

POLITECNICO DI TORINO

Master's Degree in Mechatronic Engineering
Dipartimento di Automatica e Informatica



**Politecnico
di Torino**

Master's Degree Thesis

**Design, Validation and Implementation of an
Adaptive Model Predictive Control for an
Autonomous Racing Vehicle**

Supervisors:

Prof. Andrea Tonoli

Prof. Nicola Amati

Co-supervisors:

Stefano Feraco

Sara Luciani

Candidate:

Nicolò Fiume

Anno Accademico 2020 - 2021

Abstract

In recent years, automotive control has become a significant factor in automotive innovation. Over the years, it has been necessary to use automotive control to meet lower fuel consumption and lower emissions demands. Besides, automotive control ensures greater driving safety and comfort.

In any technology area, control design is a fusion of reality, physics, modeling, and design methods. This also happens in automotive control, where extensive research and development has led to numerous descriptions, models, and design methodologies suitable for control. [1]

An autonomous vehicle's control consists mainly of three separate modules: environment perception, planning and decision-making, and vehicle control. This master thesis aims to design, validate, and implement a vehicle control strategy to automatically manage the lateral and longitudinal dynamics of a full electric all-wheel-drive racing vehicle participating in Formula SAE.

The vehicle control strategy is based on Model Predictive Control, using a combined model that manages both the lateral and longitudinal dynamics or two separated MPC, one for the lateral dynamics and the other for the longitudinal dynamics.

In the first part of the thesis work, vehicle dynamics is modeled using 3 degrees of freedom vehicle model, and simulations are performed in virtual scenarios created using Automated Driving Scenario Toolbox[®] on MATLAB[®] and Simulink[®]. In the second part, there is an integration of the Path Planning and the Vehicle Control Strategy based on acquisitions performed in real-time. The third part of the thesis work is performed on Simscape Vehicle Template[2] with the vehicle dynamics modeled using a complete vehicle model. The last part of the work consists of implementing the developed controller into Real-Time Target Hardware Platforms.

Contents

1	Introduction	1
1.1	History of Autonomous Vehicle Technologies	2
1.2	SAE Autonomous Vehicle Standard levels	7
1.2.1	Driving-Assistance Systems	8
1.2.2	Advanced Driving-Assistance Systems	10
1.3	Formula Student Competition	13
1.4	State of Art	15
1.4.1	Overview Lane Following	16
1.5	Thesis outline	22
2	Modeling	24
2.1	Reference Frames and Vehicle's Coordinates	25
2.2	3 DOF Vehicle Model	27
2.2.1	Vehicle Body 3 DOF Dual-Track	28
2.2.2	Vehicle Body 3 DOF Single-Track	31
2.2.3	Aerodynamic Drag Force	39
2.2.4	Static Load Distribution	40
2.2.5	Understeering / Oversteering	40
2.3	Parameterized Vehicle Model for Adaptive MPC	41
2.3.1	Adaptive MPC Model - Separated Dynamics	42
2.3.2	Adaptive MPC Model - Combined Dynamics	44
2.4	15 DOF Vehicle Model	46
2.4.1	Double-Wishbone Suspension	54
2.4.2	Steering System - Rack and Pinion Steering	54
2.4.3	Anti Roll Drop Link	55
3	Model Predictive Control Strategy and Trajectory Planning	57
3.1	Autonomous Driving Building Blocks	59
3.2	Problem Formulation	61
3.2.1	Combined Dynamics Configuration	62
3.2.2	Separated Dynamics Configuration	63
3.3	Reference Path Generator	63
3.4	Reference Velocity Generator	67
3.5	Wheel Torque Calculation for Desired Acceleration	68

4	Validation and Results	71
4.1	Driving Scenario Simulator	72
4.1.1	3 Degrees of Freedom validation and results	72
4.1.2	15 Degrees of Freedom validation and results	79
4.2	Path Planning and Lane Following	85
4.2.1	3 Degrees of Freedom validation and results	85
4.2.2	15 Degrees of Freedom validation and results	88
4.3	Hardware Implementation	91
5	Conclusions and future works	94
	Acronyms	100
	Symbols	103

Design, Validation and Implementation of an Adaptive Model Predictive Control for an Autonomous Racing Vehicle

CHAPTER 1

Introduction

This chapter aims to introduce this thesis's topic, presenting a brief history of autonomous vehicle technologies, standard autonomous driving levels, and some famous Driving Assistance Systems(DAS) equipped in the ground vehicles. The development of these systems has grown in the last decades due to car accidents connected to driver distraction or misjudgment.

A description of Formula Student's competition is provided, analyzing the different vehicle classes and the competition's characteristics briefly, focusing on the driverless aspect. Squadra Corse Politecnico has to build a single-seat formula racecar that competes against teams from all over the world. The team that wins the competition is not only the one with the fastest car, but is the one with the best overall package of construction, performance, and financial planning.

Finally, an overview of the State of Art of autonomous vehicles and Lane following are presented. Lane following control is a crucial part of autonomous driving to maintain vehicles' road to avoid dangerous situations. The control strategy used in this thesis work is based on Model Predictive Control approach with which it is possible to control the lateral and longitudinal dynamics.

1.1 History of Autonomous Vehicle Technologies

The expectation of autonomous cars can seem extraordinarily futuristic. This evolutionary process began with Leonardo Da Vinci's inventions and was improved over time up to the present day. In the not too distant future, we will be able to get into a vehicle and be transported to any destination without putting our hands on the steering wheel and pressing the accelerator pedal.

Companies like Ford, Mercedes, and Tesla are continually working to build autonomous vehicles for a world that will undergo a radical change.

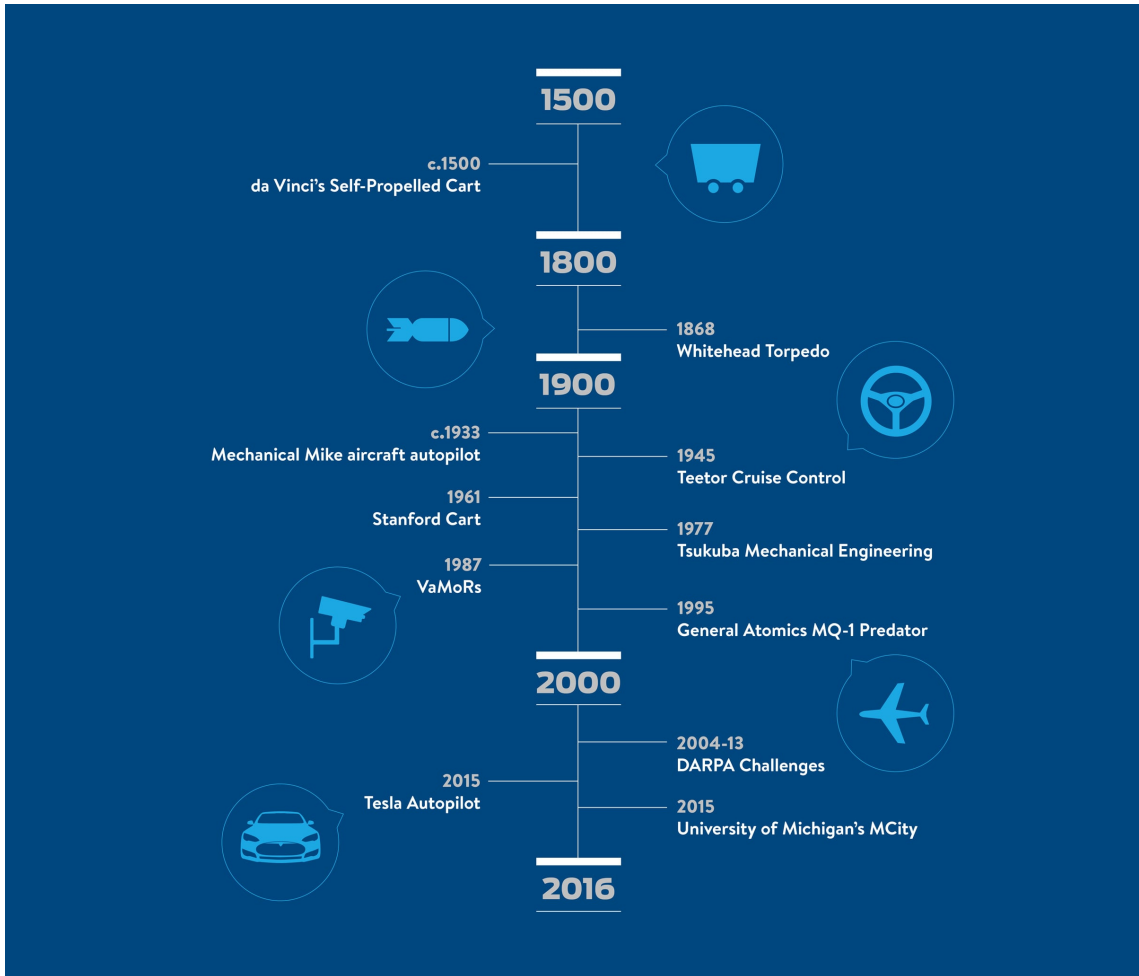


Figure 1.1: History of Autonomous Vehicle Technologies

Da Vinci's Self-Propelled Cart—c. 1500 In the sixteenth century, long before the first automobile invention, Leonardo da Vinci designed an autonomous cart. This Cart did not need to be pushed, but it moved through a mechanism formed by high tension springs.

The path to be followed was set in advance, so there was no need for steering actions. The device is sometimes considered the first robot in the world.

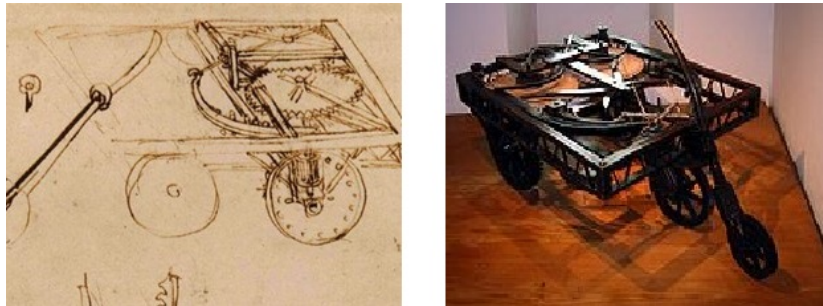


Figure 1.2: Da Vinci's Self-Propelled Cart [3]

Whitehead Torpedo—1868 Robert Whitehead's invention, a torpedo capable of moving underwater, has proved a turning point for naval wars. The Whitehead torpedo could travel several hundred meters underwater and maintain depth, thanks to a pressurization system dubbed "The Secret." Torpedo guidance would evolve dramatically after that and lead to a wide range of weapons, aircraft, and other autonomous devices.

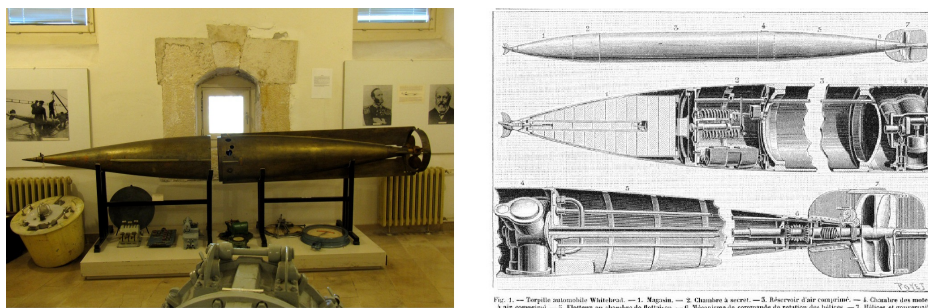


Figure 1.3: Whitehead Torpedo [4]

Mechanical Mike aircraft autopilot—1933 Prolonged travel times have forced the development of autopilot systems to be incorporated into aerial vehicles. One of the prototypes of an autonomous pilot was the Mechanical Mike. This prototype was designed by Sperry Gyroscope Co. and was used in 1933 by Wiley Post, who, through this device, was able to make a world tour in an airplane. The gyroscopes acquired data related to the plane's direction and collaborated with the controls to ensure a precise route. In today autonomous vehicle technology, Gyroscopes are of great importance.



Figure 1.4: Mechanical Mike aircraft autopilot [5]

Teetor Cruise Control—1945 Ralph Teetor was an engineer who developed one of the first cruise control systems. This system used a mechanical throttle valve capable of setting the speed of the vehicle. "Speedostat" was the name given to the invention. The name that was given later was "Cruise Control." The device was not used in cars until 1958 when Chrysler tried to install it.

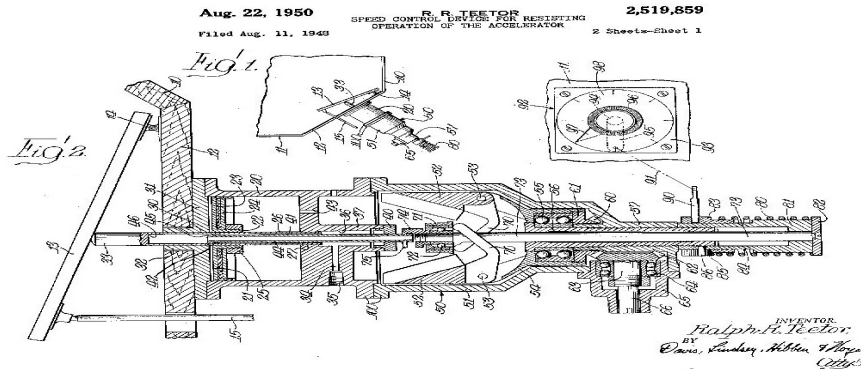


Figure 1.5: Teetor Cruise Control [6]

Stanford Cart—1961 During the 1960s, the space race was at the center of the plans of researchers who began to think and develop about vehicles capable of landing on the moon and moving on its surface. Initially, the engineers thought of vehicle remote control, but they discarded the idea due to the delay between command and execution. For this reason, the development of an autonomous wheeled vehicle was designed. The Cart was equipped with cameras and programmed to move independently. In modern autonomous cars, cameras are essential elements for the proper functioning of the vehicle.

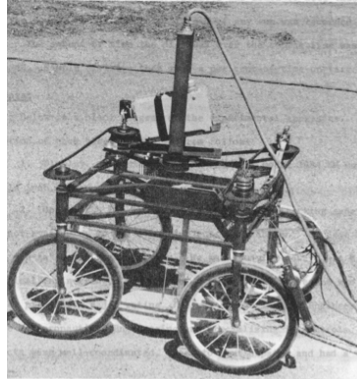


Figure 1.6: Stanford Cart [7]

Tsukuba Mechanical Engineering—1977 Tsukuba Mechanical has produced an autonomous passenger vehicle capable of recognizing road signs with speed slightly below 32 kilometers per hour. The functioning of this vehicle was made possible thanks to cameras mounted in the car.



Figure 1.7: Automatically Operated Car [8]

VaMoRs—1987 German engineer Ernst Dickmanns equipped a vehicle with a series of cameras and several micro-processing modules to detect objects on the road. He was remembered primarily for his "dynamic vision," which filters out the "noise" and detects only relevant objects. Today, this is a fundamental mechanism for autonomous driving.

The VaMoRs were so effective that they were tested up to speeds close to 100km/h on German motorways.



Figure 1.8: VaMoRs [9]

General Atomics MQ-1 Predator—1995 Some autonomous devices are designed to travel entirely on their own, such as drones. One of the most famous is the General Atomics Predator. The Predator is equipped with technologies adapted for cars, including radar that can see through smoke or clouds and thermal cameras that allow travel at night.



Figure 1.9: General Atomics MQ-1 Predator [10]

DARPA Challenges—2004-2013 The US Department of Defense research arm, DARPA, sponsored several challenges to foster the development of autonomous technologies. In 2004, the competition consisted of a 150-mile long route in the desert that the vehicles had to drive autonomously. Although any vehicles did not complete the route in that year, this challenge involved more cars in the following years, giving a significant contribution to autonomous vehicle technologies.



Figure 1.10: DARPA Challenges [11]

Tesla Autopilot—2015 Tesla’s semi-autonomous ”Autopilot” feature was introduced in vehicles in late 2015. This feature enabled control for self-driving on the highway and was provided in the form of a software update to Model S owners. [13]

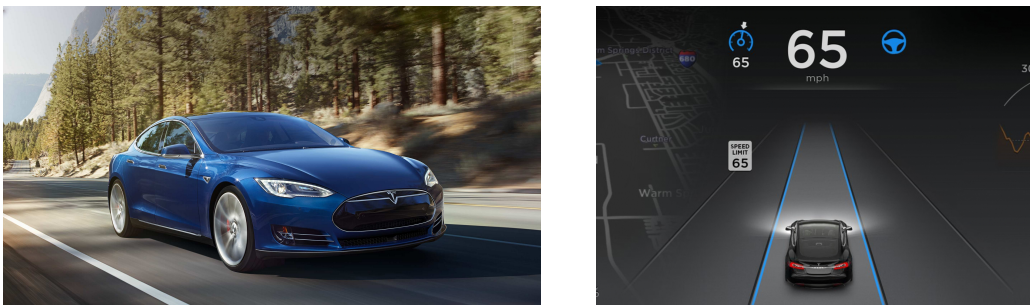


Figure 1.11: Tesla Model S [12]

1.2 SAE Autonomous Vehicle Standard levels

SAE International defines the six levels of driving automation, from no automation to full automation, through a chart with more "consumer-friendly" terms and definitions for each class.

The infographic aims to eliminate confusion, provide clearness, and use terms and expressions most used in ordinary language.

"SAE J3016™: Taxonomy and Definitions for Terms Related to On-Road Motor Vehicle Automated Driving Systems" is a reference document that aims to speed the delivery of an initial regulatory framework and best practices to guide manufacturers and other entities in the safe design, development, testing, and deployment of highly automated vehicles (HAVs).

The document has gained more and more fame to become a global standard in automated vehicle technology.

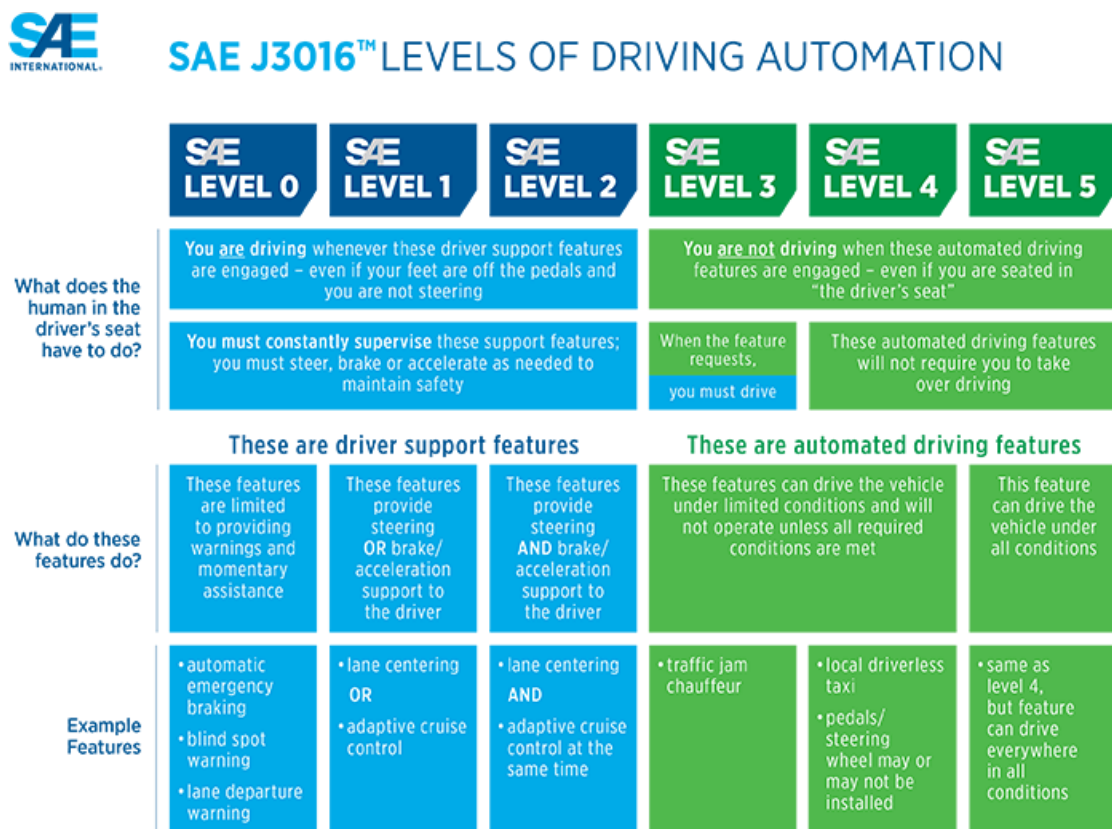


Figure 1.12: SAE Autonomous Vehicle Standard levels [14]

The six levels of driving automation are briefly described below:

- **Level 0 - No Automation.** The full-time performance is of the human driver on all aspects of the dynamic driving activity, even if enhanced by warning or intervention systems.
- **Level 1 - Driver Assistance.** The driving mode-specific execution is done by a driver assistance system (steering or acceleration/deceleration) using information about the

driving environment and the expectation that the human driver performs all remaining aspects of the dynamic driving task.

- **Level 2 - Partial Automation.** The vehicle can control both acceleration/deceleration and steering using the information about the driving environment, but the human driver must be ready to take control at any moment.
- **Level 3 - Conditional Automation.** The driving mode-specific execution is done by an automated driving system capable of managing all aspects of the dynamic driving task with favorable conditions. The human driver must intervene in case of unfavorable driving conditions.
- **Level 4 - High Automation.** Vehicles can drive themselves without human interactions except for some complicated scenarios.
- **Level 5 - Full Automation.** The vehicles should be able to monitor and maneuver through all road conditions and require no human interventions.

Level 4 autonomy is expected to be available between 2020 and 2022, while full autonomy with Level 5 technology is projected to arrive by 2030 at the earliest. Advanced Driving-Assistance Systems (ADAS) are vital components in achieving the goal of fully autonomous driving. The main ADAS will be briefly described in the following two paragraphs.

1.2.1 Driving-Assistance Systems

Driving-Assistance Systems (DAS) are based on proprioceptive sensors, i.e., sensors measuring internal vehicle variables, such as velocity, acceleration, and wheel rotational velocity, to support the driver's action and improve vehicle safety during critical driving conditions.

The first introduced DAS were:

- **Anti-lock Braking System (ABS).** Emergency braking or even braking on a wet or slippery surface can cause the wheels of the vehicle to lock. Locking wheels reduce the adhesion between tires and the road surface and make the vehicle unsteerable. The antilock braking system (ABS) prevents the wheels from locking and enables safe braking.[15]

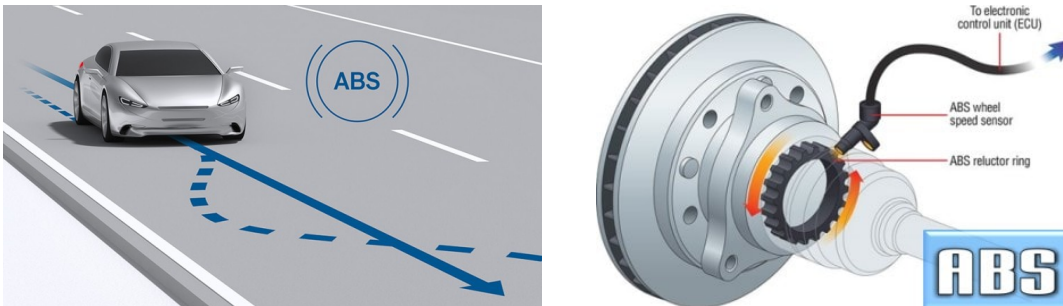


Figure 1.13: Anti-lock Braking System

- **Electronic Stability Control (ESC).** It is a system for controlling the car's stability, which acts when skidding, adjusting the engine power, and braking the individual wheels with different intensity to re-stabilize the car's attitude. This device is effective in correcting both any oversteer or understeer situations, which may occur in the event of a wrong setting of a curve, and in the event of sudden deviation of the trajectory, avoiding the skidding of the vehicle. [16]

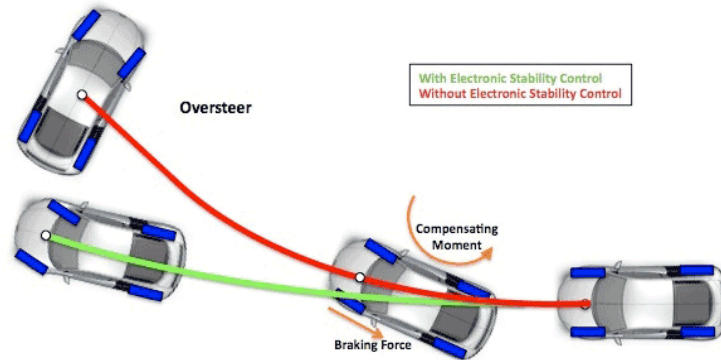


Figure 1.14: Electronic Stability Control

- **Cruise Control (CC).** Cruise control is an electronic system that allows the automatic speed adjustment of a vehicle. The driver selects the desired speed, and it is maintained compatibly with the trim conditions of the car itself. Suppose the driver decides to overtake another car. In that case, he can press the accelerator pedal and increase the speed, which will return to the previously set one only when he stops accelerating. There is also the system's deactivation in pressure on the brake, clutch, handbrake, activation of a safety system, or faults in the electrical circuits.

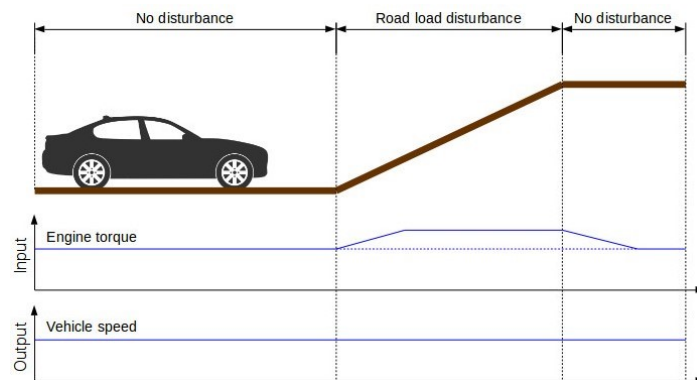


Figure 1.15: Cruise Control[17]

- **Traction Control System (TCS).** The traction control, also called Anti-Slip Regulation, is an electronic control unit or integrated system with electronic management, which prevents the drive wheels of a vehicle from spinning during acceleration and which, especially for motorcycles, can also be used as an anti-rearing system.[18]

1.2.2 Advanced Driving-Assistance Systems

Thanks to the recent ICT technology advances, sensors and microcontrollers have been introduced in commercial vehicles to support drivers in various driving tasks. Advanced Driver Assistance Systems (ADAS) are the evolution of DAS based on exteroceptive sensors, i.e., sensors that acquire information about road and traffic environment.

- **Adaptive Cruise Control (ACC).** Adaptive cruise control is an electronic control system that adjusts the vehicle's speed on which it is equipped while automatically maintaining a safe distance from the vehicles in front.

The control is based on the onboard sensors' information that allows the device to brake the car when approaching another vehicle in front and then accelerate when traffic permits.

ACC technology is considered a key component for future generations of smart cars. They affect the driver's safety and comfort and the smoothness of traffic, maintaining an optimal distance between vehicles and reducing the likelihood of driver error.

Vehicles equipped with adaptive cruise control are considered autonomous level 1, according to the SAE International classification. When combined with another driver assistance function such as the lane-keeping system, it allows the vehicle in question to achieve a level 2 range.[19]



Figure 1.16: Adaptive Cruise Control

- **Autonomous Emergency Braking (AEB).** Many accidents are caused by late use of the brakes or insufficient braking force. The driver may brake late for several reasons. He may be distracted or fatigued, or he may find himself in conditions of poor visibility; in other cases, it may not have the time necessary for the sudden and unexpected braking of the vehicle in front.

Some manufacturers have developed technologies that help the driver avoid accidents or at least reduce their severity. The systems designed can be grouped in the Autonomous Emergency Braking category (Emergency braking assistant).

AEB systems improve safety in two ways: first, they help avoid impact by identifying critical situations in time and alerting the driver; secondly, they reduce the severity of

unavoidable accidents, reducing the collision speed and, in some cases, preparing the car and seat belts for impact.[20]

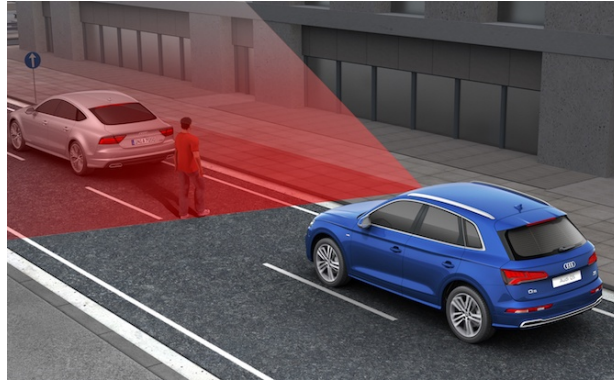


Figure 1.17: Autonomous Emergency Braking

- **Lane Keeping (LK).** Lane departures are among the most significant causes of fatal accidents and account for about 40 % of the victims due to accidents. Lane Keeping support functions have been introduced on commercial vehicles to prevent accidents due to unintentional lane departures.

Lane-keeping support systems detect the lane markings ahead of the vehicle and give the information of its' position in the lane. If the vehicle's distance to the lane markings falls below a defined threshold, the system steps in.

Lane-keeping support systems can be divided in:

- **Warning functions** do not directly modify the vehicle trajectory and alert the driver through a sound to establish a suitable driving action to avoid lane departure.

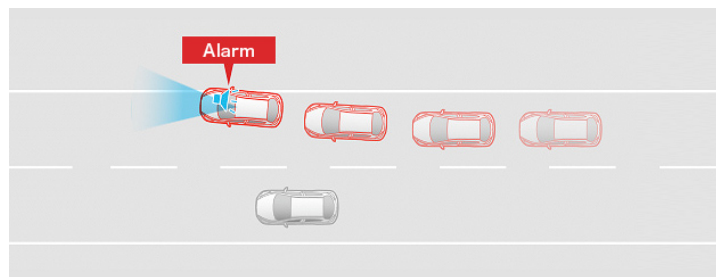


Figure 1.18: Lane Departure Warning System [21]

- **Intervention functions** have limited authority to vehicle direction change and superimpose a limited steering command to the one issued by the driver.

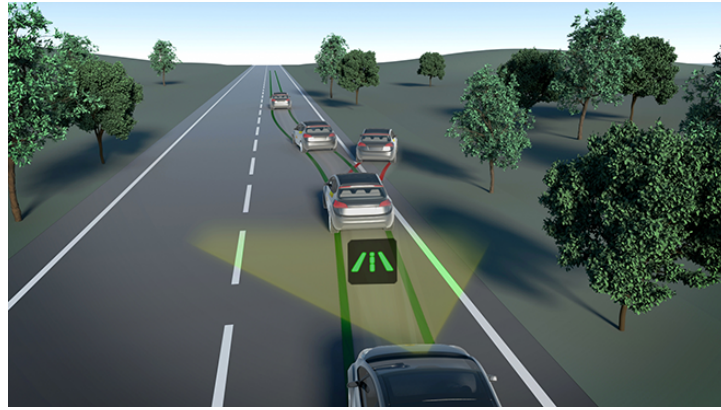


Figure 1.19: Lane Keep Assist [22]

- **Control functions** have full authority to steer the vehicle; an automatic control algorithm substitutes the manual driving action from the loop. Automatic Lane Keeping Control automatically steers the vehicle to keep the center of the lane detected by a vision system and it is used in conjunction with the Adaptive Cruise Control system to support autonomous driving SAE level 2.



Figure 1.20: Automatic Lane Keeping Control [23]

- **Park Assist (PA)** is a system capable of actively assisting the driver in parking maneuvers. It autonomously manages the search for parking, calculating the necessary space, and the steering maneuvers. However, it does not control the throttle control, the gearbox, and the brakes, which the driver must still operate.[32]



Figure 1.21: Parking Assist System [24]

1.3 Formula Student Competition

Formula Student (FS) is a competition that challenges students from various universities around the world. It represents Europe's most established educational engineering competition, which uses motorsport to inspire students. It was born in 1981 in the United States when the Society of Automotive Engineers (SAE) started running its first Formula SAE program.

This competition challenges young engineers and encourages more young people to take a career in engineering. Furthermore, the competition has become bigger and bigger thanks to the famous companies interested in the event.



Figure 1.22: Partners Formula Student Germany 2021

The format provides an ideal opportunity for students to demonstrate their engineering knowledge and test and improve their capabilities to deliver a complex and integrated product in the demanding environment of a motorsport competition.

Thanks to the competition, young engineers' technical, design, engineering, and production skills are tested while meeting a strict deadline. This competition will give them experience in the skills prospective employers will be looking for and setting them up for a career in engineering.[25]



Figure 1.23: Formula Student Competition

The competition is divided into 3 classes:

- FS Combustion (FSC)
- FS Electric (FSE)
- FS Driveless (FSD)



Figure 1.24: Formula Student Competition Classes

The Formula Student Germany competition introduces the participating students to today's automotive industry's interdisciplinary approach, including technical understanding and economic and communication abilities such as presentation techniques or financial planning skills. These are three static events that demand collaboration across the team in design and layout, construction, marketing, and pricing of a product. They also require specialized expertise from various technical and financial courses of study. Each event has a different weight depending on the discipline covered and the type of vehicle class. A panel of experienced experts from the automobile, motorsport, and supply industries judge each team's performance.[26]

During the current year, due to the Covid 19, the events did not take place; the roadmap for next years competitions, presented by Formula Student Germany (FSG), expect to integrate by the 2022 FS Driverless event directly into both FS Combustion and FS Electric events and to eliminate FS Combustion by 2023.



Figure 1.25: Formula Student Driveless vehicle during Formula Student Germany 2019

Formula Student Germany competition is divided into eight disciplines, 3 Static and 5 Dynamic. All the cars must attend a series of inspections for all autonomous systems (AS) and hardware elements to check compliance with regulations and be admitted to the competition. Furthermore, each driverless vehicle must respect the base requirements for the combustion or the electric class. The vehicle must be able to be operated in both driverless and with driver modes.

The competition is not won solely by the team with the fastest car, but rather by the team with the best overall package of construction, performance, and financial and sales planning and challenges students to build the vehicle considering the manufacturing feasibility in automotive sectors.

Table 1.1: Formula Student Competition disciplines points:

	Discipline	FSC,FSE	FSD
Statics	Business Plan	75 points	75 points
	Cost and Manufacturing	100 points	100 points
	Engineering Design	150 points	300 points
Dynamics	Acceleration	75 points	75 points
	Skid Pad	75 points	75 points
	Autocross	100 points	100 points
	Endurance	325 points	- - -
	Track Drive	- - -	200 points
	Efficiency	100 points	75 points
	Overall	1000 points	1000 points

1.4 State of Art

Considering the massive shift towards autonomous driving that the automotive industry is facing, it is of the utmost importance to optimize control techniques. This thesis work addresses finding an optimal control algorithm for managing the lateral and longitudinal dynamics of an autonomous vehicle that will face the various disciplines in the Formula Student Competition. State of the art regarding the development of vehicle control for autonomous driving has been analyzed. The methodology adopted for the project mainly consists of modeling, tuning, validation, and implementation of the system.

The flow chart below illustrates the progress of the work. The first part of the work was dedicated to the Review of the Literature. This review is done to get an idea of the project's nature and to familiarize with the symbols and formulas used in the reference model. The reference model is taken from MATLAB MPC examples, and it is explained extensively in the MPC User Guide from MATLAB documentation.

Starting from a reference model and adapting it to Squadra Corse's vehicle's parameters, the Lane Following section and the Path Planning section were developed in parallel. These two sections have been merged upon their completion to have a complete control algorithm.

The Validation section consists of testing the control algorithm in different scenarios and different vehicle models. For the Validation section Automated Driving Scenario Toolbox[®] is used to create the different scenarios, and Simscape Vehicle Template is used for modeling the vehicle dynamics.

The last part of the State of Art is the Implementation section, where the developed controller is implemented into real-time-target machines like SCALEXIO (DSpace's Hardware-in-the-loop system).

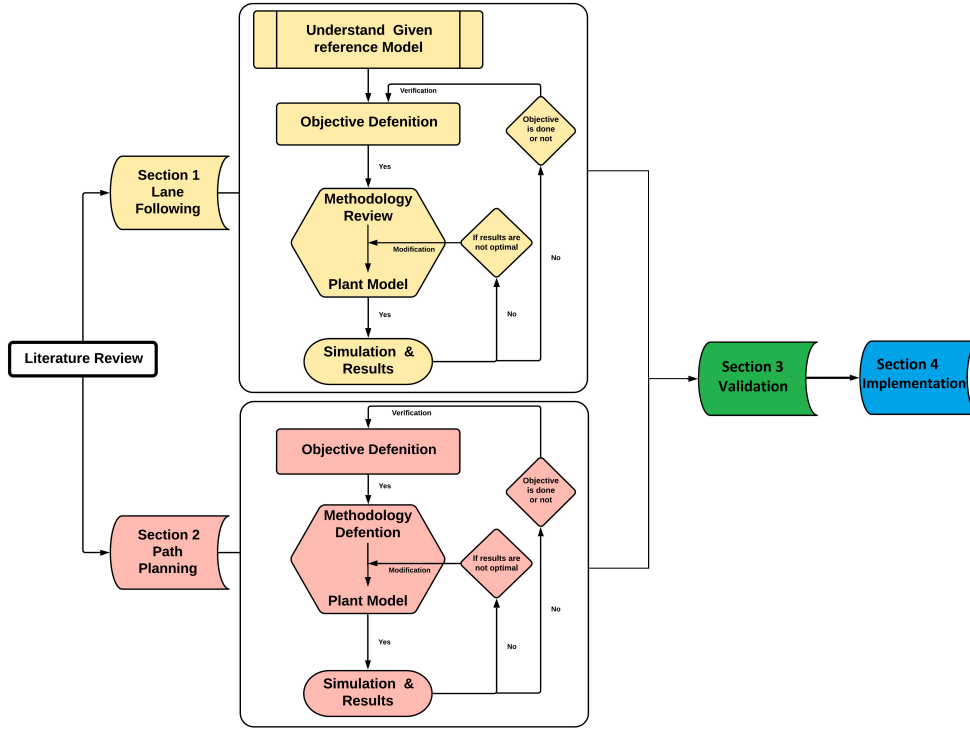


Figure 1.26: State of Art Flow Chart

1.4.1 Overview Lane Following

Vehicle control is a crucial part of autonomous driving, both in terms of comfort and driving safety. This thesis work mainly focuses on developing an autonomous vehicle control algorithm, and this subsection briefly describes the design of the control architecture to implement this control algorithm.

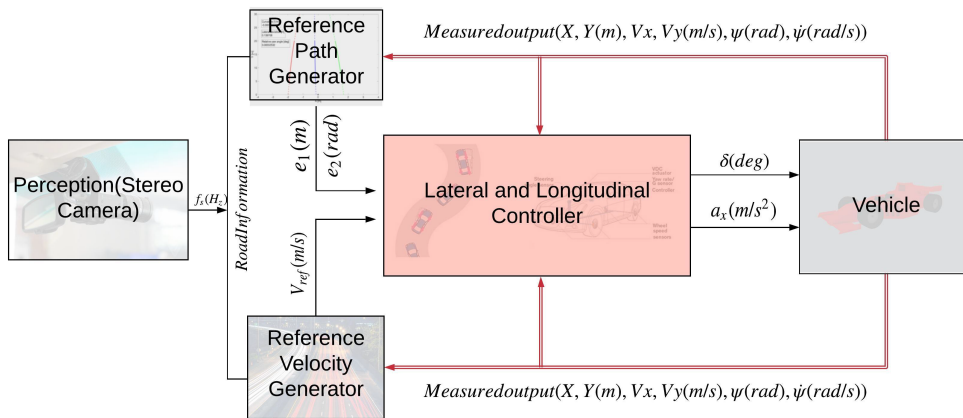


Figure 1.27: Autonomous Vehicle Control Architecture

For this thesis, an Adaptive Model Predictive Control is adopted as a control algorithm. Model predictive control is an advanced method of process control used to control a process while satisfying a set of constraints based on online optimization.

The main advantage of MPC is that it allows the current timeslot to be optimized while keeping future timeslots into account. This optimization is achieved by optimizing a finite time-horizon, but only implementing the current timeslot and then optimizing again, repeatedly. MPC can anticipate future events and can take control actions accordingly.

MPC is nearly universally implemented as digital control, although there is research into achieving faster response times with specially designed analog circuitry.[27]

For this thesis work, two types of control algorithms have been developed. The first considers together the longitudinal and lateral dynamics, while the second considers these dynamics separately.

Another key element of the control architecture is the vehicle model. It can be modeled with 3 DOF or a more advanced model that considers multiple aspects of dynamics. The model receives the acceleration and steering angle signals from the controller and uses them to modify its longitudinal and lateral dynamics.

Through the changes received through the controller's signals, the vehicle sends the measured outputs to the sensors that use the information to analyze the environment to give the input to the controller.

The Reference Velocity Generator elaborates the information from the curves and calculates the correct velocity that the vehicle must maintain to perform the turn correctly.

The Reference Path Generator brings information about the environment, finds the road's left and right limits, and computing the center between them. The founded points are the ones that the vehicle uses as the trajectory.

First Controller Architecture

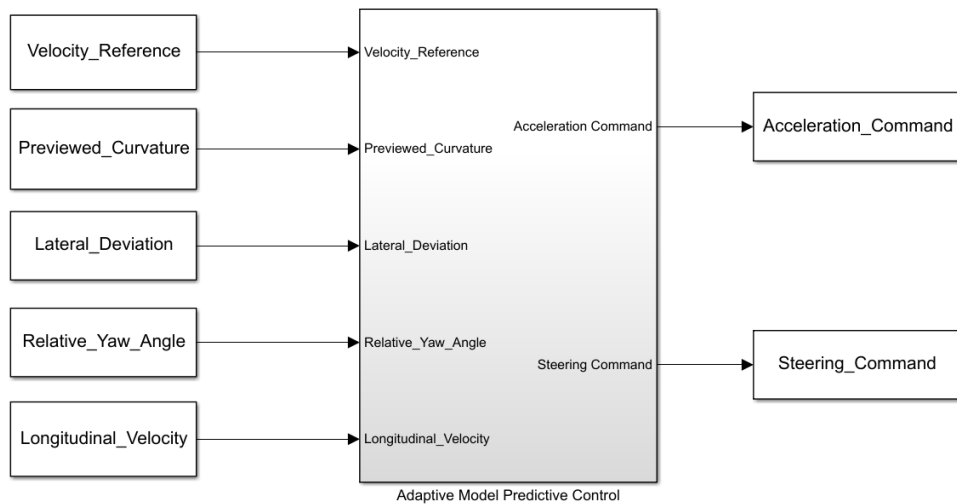


Figure 1.28: First Controller Architecture

As shown in the Figure 1.28, the First Controller Architecture receives as inputs the following signals:

- *Velocity Reference*
- *Previewed Curvature*
- *Lateral Deviation*
- *Relative Yaw Angle*
- *Longitudinal Velocity*

The controller elaborates the input data and calculates the Acceleration and Steering commands to provide to the vehicle model. This process is done using an Adaptive Model Predictive Controller that uses a variable parametrized vehicle model to calculate the optimized controls.

Velocity Reference and constant zero are used as references for the measured outputs of the controller.

The measured outputs are the vehicle's Longitudinal Velocity, the Lateral Deviation derived from the distance between the center lane of the road and the center of gravity of the car, and the Relative Yaw Angle derived from the difference between the yaw angle of the vehicle and the street angle.

The measured disturbance is calculated performing the product of the Longitudinal Velocity and the Previewed Curvature.

Providing all these signals, the Adaptive MPC can calculate the manipulated variables in the form of Acceleration and Steering commands for the vehicle.

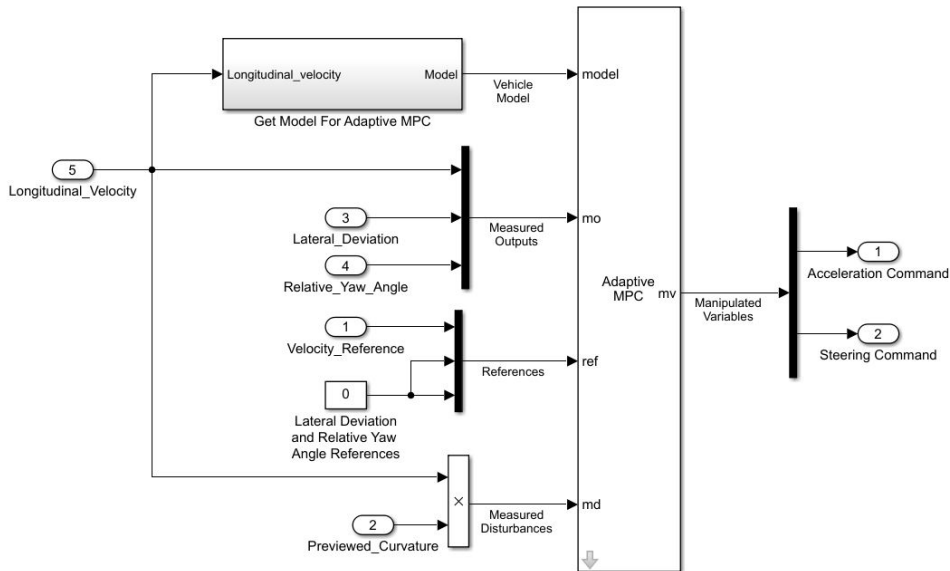


Figure 1.29: First Controller Architecture

Second Controller Architecture

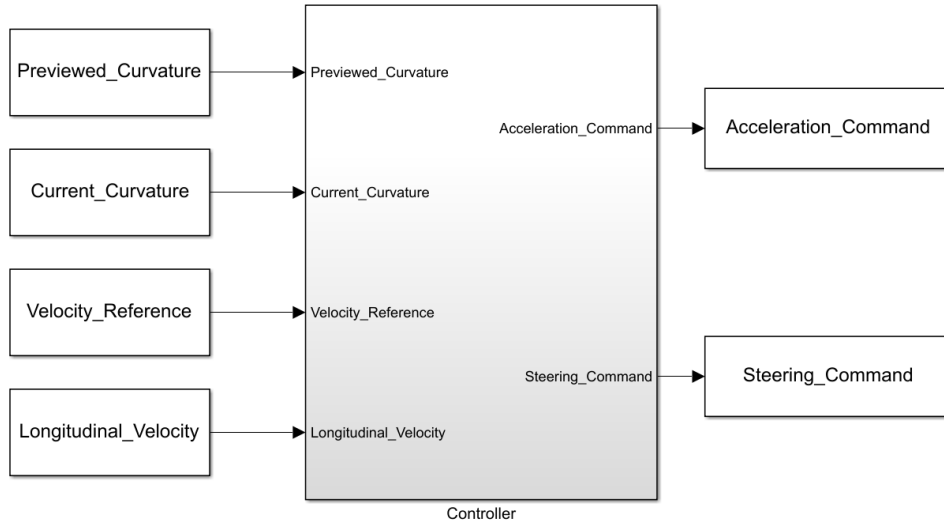


Figure 1.30: Second Controller Architecture

As shown in the Figure 1.30, the Second Controller Architecture receives as inputs the following signals:

- *Previewed Curvature*
- *Current Curvature*
- *Velocity Reference*
- *Longitudinal Velocity*

Unlike the first architecture, this second architecture receives only four inputs, including the Current Curvature, representing the Previewed Curvature vector's first value.

The main difference between the two architectures is the decoupling of the lateral and longitudinal dynamics, as shown in Figure 1.31.

Previewed Curvature, Current Reference, and Longitudinal Velocity signals are the lateral controller inputs that provide the vehicle's Steering command.

The Longitudinal Velocity and the Velocity Reference signals are the longitudinal controller inputs that provide the vehicle's Acceleration command.

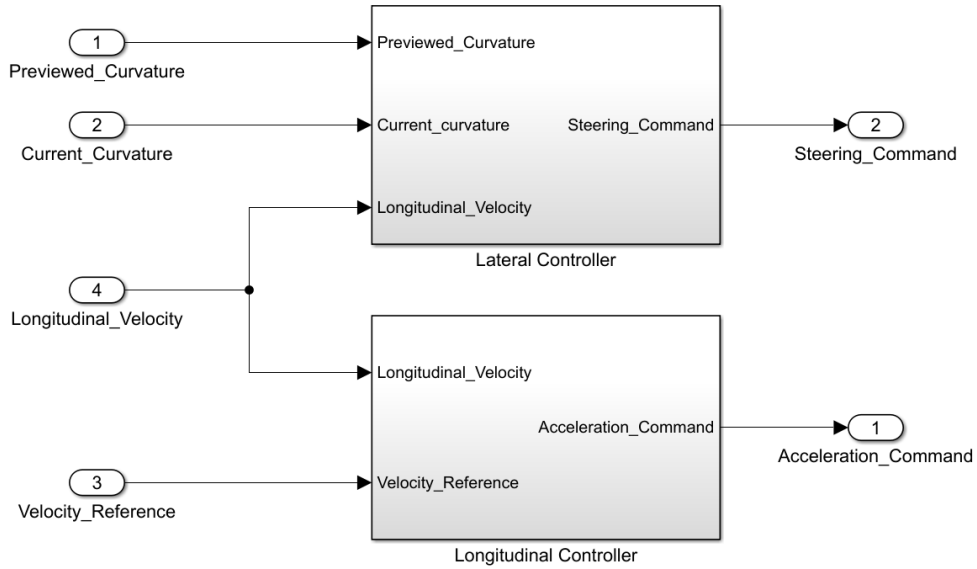


Figure 1.31: Second Controller Architecture

The lateral controller is composed of two blocks:

- The Adaptive MPC that uses the vehicle’s longitudinal velocity, the previewed curvature, the lateral deviation, and the relative yaw angle to calculate the manipulated variable Steering command. The controller uses a parametrized vehicle model and can be set tuning some parameters related to the controller’s behavior. The controller can assume robust behavior or aggressive behavior.
- A block used to find Lateral Deviation and Relative Yaw Angle from the Steering feedback signal, Longitudinal Velocity, and Current Curvature.

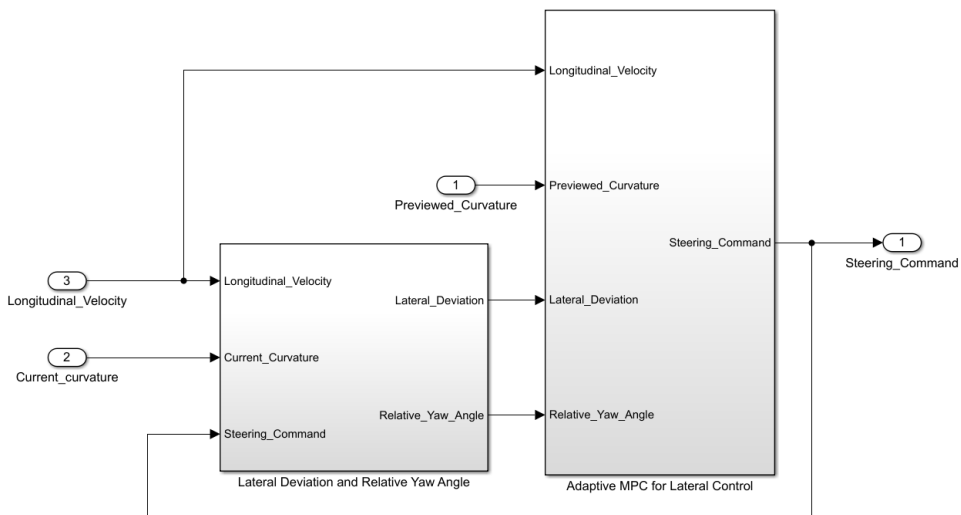


Figure 1.32: Lateral Controller

The longitudinal controller consists of an MPC receiving as Reference the Reference Velocity and as Measured Output the vehicle's Longitudinal Velocity.

This controller aims to control only the longitudinal dynamics, so the Manipulated Variable is an Acceleration Command that acts only in the longitudinal direction.

The Reference Velocity considers the curvature of the road. In the case of a curved road, the value decreases, while it increases in the case of a straight road. The Reference Velocity is calculated considering the maximum curvature between the ones provided in the Previewed curvature signals.

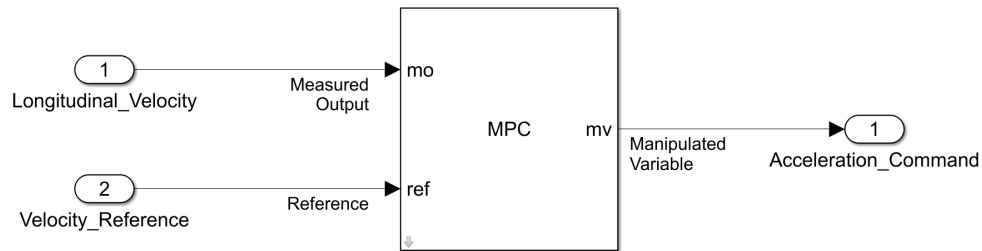


Figure 1.33: Longitudinal Controller

1.5 Thesis outline

The thesis is organized as follows:

- **Chapter 2 - Modeling** consists of a detailed description of the vehicle models used in the simulation and validation phases.

This chapter is divided into four subsections:

- The first part introduces the conventions used in this thesis work.
 - The second subsection is related to a detailed description of the 3 degrees of freedom rigid vehicle model.
 - The third subsection is related to the vehicle model's linearization for the Adaptive MPC control design.
 - The last subsection is related to a detailed description of the 15 degrees of freedom vehicle model provided by Simscape Vehicle Template.
- **Chapter 3 - Model Predictive Control Strategy and Trajectory Planning** aims to explain the problem formulation related to the MPC strategy and to give a brief introduction to the problem of trajectory planning.

The final goal of the thesis is to merge the planning part and the control part together in order to have a greater realism in the simulations. Additionally, subsections related to the reference velocity generation and to the conversion from Acceleration command to Torque Command are presented.

- **Chapter 4 - Validation and Results** is related to the final results of this master thesis work. Every subsection presents the results obtained from the 3 DOF vehicle model and the model presented in the Simscape Vehicle Template.

It is divided into three subsections:

- The first subsection is related to the results obtained into Driving Scenario Simulator.
 - The second subsection is related to the results obtained merging the path planning and lane following parts.
 - The last subsection is related to the results of the Hardware implementation.
- **Chapter 5 - Conclusions and future works** reports the final considerations about this master thesis work and possible improvements on the controller and the vehicle model.

CHAPTER 2

Modeling

This chapter aims to present the vehicle models used for the simulation and validation parts of the controller. This chapter describes three models, including two models for modeling vehicle dynamics in the surrounding environment and one parameterized model used in the Adaptive MPC.

The first part of this chapter deals with the conventions used to describe vehicle references in the environment to familiarize with the symbology used in this thesis work.

The second part describes in detail the 3 degrees of freedom vehicle model. This model does not give accurate predictions like other more complex models but is still used due to its limited computational demand. Since the Adaptive MPC will be evaluated through simulations, the 3 degrees of freedom vehicle model is used for the controller's first design to have faster simulations.

The parametrized vehicle model used for the Adaptive MPC is presented in the third part of this chapter. The parameterization is performed to consider the vehicle dynamics variations and to speed up the controller's operations.

The last part of the chapter is dedicated to the description of the complex model taken from Simscape Vehicle Template. After completing the simpler model's validation with 3 degrees of freedom, the controller is validated using a more complex model with 15 degrees of freedom. This model has a high computational demand, but it is capable of providing very accurate results. Given the model's complexity, the controller is adapted to the vehicle parameters in the validation phase.

2.1 Reference Frames and Vehicle's Coordinates

For an accurate description of vehicle model equations, the ISO 8855-2011 is adopted to describe the vehicle axis system. The local coordinate system is denoted as the vehicle fixed system.

In Figure 2.1 the local coordinates system is presented:

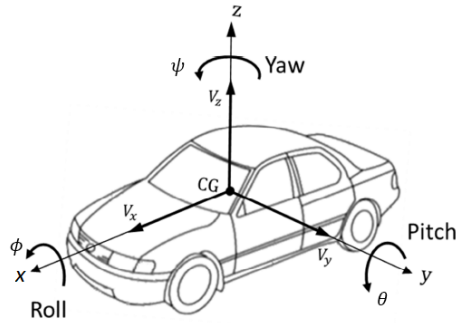


Figure 2.1: Local Coordinates System [28]

The symbol **CG** indicates the Center of Gravity, sometimes referred to as Point of Equilibrium. It is the geometric point corresponding to the mean value of the system's mass distribution in space. The Center of Gravity is the point where the local reference frame develops itself.

As shown in the figure above, the vehicle can perform various movements, divided into translational and rotational movements. The translational movements can be developed along the main axis:

- Longitudinal movement along x
- Lateral movement along y
- Vertical movement along z

Velocities along the axes are indicated with v followed by a subscript representing the axis along which the velocity propagates. The same convention is used for accelerations, but they are indicated with a .

- Longitudinal velocity v_x, \dot{x}
- Lateral velocity v_y, \dot{y}
- Vertical velocity v_z, \dot{z}
- Longitudinal acceleration a_x, \dot{v}_x, \ddot{x}
- Lateral acceleration a_y, \dot{v}_y, \ddot{y}
- Vertical acceleration a_z, \dot{v}_z, \ddot{z}

The rotational movements do not change the position of the Center of Gravity. They can be divided into three different rotations around the main axes:

- **Roll** causes a vehicle to rotate about its longitudinal axis. It is indicated with ϕ
- **Pitch** causes a vehicle to rotate about its lateral axis. It is indicated with θ
- **Yaw** causes a vehicle to rotate about its vertical axis. It is indicated with ψ

Angular velocities around the axes are indicated with ω followed by a subscript representing the rotation axis. The same convention is used for the angular accelerations, but they are indicated with α .

- Angular velocity around longitudinal axis \mathbf{x} , also called **Roll Rate**, indicated with ω_x , $\dot{\phi}$
- Angular velocity around lateral axis \mathbf{y} , also called **Pitch Rate**, indicated with ω_y , $\dot{\theta}$
- Angular velocity around vertical axis \mathbf{z} , also called **Yaw Rate**, indicated with ω_z , ω , Ψ , $\dot{\psi}$, r . For simplicity, this parameter will be referred to as **angular velocity** from this point on
- Angular acceleration around longitudinal axis \mathbf{x} , indicated with α_x , $\dot{\omega}_x$, $\ddot{\phi}$
- Angular acceleration around lateral axis \mathbf{y} , indicated with α_y , $\dot{\omega}_y$, $\ddot{\theta}$
- Angular acceleration around vertical axis \mathbf{z} , also called **Yaw Angular Acceleration**, indicated with α_z , α , $\dot{\omega}_z$, $\dot{\omega}$, $\ddot{\Psi}$, $\ddot{\psi}$, \dot{r} . For simplicity, this parameter will be referred to as **angular acceleration** from this point on

The local reference frame is fixed in the Center of Gravity, so it moves following the vehicle's movement. Unlike the local reference system, the global reference system does not follow the vehicle's movement but remains fixed in the environment.

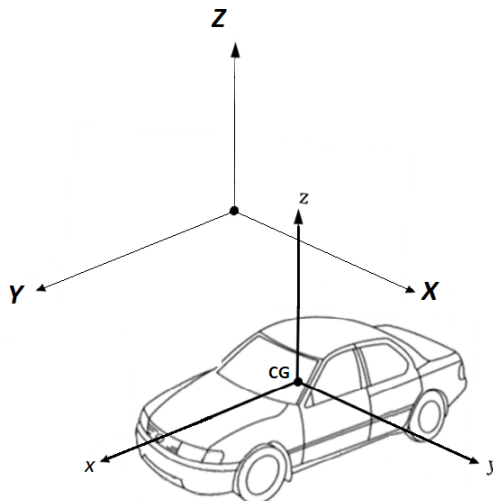


Figure 2.2: Global Coordinates System

The global coordinates are indicated with bold-capital letters. There are 3 main axes:

- Longitudinal global direction \mathbf{X}
- Lateral global direction \mathbf{Y}
- Vertical global direction \mathbf{Z}

2.2 3 DOF Vehicle Model

For the first controller design, a 3 degrees of freedom vehicle model was used. The 3 degrees of freedom model is a simplistic model of the vehicle that takes into account only three directions:

- Longitudinal direction
- Lateral direction
- Yaw direction

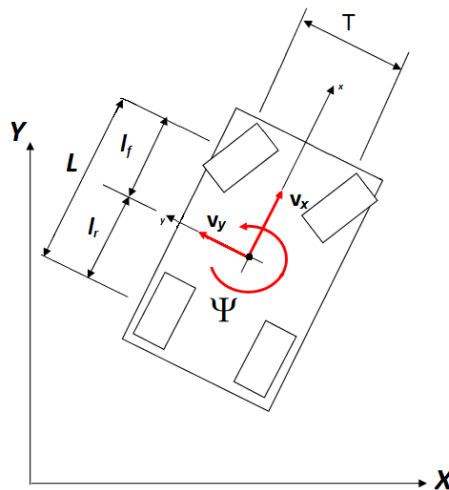


Figure 2.3: 3 DOF Vehicle Model

As shown in Figure 2.3, the vehicle is shown with a top view, so it is possible to see only the translational movement along the x-y axes and the rotational movement around the vertical axis with a positive direction defined by the right-hand rule.

The distance between the front axle and the Center of Gravity is defined as front wheelbase indicated with l_f , while the distance between the Center of Gravity and the rear axle is defined rear wheelbase indicated with l_r .

The sum of front wheelbase and rear wheelbase is called Wheelbase indicated with L . The axle's width, which corresponds to the distance between the right wheel and the left one, is defined as Track indicated with T .

2.2.1 Vehicle Body 3 DOF Dual-Track

To design control algorithms is necessary to know the equations of motion and write the physical interactions between the various subsystems in mathematical equations. One method to model the vehicle consists of Modeling as simply as possible and with as little computing-time as possible.

This subsection describes a simplified vehicle model, considering only 3 degrees of freedom.

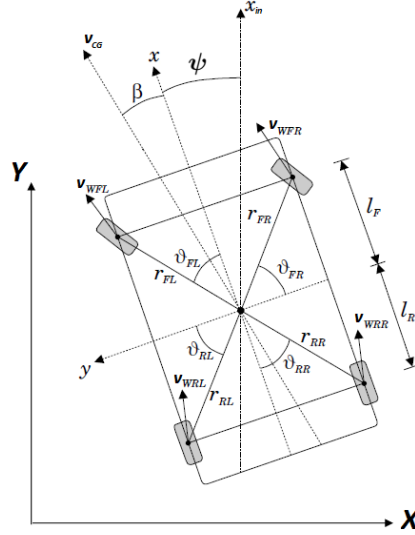


Figure 2.4: Vehicle Body 3 DOF Dual-Track [29]

\mathbf{X} and \mathbf{Y} are the fixed global axes. They do not change with the vehicle's motion. The axes \mathbf{x} and \mathbf{y} are the local axes. They start from the Center of Gravity of the vehicle and move following the vehicle's movements. The parameter \mathbf{x}_{in} represents the initial position of the local axis \mathbf{x} .

As mentioned above, the velocity can propagate along the longitudinal or the lateral direction. The resultant of the two velocities define the direction and intensity of the Center of Gravity's velocity vector, denoted by \mathbf{v}_{CG} .

The angle between the \mathbf{x} local axis and the direction defined by the velocity vector \mathbf{v}_{CG} defined the vehicle body **Side Slip Angle** β . This angle can not be measured on-board of a normal production vehicle (too expensive) and can not be at the moment precisely estimated with virtual sensors.

Rotation along the vertical z -axis is indicated with ψ . This rotation is defined by the angle between local axis \mathbf{x} and the initial position of this axis \mathbf{x}_{in} . The amplitude of this angle represents the rotation made by the vehicle concerning its initial position. It assumes positive values if the rotation is done counterclockwise and negative values if it is done clockwise.

The distance between the center of gravity and contact point between wheel and ground is indicated with r and subscripts representing the wheel to which this distance refers. These distances create angles with which it is possible to derive the velocities mathematically for each wheel.

- \mathbf{r}_{FL} distance from CG to front left wheel ground contact point
- \mathbf{r}_{FR} distance from CG to front right wheel ground contact point
- \mathbf{r}_{RL} distance from CG to rear left wheel ground contact point
- \mathbf{r}_{RR} distance from CG to rear right wheel ground contact point
- θ_{FL} angle between chassis coordinate system and front left wheel ground contact point
- θ_{FR} angle between chassis coordinate system and front right wheel ground contact point
- θ_{RL} angle between chassis coordinate system and rear left wheel ground contact point
- θ_{RR} angle between chassis coordinate system and rear right wheel ground contact point

In vehicle body 3 DOF Dual-Track model, each wheel has its velocity, with a direction different from the speed of the center of gravity v_{CG} . These speeds have a different direction to perform curves correctly. The wheels on the outside will have to front a more significant curve than the wheels inside the curve.

Wheel speeds are indicated with v and subscript W to indicate the wheel. Each speed has two more subscripts to indicate to which wheel the speed refers. One subscript indicates the reference axle, F for front and r for rear, the other subscript indicates the side to which the speed refers, L for left and R for right.

- \mathbf{v}_{WFL} front left wheel velocity
- \mathbf{v}_{WFR} front right wheel velocity
- \mathbf{v}_{WRL} rear left wheel velocity
- \mathbf{v}_{WRR} rear right wheel velocity

Velocities can be divided into two components, one in the longitudinal direction, indicated with \vec{e}_X , and one in the lateral direction, indicated with \vec{e}_Y .

$$\vec{v}_{WFL} = (v_{CG} \cos\beta - \dot{\psi} r_{FL} \sin\theta_{FL}) \vec{e}_X + (v_{CG} \sin\beta + \dot{\psi} r_{FL} \cos\theta_{FL}) \vec{e}_Y$$

$$\vec{v}_{WFR} = (v_{CG} \cos\beta + \dot{\psi} r_{FR} \cos\theta_{FR}) \vec{e}_X + (v_{CG} \sin\beta + \dot{\psi} r_{FR} \sin\theta_{FR}) \vec{e}_Y$$

$$\vec{v}_{WRL} = (v_{CG} \cos\beta - \dot{\psi} r_{RL} \cos\theta_{RL}) \vec{e}_X + (v_{CG} \sin\beta - \dot{\psi} r_{RL} \sin\theta_{RL}) \vec{e}_Y$$

$$\vec{v}_{WRR} = (v_{CG} \cos\beta - \dot{\psi} r_{RR} \sin\theta_{RR}) \vec{e}_X + (v_{CG} \sin\beta - \dot{\psi} r_{RR} \cos\theta_{RR}) \vec{e}_Y$$

The wheel velocities' amplitude is calculated using the squared longitudinal and lateral components' square root. After defining the wheel speed directions, it is possible to define other fundamental parameters in vehicle dynamics.

Side Slip Angle

As mentioned above, the Side Slip Angle is angle between the x local axis and the direction defined by the velocity vector v_{CG} . β can be roughly defined by the following formula:

$$\beta \triangleq -\arctan\left(\frac{v_y}{|v_x|}\right)$$

Due to the deformation of the carcass and the tire tread, a non-zero slip angle is created. When the tire rotates, the friction between the contact patch and the road causes the tread elements to remain stationary relative to the road. If a lateral sliding speed is introduced, the contact zone will be deformed, as shown in Figure 2.6.

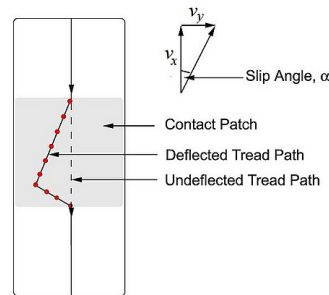


Figure 2.6: Deflected tread path and slip angle

β results in the cornering force, located in the plane of the contact patch and perpendicular to the intersection of the contact patch and the wheel's midplane. This cornering force increases approximately linearly for the first few slip angles, then increases non-linearly to a maximum before decreasing.[30]

2.2.2 Vehicle Body 3 DOF Single-Track

The 3 DOF single track model is used to approximate the vehicle dynamics without excessive effort. This model does not give accurate predictions like other more complex models but is still used due to its limited computational demand.

Since the Adaptive MPC will be evaluated through simulations, the 3 degrees of freedom Single -Track vehicle model is used for the controller's first design to have faster simulations. [31]

The model is based on a series of simplifications:

- All Roll, Pitch and Lift movements are not considered
- The mass of the vehicle is concentrated on the center of gravity v_{CG}
- The wheels of the front axle and rear axle are represented by a single wheel for each axle
- The point of contact between the wheel and the ground is in the same plane of the axles

- The wheel load distribution between the front and rear axles is constant
- The longitudinal forces on the tires are neglected

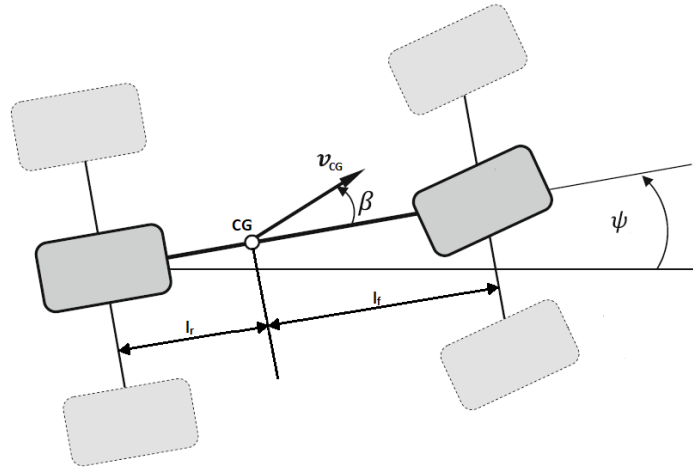


Figure 2.7: Vehicle Body 3 DOF Single-Track

The first assumption leads to a decrease in the degrees of freedom from six to three. The only movements allowed are longitudinal movements along the local axis x , lateral movements along the local axis y , and rotational movement around the local vertical axis z .

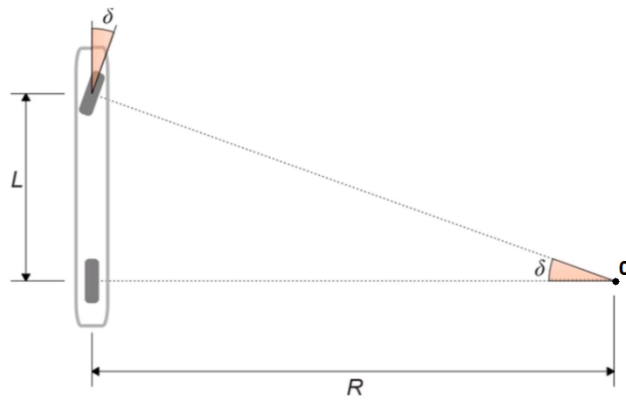


Figure 2.8: Ackermann Angle

As shown in Figure 2.8, the directions perpendicular to the wheels converge at a point indicated as 0. The angle between these two directions is indicated as the **Ackermann angle** δ_{Ack} .

Defining L as the distance between the two axles and R as the distance between the wheel and point 0, the Ackermann angle δ_{Ack} can be approximated with the following formula:

$$\delta_{Ack} = \arctan\left(\frac{L}{R}\right)$$

Kinematic Model

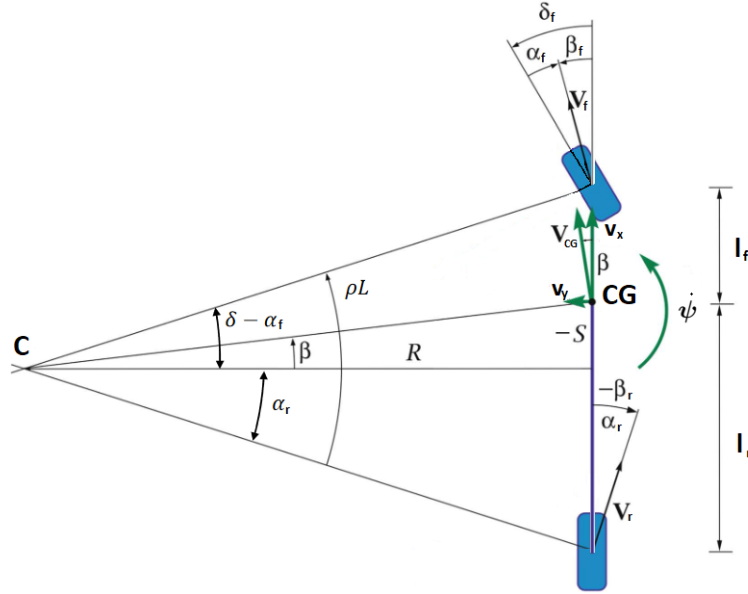


Figure 2.9: Single-Track Kinematic

Figure 2.9 shows a model of a single track 3 degrees of freedom vehicle. The versors indicate the principal directions. \vec{i} is the longitudinal versor, \vec{j} is the lateral versor, and \vec{k} is the versor which represents the rotation around the vertical axis.

The vehicle speed is indicated with \mathbf{v}_{CG} and has two components, the longitudinal one \mathbf{v}_x and the lateral one \mathbf{v}_y . The direction of the rotational velocity is defined by the versor \mathbf{k} and it is denoted by $\dot{\psi}$.

$$\begin{aligned}\vec{v}_{CG} &= v_x \vec{i} + v_y \vec{j} \\ \vec{\Psi} &= \Psi \vec{k} = r \vec{k}\end{aligned}$$

The angle between the longitudinal component of the velocity v_x and the vehicle velocity \mathbf{v}_{CG} is the **side slip angle** β .

$$\beta = -\arctan\left(\frac{v_y}{|v_x|}\right)$$

The side slip angle can be approximated as following:

$$\beta \simeq -\arctan(\beta)$$

$$\beta = -\left(\frac{v_y}{|v_x|}\right)$$

The perpendiculars to the wheels' velocity vectors define the center of instantaneous motion **ICM**, which in Figure 2.9 is indicated by C.

The distance between the instantaneous center of motion C and the center of gravity GC defines the **curvature radius** of the vehicle.

$$curvature\ radius = S\vec{i} + R\vec{j}$$

From point C, a line is drawn in a perpendicular direction up to the vehicle, and it is indicated by \mathbf{R} . The angle between this line and the radius of curvature is equal to the sideslip angle β . The velocity can be described as:

$$\vec{v}_{CG} = r\vec{k} \times (-curvature\ radius)$$

$$\vec{v}_{CG} = r\vec{k} \times (-R\vec{j} - S\vec{i}) = rR\vec{i} - rS\vec{j} = \vec{v}_x + \vec{v}_y$$

$$R = \frac{v_x}{r} = \frac{1}{\rho} \quad S = -\frac{v_y}{r}$$

The distance between the front axle and the Center of Gravity is defined as front wheelbase indicated with \mathbf{l}_f , while the distance between the Center of Gravity and the rear axle is defined rear wheelbase indicated with \mathbf{l}_r .

The sum of front wheelbase and rear wheelbase is called Wheelbase indicated with \mathbf{L} . Unlike the 3 DOF Dual Track vehicle model, in this model, the vehicle width is neglected.

$$L = l_f + l_r$$

The **Ackermann angle** δ_{Ack} is equal to:

$$\delta_{Ack} = \arctan\left(\frac{L}{R}\right) \approx \frac{L}{R} = L\rho = L\frac{r}{v_x}$$

During a rotation, the wheels have a different velocity than the vehicle velocity v_{CG} , both in intensity and in direction. Wheel velocities are indicated with \mathbf{v}_f for the front wheel and \mathbf{v}_r for the rear wheel.

For each wheel, a steering angle is defined, necessary to perform a rotation. They are indicated with δ_f for the front wheel and δ_r for the rear wheel. The **Steering Angle** δ for the vehicle is defined as the command input that must be provided to the vehicle in order to perform a rotation correctly. Defining τ as the **steer gear ratio**, the Steering Angle δ can be associated to the steering angle for each wheel with the following formula:

$$\delta_f = \tau_f \delta$$

$$\delta_r = \tau_r \delta$$

Assuming:

$$\tau = \tau_f$$

$$\chi \ll 1$$

$$\tau_r = \chi\tau$$

The steering angles associated to the wheel can be written as follows:

$$\delta_f = \tau \delta$$

$$\delta_r = \chi \tau \delta$$

From these formulas, it is possible to note how the steering angle on the rear wheel is much smaller than the front wheel's angle.

The angle between the velocity and the direction of the wheel is defined as the **tire sideslip angle**. Tire sideslip angles are indicated with α_f for the front wheel and α_r for the rear wheel.

$$\alpha_f = \tau \delta - \frac{v_y + r l_f}{v_x} = \delta_f - \frac{v_y + r l_f}{v_x}$$

$$\alpha_r = \chi \tau \delta - \frac{v_y - r l_r}{v_x} = \delta_r - \frac{v_y - r l_r}{v_x}$$

From the geometry is possible to derive the relation between the **Ackermann Angle** and the **Steering Angle**, using the tire slip angles:

$$\delta - \alpha_f + \alpha_r = \frac{L}{R}$$

or

$$\delta - \alpha_f + \alpha_r = \rho L$$

Recall that:

$$\frac{d\vec{i}}{dt} = r \vec{j} \quad \frac{d\vec{j}}{dt} = -r \vec{i}$$

The acceleration of the vehicle is equal to:

$$\vec{a}_{CG} = \frac{d\vec{v}_{CG}}{dt} = \dot{v}_x \vec{i} + v_x r \vec{j} + \dot{v}_y \vec{j} - v_y r \vec{i}$$

$$\vec{a}_{CG} = (\dot{v}_x - v_y r) \vec{i} + (\dot{v}_y + v_x r) \vec{j} = a_x \vec{i} + a_y \vec{j}$$

The longitudinal component of the vehicle acceleration is equal to:

$$a_x = \dot{v}_x - v_y r = \dot{v}_x - v_x^2 \rho \beta$$

The lateral component of the vehicle acceleration is equal to:

$$a_y = \dot{v}_y + v_x r = v_x \dot{\beta} + \dot{v}_x \beta + v_x^2 \rho$$

The steady-state lateral acceleration is equal to:

$$\tilde{a}_y = v_x r = v_x^2 \rho = \frac{v_x^2}{R}$$

Dynamic Model

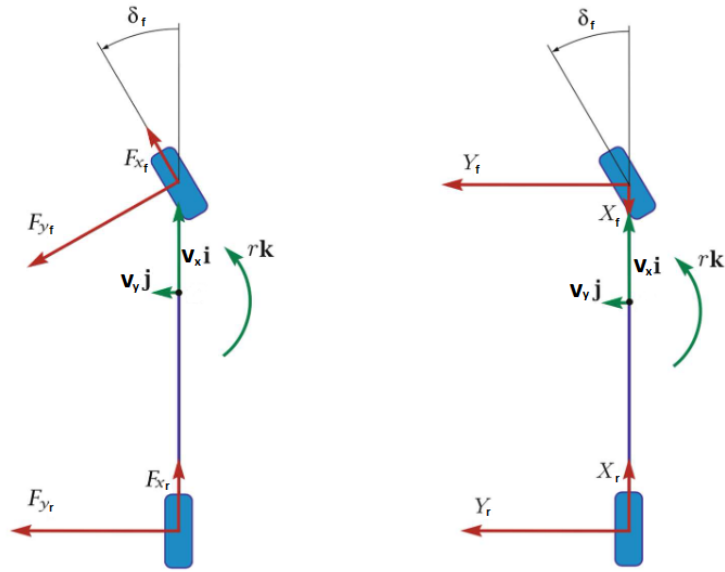


Figure 2.10: Single-Track Dynamic

The kinematic model is valid only in the case of low velocities. A dynamic model is considered to have more accurate results. The motion can propagate in three directions, longitudinal, lateral, and rotational.

The front and rear wheels of the model are considered a single-center. The forces acting on the vehicle are described in Figure 2.10.

The directions of the forces are the same as the main directions of the wheels. The longitudinal force is indicated with \mathbf{F}_x , the lateral force is indicated with \mathbf{F}_y , while the normal force acting on the wheel center is indicated with \mathbf{F}_z . A subscript indicates which axle the force refers to.

- \mathbf{F}_{xf} longitudinal force acting on the front axle
- \mathbf{F}_{xr} longitudinal force acting on the rear axle
- \mathbf{F}_{yf} lateral force acting on the front axle
- \mathbf{F}_{yr} lateral force acting on the rear axle
- \mathbf{F}_{zf} normal force acting on the front axle
- \mathbf{F}_{zr} normal force acting on the rear axle

Forces can be translated along the local vehicle axes. These forces are indicated with \mathbf{X} and \mathbf{Y} with a subscript to indicate the reference axes.

- \mathbf{X}_f longitudinal force on the front axle along x local axis
- \mathbf{X}_r longitudinal force on the rear axle along x local axis

- Y_f lateral force on the front axle along y local axis
- Y_r lateral force on the rear axle along y local axis

The following formulas describe the forces equilibrium equations along with longitudinal, lateral e vertical directions. The first two represent an equilibrium of forces, while the third represents an equilibrium of moments.

$$m a_x = m v_y r + F_{xf} + F_{xr} - F_{aero}$$

$$m a_y = -m v_x r + F_{yf} + F_{yr}$$

The equilibrium of moments is done around the center of gravity CG. I_{zz} indicates the moment of inertia referred to the local vertical axis z. This value measures the inertia of the body as its angular velocity varies.

$$I_{zz} \dot{r} = l_f F_{yf} \cos \delta_f - l_r F_{yr}$$

These formulas can be described using the translate forces in the local vehicle axes.

$$m a_x = -X_f + X_r$$

$$m a_y = Y_f + Y_r$$

$$I_{zz} \dot{r} = l_f Y_f - l_r Y_r$$

For assumptions, small longitudinal forces and a rear-wheel-drive single track model are considered.

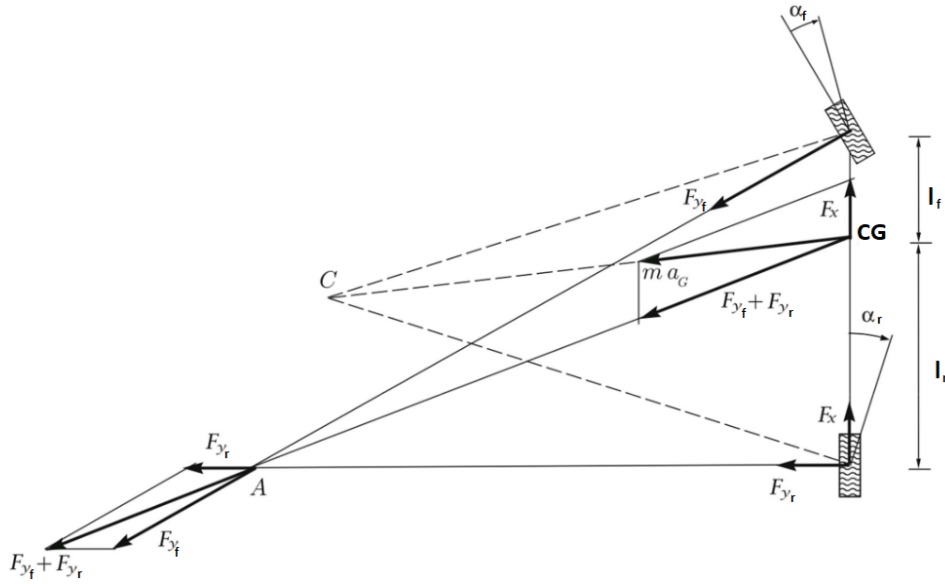


Figure 2.11: Equilibrium of Vehicle Forces

The aerodynamic drag force and drag due to tire slip are not shown in Figure 2.11, and they must be taken into account for the equilibrium of the forces. In the longitudinal direction, the equilibrium of forces is equal to:

$$(F_x - F_{yf} \delta_f) v_x + F_{yf} (v_y + r l_f) + F_{yr} (v_y - r l_r) - \left(\frac{1}{2} \rho S C_x v_x^2\right) v_x = 0$$

From this equation is possible to obtain the **driving force**:

$$F_x = F_{yf} \left(\delta_f - \frac{v_y + r l_f}{v_x}\right) + F_{yr} \left(-\frac{v_y - r l_r}{v_x}\right) + \left(\frac{1}{2} \rho S C_x v_x^2\right)$$

$$F_x = F_{yf} \alpha_f + F_{yr} \alpha_r + \left(\frac{1}{2} \rho S C_x v_x^2\right)$$

In the linear field (small tire slip angle α), the axle characteristic may be approximated as a linear function of α . The coefficient of the linear equation is the **Cornering Stiffness C**.

$$Y_i = C_i \alpha_i$$

The linearized axle equations are:

$$Y_f = C_f \alpha_f = C_f \left(\tau \delta - \frac{v_y + r l_f}{v_x}\right)$$

$$Y_r = C_r \alpha_r = C_r \left(-\frac{v_y - r l_r}{v_x}\right)$$

The forces along the local vehicle axes depend on the tire slip angle.

$$Y_f = Y_f(\alpha_f)$$

$$Y_r = Y_r(\alpha_r)$$

Considering the steady-state lateral acceleration, the equilibrium of forces and the rotation equilibrium about the center of gravity are equal to:

$$m \tilde{a}_y = Y_f(\alpha_f) + Y_r(\alpha_r)$$

$$0 = Y_f(\alpha_f) l_f - Y_r(\alpha_r) l_r$$

From these equations, it is possible to derive the following formulas:

$$Y_f(\alpha_f) = \frac{m l_r}{L} \tilde{a}_y$$

$$Y_r(\alpha_r) = \frac{m l_f}{L} \tilde{a}_y$$

By dividing these two formulas by the acceleration of gravity, it is possible to identify the relationship between lateral acceleration and vertical loads for each axle.

$$\frac{Y_f(\alpha_f) L}{m g l_r} = \frac{Y_f(\alpha_f)}{F_{zf}^0} = \frac{\tilde{a}_y}{g}$$

$$\frac{Y_r(\alpha_r) L}{m g l_f} = \frac{Y_r(\alpha_r)}{F_{zr}^0} = \frac{\tilde{a}_y}{g}$$

The tire slip angles can be described as:

$$\alpha_f = \tau \delta - \frac{v_y + r l_f}{v_x} = \frac{m l_r}{C_f L} \tilde{a}_y$$

$$\alpha_r = -\frac{v_y - r l_r}{v_x} = \frac{m l_f}{C_r L} \tilde{a}_y$$

If the longitudinal velocity v_x grows, the lateral acceleration a_y , the tire slip angles α_f and α_r increase.

Moreover, $\delta - \alpha_f + \alpha_r = L/R$ can be rewritten as:

$$\delta - \frac{L}{R} = \alpha_f - \alpha_r = \left(\frac{l_r}{C_f} - \frac{l_f}{C_r} \right) \frac{m}{L} \tilde{a}_y$$

2.2.3 Aerodynamic Drag Force

An Aerodynamic Drag Force is a force exerted on a body by the air in which the body is immersed and is due to relative motion between body and gas. This force interferes with the longitudinal movement of the vehicle.

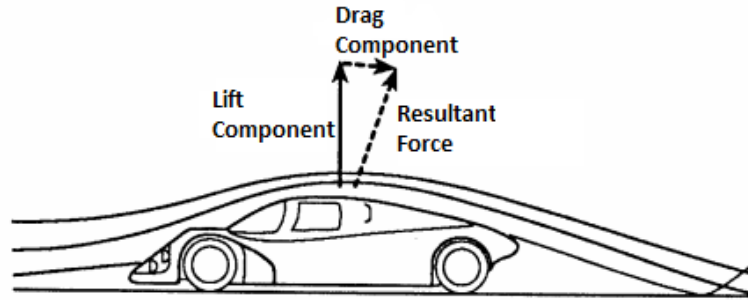


Figure 2.12: Aerodynamic Drag Force

The following formula describes this force:

$$F_{aero} = \frac{1}{2} \rho_{air} S c_x v_x^2$$

where:

- ρ_{air} is the air density equal to 1.225 kg/m^3
- S is the cross-sectional area of the vehicle. This value is the total area of the orthographic projection of the frontal area of the vehicle.
- v_x is the longitudinal velocity of the vehicle
- c_x is the drag coefficient, a dimensionless factor that depends on the shape of the vehicle and on the Reynolds number

In Figure 2.12, there is a lift force which in the vehicle model 3 DOF Single Track is neglected.

2.2.4 Static Load Distribution

The Static Load Distribution is the equilibrium of the vertical forces when the velocity is equal to 0.

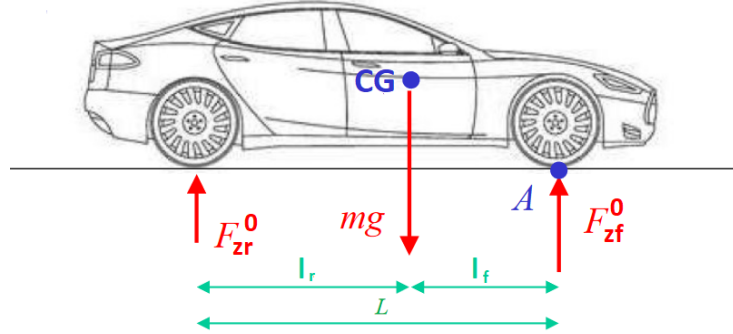


Figure 2.13: Static Load Distribution

The following equations describe the vertical balance of forces and the rotation around point A.

$$\begin{aligned} F_{zf}^0 + F_{zr}^0 - mg &= 0 \\ F_{zr}^0 L - mg l_f &= 0 \end{aligned}$$

Through these equations, it is possible to derive the static vertical loads on each axle.

$$\begin{aligned} F_{zf}^0 &= mg \frac{l_r}{L} \\ F_{zr}^0 &= mg \frac{l_f}{L} \end{aligned}$$

2.2.5 Understeering / Oversteering

As shown previously, $\delta - \alpha_f + \alpha_r = L/R$ can be rewritten as:

$$\delta - \frac{L}{R} = \alpha_f - \alpha_r = \left(\frac{l_r}{C_f} - \frac{l_f}{C_r} \right) \frac{m}{L} \tilde{a}_y$$

According to SAE J266 Standard, Steady-State Directional Control Test Procedures For Passenger Cars and Light Trucks, "understeer/oversteer gradient K is defined as the difference between steer angle gradient and Ackermann steer angle gradient."

$$\begin{aligned} K &= \frac{d}{d\tilde{a}_y} \left(\delta - \frac{L}{R} \right) \\ K &= \frac{m}{L} \frac{C_r l_r - C_f l_f}{C_f C_r} = \left(\frac{l_r}{C_f} - \frac{l_f}{C_r} \right) \frac{m}{L} \end{aligned}$$

- if $C_f l_f - C_r l_r > 0$, K assumes negative values and there is an oversteering vehicle
- if $C_f l_f - C_r l_r = 0$, K assumes null values and there is a neutral vehicle

- if $C_f l_f - C_r l_r < 0$, K assumes positive values and there is an understeering vehicle

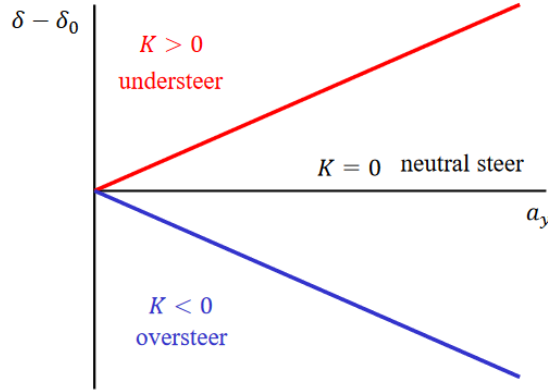


Figure 2.14: Understeering / Oversteering

In this case the system is stable, it is possible to define a critical velocity, that is the velocity at which the vehicle becomes unstable. It is equal to:

$$v_{cr} = \sqrt{\frac{C_f C_r L^2}{m (C_f l_f - C_r l_r)}}$$

The vehicle is unstable if the longitudinal velocity v_x is greater than the critical velocity v_{cr} . The critical velocity exists only if $(C_f l_f - C_r l_r) > 0$, so in the case of oversteering vehicle.

2.3 Parameterized Vehicle Model for Adaptive MPC

The dynamic equations of the longitudinal, lateral and yaw dynamics are expressed as:

$$\begin{aligned} a_x &= \dot{v}_x \\ a_y = \dot{v}_y &= -\frac{C_f + C_r}{m v_x} v_y + \frac{C_r l_r - C_f l_f - m v_x^2}{m v_x} r + \frac{C_f}{m} \delta \\ \dot{r} &= \frac{C_r l_r - C_f l_r}{I_{zz} v_x} v_y - \frac{C_r l_r^2 + C_f l_f^2}{I_{zz} v_x} r + \frac{C_f l_f}{I_{zz}} \delta \end{aligned}$$

In the equations above, the steering angle δ is the manipulable input.

A 2 degree of freedom vehicle model defines the vehicle's lateral dynamics for the controller internal plant model. To design an MPC control for automated lane-keeping is useful to describe the lateral dynamics in terms of:

- **lateral deviation \mathbf{e}_1** , the distance of the center of gravity of the vehicle from the centerline of the road
- **relative yaw angle \mathbf{e}_2** , the orientation error of the vehicle with respect to the road.

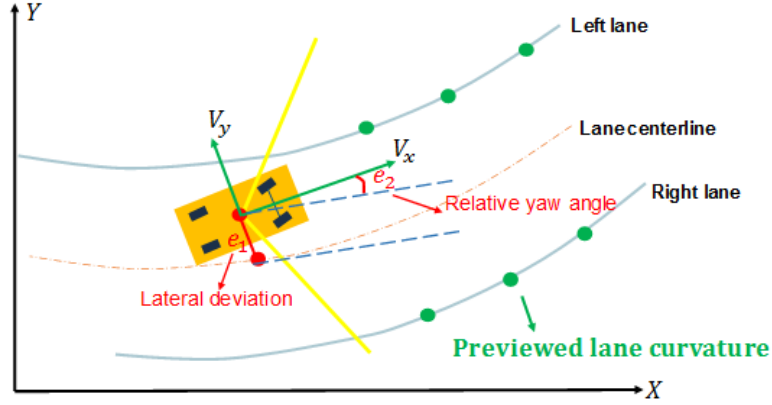


Figure 2.15: Lateral Deviation and Relative Yaw Angle[32]

The equation of lateral deviation, relative yaw angle and their derivatives are shown below:

$$\begin{aligned} e_1 &= y - y_{cl} \\ e_2 &= \psi - \psi_{des} \\ \dot{e}_1 &= v_y + v_x e_2 \\ \dot{e}_2 &= \dot{\psi} - \dot{\psi}_{des} \end{aligned}$$

where:

- y_{cl} is the position of the center line of the lane in the global coordinate Y
- ψ_{des} is the desired yaw angle, the angle of the curvature of the road
- $\dot{\psi}_{des}$ is the desired yaw rate

The desired yaw rate is equal to:

$$\dot{\psi}_{des} = \frac{v_x}{R} = v_x \kappa$$

R is the road curvature radius, while $\kappa = 1/R$ is the road curvature.

As mentioned above, in this thesis, two MPC models have been designed. One controller considers the lateral and longitudinal dynamics separately, while the other considers the dynamics together.

2.3.1 Adaptive MPC Model - Separated Dynamics

The equations for the longitudinal dynamics can be described in matrix form as follows:

$$\begin{bmatrix} \ddot{v}_x \\ \dot{v}_x \end{bmatrix} = \begin{bmatrix} -\frac{1}{\tau} & 0 \\ 1 & 0 \end{bmatrix} \begin{bmatrix} \dot{v}_x \\ v_x \end{bmatrix} + \begin{bmatrix} \frac{1}{\tau} \\ 0 \end{bmatrix} v_x$$

$$y = \begin{bmatrix} 0 & 1 \end{bmatrix} \begin{bmatrix} \dot{v}_x \\ v_x \end{bmatrix}$$

\ddot{v}_x is the longitudinal jerk, τ is the time constant. The **state vector** is composed of the longitudinal acceleration and the longitudinal velocity:

$$\begin{bmatrix} \dot{v}_x & v_x \end{bmatrix}$$

The equations for the lateral dynamics can be described in matrix form as follows:

$$\begin{bmatrix} \dot{v}_y \\ \dot{\psi} \end{bmatrix} = \begin{bmatrix} -\frac{(2C_f + 2C_r)}{m v_x} & -v_x - \frac{(2C_f l_f - 2C_r l_r)}{m v_x} \\ -\frac{(2C_f l_f - 2C_r l_r)}{I_{zz} v_x} & -\frac{(2C_f l_f^2 + 2C_r l_r^2)}{I_{zz} v_x} \end{bmatrix} \begin{bmatrix} v_y \\ \psi \end{bmatrix} + \begin{bmatrix} 2\frac{C_f}{m} \\ 2\frac{C_f l_f}{I_{zz}} \end{bmatrix} \delta$$

The equations on the lateral deviation and relative yaw angles are described in matrix form:

$$\begin{bmatrix} \dot{e}_1 \\ \dot{e}_2 \end{bmatrix} = \begin{bmatrix} 1 & 0 & 0 & v_x \\ 0 & 1 & 0 & 0 \end{bmatrix} \begin{bmatrix} v_y \\ \psi \\ e_1 \\ e_2 \end{bmatrix} + \begin{bmatrix} 0 \\ -\kappa \end{bmatrix} v_x$$

Combining the part relating to the longitudinal dynamics to the part relating to the lateral deviation and relative yaw angle, the parameterized model for the lateral control of the MPC in matrix form is equal to:

$$\begin{bmatrix} \dot{v}_y \\ \dot{\psi} \\ \dot{e}_1 \\ \dot{e}_2 \end{bmatrix} = \begin{bmatrix} -\frac{(2C_f + 2C_r)}{m v_x} & -v_x - \frac{(2C_f l_f - 2C_r l_r)}{m v_x} & 0 & 0 \\ -\frac{(2C_f l_f - 2C_r l_r)}{I_{zz} v_x} & -\frac{(2C_f l_f^2 + 2C_r l_r^2)}{I_{zz} v_x} & 0 & 0 \\ 1 & 0 & 0 & v_x \\ 0 & 1 & 0 & 0 \end{bmatrix} \begin{bmatrix} v_y \\ \psi \\ e_1 \\ e_2 \end{bmatrix} + \begin{bmatrix} 2\frac{C_f}{m} \\ 2\frac{C_f l_f}{I_{zz}} \\ 0 \\ 0 \end{bmatrix} \delta + \begin{bmatrix} 0 \\ 0 \\ 0 \\ -\kappa \end{bmatrix} v_x$$

$$y = \begin{bmatrix} 0 & 0 & 1 & 0 \\ 0 & 0 & 0 & 1 \end{bmatrix} \begin{bmatrix} v_y \\ \psi \\ e_1 \\ e_2 \end{bmatrix}$$

The **state vector** is composed of lateral velocity, angular velocity, lateral deviation and relative yaw angle:

$$\begin{bmatrix} \dot{v}_y & \dot{\psi} & e_1 & e_2 \end{bmatrix}$$

2.3.2 Adaptive MPC Model - Combined Dynamics

The other configuration of the controller involves the fusion of longitudinal and lateral dynamics. The equations used are the same as those used in the model with separate dynamics.

$$\begin{aligned}
 \begin{bmatrix} \ddot{v}_x \\ \dot{v}_x \\ \dot{v}_y \\ \dot{\psi} \\ \dot{e}_1 \\ \dot{e}_2 \end{bmatrix} &= \begin{bmatrix} -\frac{1}{\tau} & 0 & 0 & 0 & 0 & 0 & 0 \\ 1 & 0 & 0 & 0 & 0 & 0 & 0 \\ 0 & 0 & -\frac{(2C_f+2C_r)}{m v_x} & -v_x - \frac{(2C_f l_f - 2C_r l_r)}{m v_x} & 0 & 0 & 0 \\ 0 & 0 & -\frac{(2C_f l_f - 2C_r l_r)}{I_{zz} v_x} & -\frac{(2C_f l_f^2 + 2C_r l_r^2)}{I_{zz} v_x} & 0 & 0 & 0 \\ 0 & 0 & 1 & 0 & 0 & v_x & 0 \\ 0 & 0 & 0 & 1 & 0 & 0 & 0 \end{bmatrix} \begin{bmatrix} \dot{v}_x \\ v_x \\ v_y \\ \dot{\psi} \\ e_1 \\ e_2 \end{bmatrix} + \\
 &+ \begin{bmatrix} \frac{1}{\tau} & 0 \\ 0 & 0 \\ 0 & 2\frac{C_f}{m} \\ 0 & 2\frac{C_f l_f}{I_{zz}} \\ 0 & 0 \\ 0 & 0 \end{bmatrix} \begin{bmatrix} \dot{v}_x \\ \delta \end{bmatrix} + \begin{bmatrix} 0 \\ 0 \\ 0 \\ 0 \\ 0 \\ -\kappa \end{bmatrix} v_x \\
 \begin{bmatrix} v_x \\ e_1 \\ e_2 \end{bmatrix} &= \begin{bmatrix} 0 & 1 & 0 & 0 & 0 & 0 \\ 0 & 0 & 0 & 0 & 1 & 0 \\ 0 & 0 & 0 & 0 & 0 & 1 \end{bmatrix} \begin{bmatrix} \dot{v}_x \\ v_x \\ v_y \\ \dot{\psi} \\ e_1 \\ e_2 \end{bmatrix}
 \end{aligned}$$

The current **measured outputs** are compared to the outputs of the prediction model, and the error is added to the future predictions. The measured outputs are:

$$\begin{bmatrix} v_x & e_1 & e_2 \end{bmatrix}$$

The **state vector** is composed of longitudinal acceleration, longitudinal velocity, lateral velocity, angular velocity, lateral deviation and relative yaw angle:

$$\begin{bmatrix} \dot{v}_x & v_x & \dot{v}_y & \dot{\psi} & e_1 & e_2 \end{bmatrix}$$

Analyzing the matrix above, the **manipulated variables** are the **longitudinal acceleration** \dot{v}_x and the **steering angle** δ .

$$\begin{bmatrix} \dot{v}_x & \delta \end{bmatrix}$$

The product of the longitudinal velocity v_x and the road curvature κ is defined as **measured disturbance**.

$$\dot{\psi}_{des} = v_x \kappa = \frac{v_x}{R}$$

The plant model used as the basis for adaptive MPC is an LTI discrete-time, state-space model with a **sampling time** T_s equal to 100 ms. The combined state space model for lateral and longitudinal dynamics which is used as the internal plant model for MPC is represented below:

$$\begin{aligned} x(k+1) &= Ax(k) + B_u u(k) + B_d v(k) \\ y(k) &= Cx(k) \end{aligned}$$

where:

- \mathbf{k} is the time index (current control interval)
- \mathbf{x} is the state vector
- \mathbf{u} is the manipulated variables input vector
- \mathbf{v} is the measured disturbance input vector
- \mathbf{y} is the output vector
- \mathbf{A} is the state matrix
- \mathbf{B}_u is the input matrix
- \mathbf{B}_v is the disturbance input matrix
- \mathbf{C} is the output matrix

The vehicle model refers to a high-performance autonomous car characterized by the parameters listed below.

- $m = 193$ kg, mass of the vehicle
- $I_{zz} = 95.81$ kg m^2 , moment of inertia about vertical axis
- $l_f = 0.839$ m, front wheelbase
- $l_r = 0.686$ m, rear wheelbase
- $C_f = 44222$ N/rad, front cornering stiffness
- $C_r = 44222$ N/rad, rear cornering stiffness

- $\tau = 0.5$ s, time constant
- $v_0 = 0.001$ m/s, initial longitudinal velocity
- $f = 0.0182$, rolling resistance coefficient
- $\mu = 0.8$, friction coefficient
- $r_{\text{wheel}} = 0.33$ m, wheel radius

2.4 15 DOF Vehicle Model

After completing the controller validation with the single track 3 degrees of freedom vehicle model, another controller validation step is performed.

This step is done with a vehicle model with 15 degrees of freedom to obtain more accurate results and perform simulations in 3D. Even if the model can lead to very truthful results, the model's problem will be the high computational demand. The simulations performed with this model will be slower than the simulations performed previously.

The 15 DOF model is taken from the Simscape Vehicle Template tool and modified to make it compatible with the designed controller.

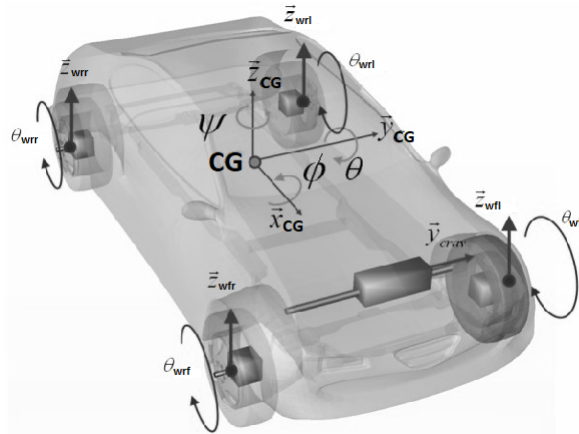


Figure 2.16: 15 DOF Vehicle Model

The model represents a four-wheel independent drive electric vehicle powered by two electric motors.

A double-wishbone suspension is used. It is an independent suspension that uses two wishbone-shaped arms to locate the wheel. Each wishbone has two mounting points to the chassis and one joint at the knuckle. The shock absorber and coil spring mount to the wishbones control vertical movement, and they are modeled linearly.

The steering system consists of a steering wheel rack system composed of a rack and pinion. The rack is a bar parallel to the front axle that moves left or right when the steering wheel is turned, aiming the front wheels in the correct direction. The pinion is a small gear at the end of the vehicle's steering column that engages the rack.

Anti-roll bar drop links are short connecting rods that link the vehicle's anti-roll bar to the suspension wishbones or shock absorbers. The torsional rigidity of the anti-roll bar limits body roll, which keeps the vehicle flat through corners.

There are 15 degrees of freedom in the vehicle:

- \mathbf{x}_{CG} , longitudinal movement along local vehicle axis
- \mathbf{y}_{CG} , lateral movement along local vehicle axis
- \mathbf{z}_{CG} , vertical movement along local vehicle axis
- **Roll** ϕ , rotation around longitudinal local vehicle axis \mathbf{x}_{CG}
- **Pitch** θ , rotation around lateral local vehicle axis \mathbf{y}_{CG}
- **Yaw** ψ , rotation around vertical local vehicle axis \mathbf{z}_{CG}
- \mathbf{z}_{wfl} , vertical movement of the front left wheel
- \mathbf{z}_{wfr} , vertical movement of the front right wheel
- \mathbf{z}_{wrl} , vertical movement of the rear left wheel
- \mathbf{z}_{wrr} , vertical movement of the rear right wheel
- θ_{wfl} , rotation of the front left wheel
- θ_{wfr} , rotation of the front right wheel
- θ_{wrl} , rotation of the rear left wheel
- θ_{wrr} , rotation of the rear right wheel
- \mathbf{y}_{craV} , movement of the front wheel angle

The equations describe the translational and rotational motion of the CG center of gravity.

Longitudinal Direction:

$$m(\dot{v}_x - v_y r + v_z \dot{\theta}) = F_{xfl} + F_{xfr} + F_{xrl} + F_{xrr}$$

Lateral Direction:

$$m(\dot{v}_y - v_z \dot{\phi} + v_x r) = F_{yfl} + F_{yfr} + F_{yrl} + F_{yrr}$$

Vertical Direction:

$$m(\dot{v}_z - v_x \dot{\theta} + v_y r) = F_{sfl} + F_{sfr} + F_{srl} + F_{srr} - m_s g$$

The vehicle's total mass is indicated with \mathbf{m} and is composed of two components. The sprung mass \mathbf{m}_s is the set of elements of the vehicle that undergo a variation in their distance from the ground. The elements that do not change their distance from the ground are part of the unsprung mass \mathbf{m}_{ui} , such as wheels. These elements are closely related to the sprung mass.

- \mathbf{m}_{ufl} , mass of front left wheel
- \mathbf{m}_{ufr} , mass of front right wheel
- \mathbf{m}_{url} , mass of rear left wheel
- \mathbf{m}_{urr} , mass of rear right wheel
- \mathbf{m}_u , total mass of the wheels

$$m_u = m_{ufl} + m_{ufr} + m_{url} + m_{urr}$$

$$m = m_s + m_{ufl} + m_{ufr} + m_{url} + m_{urr} = m_s + m_u$$

The velocities in the equations are:

- \mathbf{v}_x vehicle's longitudinal velocity
- \mathbf{v}_y vehicle's lateral velocity
- \mathbf{v}_z vehicle's vertical sprung mass velocity

The driving forces of the wheels \mathbf{F}_{xi} are the forces necessary to move the vehicle.

- \mathbf{F}_{xfl} , driving force of front left wheel
- \mathbf{F}_{xfr} , driving force of front right wheel
- \mathbf{F}_{xrl} , driving force of rear left wheel
- \mathbf{F}_{xrr} , driving force of rear right wheel

The yaw forces of the wheels \mathbf{F}_{yi} are the lateral forces necessary for the vehicle's lateral movement.

- \mathbf{F}_{yfl} , yaw force of front left wheel
- \mathbf{F}_{yfr} , yaw force of front right wheel
- \mathbf{F}_{yrl} , yaw force of rear left wheel
- \mathbf{F}_{yrr} , yaw force of rear right wheel

Suspension forces \mathbf{F}_{si} are the vertical forces experienced by suspension links. The resultant force acts to lift the sprung mass if the roll center is above ground or compress it if underground.

- \mathbf{F}_{sfl} , suspension force of front left wheel
- \mathbf{F}_{sfr} , suspension force of front right wheel
- \mathbf{F}_{srl} , suspension force of rear left wheel
- \mathbf{F}_{srr} , suspension force of rear right wheel

Rotational movement around the vertical z-axis:

$$I_{zz} \dot{r} = \frac{L}{2} (F_{xfr} + F_{xrr} - F_{xfl} + F_{xrl}) + l_f (F_{yfl} + F_{yfr}) - l_r (F_{yrl} + F_{yrr})$$

Rotational movement around the longitudinal x-axis:

$$I_{xx} \ddot{\phi} = \frac{L}{2} (F_{sfl} + F_{srl} - F_{sfr} + F_{srr}) + h_r (F_{yfl} + F_{yfr} - F_{yrl} + F_{yrr})$$

Rotational movement around the lateral y-axis:

$$I_{yy} \ddot{\theta} = l_r (F_{srl} + F_{srr}) - l_f (F_{sfl} + F_{sfr}) + h_p (F_{xfl} + F_{xfr} + F_{xrl} + F_{xrr})$$

The moment of inertia around the vehicle axes are:

- \mathbf{I}_{xx} , moment of inertia around longitudinal local axis x_{CG}
- \mathbf{I}_{yy} , moment of inertia around lateral local axis y_{CG}
- \mathbf{I}_{zz} , moment of inertia around vertical local axis z_{CG}

The distance from the center of mass of the vehicle to roll axle is indicated as \mathbf{h}_r while the distance from the center of mass of the vehicle to pitch axle is indicated as \mathbf{h}_p .

The equations of vertical dynamics between independent suspensions and unsprung masses for each wheel are equal to:

Vertical movement of front left wheel:

$$m_{ufl} \ddot{z}_{ufl} = k_{ufl} (z_{fl} - z_{ufl}) - F_{sfl}$$

Vertical movement of front right wheel:

$$m_{ufr} \ddot{z}_{ufr} = k_{ufr} (z_{fr} - z_{ufr}) - F_{sfr}$$

Vertical movement of rear left wheel:

$$m_{url} \ddot{z}_{url} = k_{url} (z_{rl} - z_{url}) - F_{srl}$$

Vertical movement of rear right wheel:

$$m_{urr} \ddot{z}_{urr} = k_{urr} (z_{rr} - z_{urr}) - F_{srr}$$

The suspension and sprung mass connection points absolute position are equal to:

- Front left suspension and sprung mass connection point \mathbf{z}_{fl} :

$$z_{fl} = \frac{L}{2} \phi - l_f \theta + z_{CG}$$

- Front right suspension and sprung mass connection point \mathbf{z}_{fr} :

$$z_{fr} = -\frac{L}{2} \phi - l_f \theta + z_{CG}$$

- Rear left suspension and sprung mass connection point \mathbf{z}_{rl} :

$$z_{rl} = \frac{L}{2} \phi + l_r \theta + z_{CG}$$

- Rear right suspension and sprung mass connection point \mathbf{z}_{rr} :

$$z_{rr} = -\frac{L}{2} \phi + l_r \theta + z_{CG}$$

where z_{CG} is the vertical position of the center of gravity.

The vertical position of the unsprung mass for each wheel is indicated with \mathbf{z}_{ui} .

- Vertical position of the front left unsprung mass \mathbf{z}_{ufl}
- Vertical position of the front right unsprung mass \mathbf{z}_{ufr}
- Vertical position of the rear left unsprung mass \mathbf{z}_{url}
- Vertical position of the rear right unsprung mass \mathbf{z}_{urr}

The vertical stiffness for each wheel is indicated with \mathbf{k}_{ui} .

- Vertical stiffness of the front left wheel \mathbf{k}_{ufl}
- Vertical stiffness of the front right wheel \mathbf{k}_{ufr}
- Vertical stiffness of the rear left wheel \mathbf{k}_{url}
- Vertical stiffness of the rear right wheel \mathbf{k}_{urr}

The rotation equilibrium equations of the wheels movements are equal to:

Rotation equilibrium of front left wheel:

$$T_{xfl} - F_{xfl} r_{wheel} - T_{bfl} - M_f = I_{wfl} \dot{\omega}_{wfl}$$

Rotation equilibrium of front right wheel:

$$T_{xfr} - F_{xfr} r_{wheel} - T_{bfr} - M_f = I_{wfr} \dot{\omega}_{wfr}$$

Rotation equilibrium of rear left wheel:

$$T_{xrl} - F_{xrl} r_{wheel} - T_{brl} - M_f = I_{wrl} \dot{\omega}_{wrl}$$

Rotation equilibrium of rear right wheel:

$$T_{xrr} - F_{xrr} r_{wheel} - T_{brr} - M_f = I_{wrr} \dot{\omega}_{wrr}$$

The driving torque of the wheel is indicated with \mathbf{T}_{xi} , while the braking torque is indicated with \mathbf{T}_{bi} . These are the torques that allow the wheels to accelerate or brake respectively. Another torque that opposes the rotation of the wheel is the rolling resistance torque, indicated with \mathbf{M}_f .

- Driving torque of the front left wheel \mathbf{T}_{xfl}
- Driving torque of the front right wheel \mathbf{T}_{xfr}
- Driving torque of the rear left wheel \mathbf{T}_{xrl}
- Driving torque of the rear right wheel \mathbf{T}_{xrr}
- Braking torque of the front left wheel \mathbf{T}_{bfl}
- Braking torque of the front right wheel \mathbf{T}_{bfr}
- Braking torque of the rear left wheel \mathbf{T}_{brl}
- Braking torque of the rear right wheel \mathbf{T}_{brr}
- Rolling resistance torque of the wheels \mathbf{M}_f

The moment of inertia around the wheels axes are:

- \mathbf{I}_{wfl} , moment of inertia of the front left wheel
- \mathbf{I}_{wfr} , moment of inertia of the front right wheel
- \mathbf{I}_{wrl} , moment of inertia of the rear left wheel
- \mathbf{I}_{wrr} , moment of inertia of the rear right wheel

The angular accelerations of each wheel are indicated with $\dot{\omega}_{wi}$.

- $\dot{\omega}_{wfl}$, angular acceleration of the front left wheel
- $\dot{\omega}_{wfr}$, angular acceleration of the front right wheel
- $\dot{\omega}_{wrl}$, angular acceleration of the rear left wheel
- $\dot{\omega}_{wrr}$, angular acceleration of the rear right wheel

Suspension forces \mathbf{F}_{si} are the vertical forces experienced by suspension links. Suspension forces of the sprung mass are equal to:

Suspension force of front left wheel:

$$F_{sfl} = k_{sfl} (z_{ufl} - z_{fl}) + b_{sfl} (\dot{z}_{ufl} - \dot{z}_{fl}) + f_{ifl}$$

Suspension force of front right wheel:

$$F_{sfr} = k_{sfr} (z_{ufr} - z_{fr}) + b_{sfr} (\dot{z}_{ufr} - \dot{z}_{fr}) + f_{ifr}$$

Suspension force of rear left wheel:

$$F_{srl} = k_{srl} (z_{url} - z_{rl}) + b_{srl} (\dot{z}_{url} - \dot{z}_{rl}) + f_{irl}$$

Suspension force of rear right wheel:

$$F_{srr} = k_{srr} (z_{urr} - z_{rr}) + b_{srr} (\dot{z}_{urr} - \dot{z}_{rr}) + f_{irr}$$

The suspension stiffness for each wheel is indicated with \mathbf{k}_{si} .

- Suspension stiffness of the front left wheel \mathbf{k}_{sfl}
- Suspension stiffness of the front right wheel \mathbf{k}_{sfr}
- Suspension stiffness of the rear left wheel \mathbf{k}_{srl}
- Suspension stiffness of the rear right wheel \mathbf{k}_{srr}

The vertical velocity of the unsprung mass for each wheel is indicated with \dot{z}_{ui} .

- Vertical velocity of the front left unsprung mass \dot{z}_{ufl}
- Vertical velocity of the front right unsprung mass \dot{z}_{ufr}
- Vertical velocity of the rear left unsprung mass \dot{z}_{url}
- Vertical velocity of the rear right unsprung mass \dot{z}_{urr}

The variations of suspension and sprung mass connection points absolute position are equal to:

- Variation of front left suspension and sprung mass connection point position \dot{z}_{fl} .
- Variation of front right suspension and sprung mass connection point position \dot{z}_{fr} .
- Variation of rear left suspension and sprung mass connection point position \dot{z}_{rl} .
- Variation of rear right suspension and sprung mass connection point position \dot{z}_{rr} .

The suspension damping for each wheel is indicated with \mathbf{b}_{si} .

- Suspension damping of the front left wheel \mathbf{b}_{sfl}
- Suspension damping of the front right wheel \mathbf{b}_{sfr}
- Suspension damping of the rear left wheel \mathbf{b}_{srl}
- Suspension damping of the rear right wheel \mathbf{b}_{srr}

In the equation the suspension initial force is considered and it is indicated with \mathbf{f}_i .

- f_{fl} , initial suspension force of front left wheel
- f_{fr} , initial suspension force of front right wheel
- f_{rl} , initial suspension force of rear left wheel
- f_{rr} , initial suspension force of rear right wheel [33]

The vehicle refers to a high-performance autonomous car characterized by the parameters listed below.

- $m = 1500$ kg, mass of the vehicle
- $I_{xx} = 432$ kg m^2 , moment of inertia about longitudinal axis
- $I_{yy} = 1922.7$ kg m^2 , moment of inertia about lateral axis
- $I_{zz} = 2066$ kg m^2 , moment of inertia about vertical axis
- $l_f = 1.2$ m, front wheelbase
- $l_r = 1.624$ m, rear wheelbase
- $T = 1.869$ m, vehicle track
- $C_f = 132000$ N/rad, front cornering stiffness
- $C_r = 132000$ N/rad, rear cornering stiffness
- $\tau = 0.5$ s, time constant
- $v_0 = 0.001$ m/s, initial longitudinal velocity
- $f = 0.0182$, rolling resistance coefficient
- $\mu = 0.8$, friction coefficient
- $r_{\text{wheel}} = 0.35$ m, wheel radius
- $m_u = 7$ kg, mass of each wheel
- $k_u = 66000$ N/m, vertical stiffness of the wheel
- $k_s = 140000$ N/m, Suspension stiffness
- $b_s = 140000$ N·s/m, Suspension damping of the wheels
- $A_{\text{cross}} = 2.81$ m^2 , cross-sectional area of the vehicle

2.4.1 Double-Wishbone Suspension

A double-wishbone suspension is an independent suspension that uses two wishbone-shaped arms to locate the wheel. Each arm has two attachment points to the frame.

The shock absorber and coil spring mount on the wishbones to control vertical movement. It is possible to control the wheel's movement during suspension travel by controlling parameters such as camber angle, caster angle, toe pattern, roll center height, slip radius, wear, and even more.

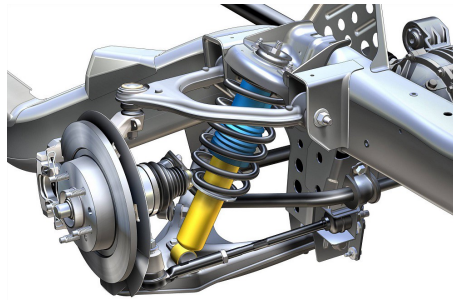


Figure 2.17: Double-Wishbone Suspension

The double-wishbone suspension provides more design choices than some other types of suspension do. It allows to work out merely the effect of moving each joint, so the suspension's kinematics can be tuned easily, and wheel motion can be optimized.

It is also easy to work out the loads that different parts will be subjected to, allowing more optimized lightweight parts to be designed.

Double wishbone suspensions may take up less space but are more complex and more expensive than other systems. Due to the increased number of components within the suspension setup, it takes much longer to service. It offers less design choice than the more expensive and complex multi-link suspension system.[34]

2.4.2 Steering System - Rack and Pinion Steering

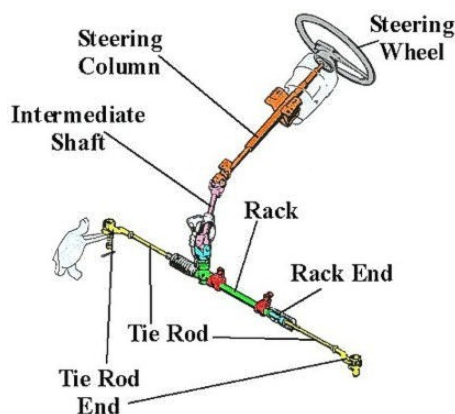


Figure 2.18: Rack and Pinion Steering System

The steering wheel connects to the steering column that runs through the vehicle's firewall into the engine bay. The steering rack can be mounted to the firewall inside the engine bay or to the engine bay's front end.

The steering column is connected to an intermediate shaft through the use of a universal joint. The intermediate shaft is connected to the steering rack's input shaft through the use of a universal joint or rubber coupling.

The ends of the steering rack protrude from both sides of the steering rack housing. The steering rack ends connect onto the steering rack. The steering rack end is a shaft with a ball and joint fitting at one end.

On the other end of the steering rack ends are screwed the tie rod end. The tie rod end is a balljoint that connects to the steering knuckle. The balljoint of the tie rod end allows the steering knuckle to move freely with the suspension.[35]

2.4.3 Anti Roll Drop Link

Anti-roll bar drop links are short connecting rods that link the vehicle's anti-roll bar to the suspension wishbones or shock absorbers.

The torsional rigidity of the anti-roll bar limits body roll, which keeps the vehicle flat through corners.

Over time the rubber mountings and anti-roll bar drop links can wear and cause play in the system. This harms the vehicles handling and road-holding and subsequently its safety.



Figure 2.19: Anti Roll Drop Link

CHAPTER 3

Model Predictive Control Strategy and Trajectory Planning

As previously mentioned, this thesis work aims to design a control strategy on lateral and longitudinal dynamics through an MPC approach. This chapter focuses on the problem of optimization and the formulation of the laws governing the controller. The developed controller must be connected to the path planner, and in this chapter, the problem of trajectory planning is also introduced.

An optimization problem is a problem of finding the best solution among all possible ones, considering a cost function to be minimized in order to find it. The MPC strategy tries to solve optimization problems for each discrete instant, considering the limits in the inputs and outputs.

To fully understand the MPC strategy, it is possible to make an analogy with chess. A chess player chooses to make a precise move based on the future game scenario and predict how the opponent will respond to such a move. If the opponent's move is unexpected, the player must predict the new future game scenario to counteract the opponent's moves. A good player can predict future game scenarios for a long time horizon.

As in chess, the MPC strategy is based on future predictions of the vehicle's behaviour in its surroundings, reacting instantly to unexpected movements.

The main advantage of MPC is that it allows the current timeslot to be optimized while keeping future timeslots into account. This optimization is achieved by optimizing a finite time-horizon, but only implementing the current timeslot and then optimizing again, repeatedly. MPC can anticipate future events and can take control actions accordingly.

Trajectory planning is a fundamental element for autonomous driving. This part is strictly connected to the control part, which needs elaborated information for the vehicle's correct behaviour.

The path planning problem is defined as follows: finding collision-free movement between an initial configuration and a final configuration within a specific environment. The initial configuration is indicated with Start, while the final configuration is indicated with Goal.

The method used in path planning consists of generating a feasible trajectory with the vision sensors' information based on the road situation. This information is constantly updated

with a period equal to the sample time.

The simulations carried out in this thesis work can be divided into two parts, those with the Scenario Driving Simulator and those through the acquisitions performed in real-time. The thesis's final goal is to merge the planning part and the control part to have a greater realism in the simulations.

After defining the controller strategy, the reference path generator's problem by acquiring information from sensors and other communication devices with the environment is introduced. The chapter introduces the reference velocity generator, which processes the information from the curves and calculates the correct velocity that the vehicle must maintain to perform the turn correctly.

The last part of the chapter focuses on converting acceleration to torque. The controller returns the desired acceleration as a signal, but this must be converted into torque supplied to the wheels.

3.1 Autonomous Driving Building Blocks

Autonomous driving can be schematized as shown in Figure 3.1.

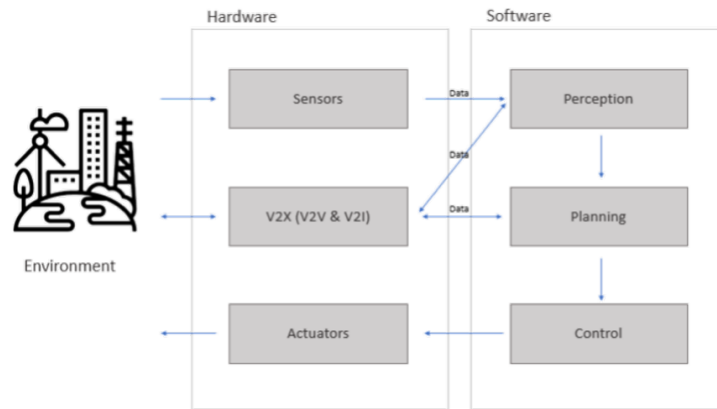


Figure 3.1: Autonomous Driving Building Blocks

There are three macro environments:

- **Environement**, everything is surrounding the vehicle, such as signs, lane lines, roads, other vehicles, etc. From the environment, it is possible to obtain all the useful information for autonomous driving
- **Hardware**, all the physical elements present in the vehicle with which it is possible to receive information from the outside or to operate the actuators necessary for movement.
- **Software**, the set of procedures and instructions in a data processing system. The software allows the processing of data from the outside and supplies the processed signals to the actuators.

Sensors:

They are part of the Hardware macro environment. Sensors are essential for taking information from the environment and supplying it to the data processor.

The sensors most used in autonomous driving are:

- **GPS** is a Global Positioning System whose essential function is to determine the position on the planet accurately.
- **Camera** is an electronic device for the acquisition of two-dimensional images in sequence at predetermined capture speeds.
- **Radar** is an electronic device that uses electromagnetic waves belonging to the spectrum of radio or microwave waves for the detection and determination of the position and speed of both fixed and mobile objects.
- **Lidar** is an electronic device that uses a remote sensing technique that allows determining the distance to an object or surface using a laser pulse. The main difference between lidar and radar is that lidar uses ultraviolet wavelengths in the visible or near-infrared.

V2X:

V2X, an abbreviation for Vehicle-to-everything, is an information communication system between the vehicle and any entity that can affect the vehicle and vice versa. In Figure 3.1, it is possible to observe how the flow of information is bilateral with the external environment and with the system software.

The different types of vehicle communication are:

- **V2I** is the communication between the vehicle and the external infrastructures.
- **V2V** is the communication between the vehicle and other vehicles in the environment.
- **V2N** is the communication between the vehicle and the network.

Actuators:

They are part of the Hardware macro environment. The actuators can be hydraulic, pneumatic, electromagnetic, or gear motors. They receive the signals coming from the control part and transform them into actions that enable movements.

The actuators most used in autonomous driving are:

- **Steering** is the device that allows controlling the steering wheels of a road vehicle to change the direction of travel.
- **Accelerator** is a device that acts on the engine regulation organs, increasing the vehicle's speed.
- **Brake** is the device capable of opposing, possibly up to stop it, the motion (rotary or translational) of one or more parts of a vehicle

Perception:

The perception system refers to the autonomous vehicle's ability to understand the information coming in through the sensors or V2X components. For example, the perception system tells the car where there is an obstacle or a moving vehicle from a given frame. This system also processes information to understand where the lane lines are located. The processed information is sent to the planning part or to the V2X components.

Planning:

The planning system refers to the autonomous vehicle's ability to make certain decisions to achieve some higher-order goals. The autonomous vehicle understands how it should act in certain situations through the planning system, organizing acceleration, braking or steering actions. The system receives information from the perception part and the external environment through the V2X devices. It then processes this information and sends it to the control part.

Control:

The control system converts intentions and derived goals from the planning system to actions. The objectives are transformed into inputs for the actuators that change the dynamics of the vehicle.

The MPC strategy used in this thesis work is designed in the following section.

3.2 Problem Formulation

Sometimes the control requirements need to be described in terms of optimization problems. The optimization problem is used when the requirements that must be met conflict with each other. To solve this problem, a cost function is considered and minimized to meet an optimal solution.

A classic optimization problem is the active control of the vehicle's suspension. The suspension system tries to isolate the vehicle from road irregularities solletications (comfort), ensuring permanent contact between wheel and road (handling). Comfort and Handling are in contrast to each other, so a possible solution would be to find a tradeoff between the two performances. To find the optimal solution, a cost function is defined, which minimizes the system's energy.

The MPC controller implemented in this thesis is based on solving a multistep optimization problem and feedback correction based on the **receding horizon principle**. Using a discrete MPC controller, for the time instant k , the RH principle is based on a recursive procedure:

- get the state $\mathbf{x}(k) = \mathbf{x}(k|k)$
where $\mathbf{x}(k|k)$ is the state vector based on the information at time instant k
- solve the optimization problem with respect to $\mathbf{u}(k|k)$
where $\mathbf{u}(k|k)$ is the input vector based on the information at time instant k
- compute the minimizer, the optimal input vector $\mathbf{u}^*(k|k)$ that minimizes the cost function along a finite **prediction horizon H_p**

$$\mathbf{u}^*(k|k) = [\mathbf{u}^*(k|k) \quad \mathbf{u}^*(k+1|k) \quad \dots \quad \mathbf{u}^*(k+H_p-1|k)]^T$$

- $\mathbf{u}(k|k) = \mathbf{u}^*(k|k)$ is applied as present control action
- the present time instant changes in $k+1$ and the procedure is repeated

The combined state space model for lateral and longitudinal dynamics which is used as the internal plant model for MPC is represented below:

$$\begin{aligned} \mathbf{x}(k+1) &= \mathbf{A}\mathbf{x}(k) + \mathbf{B}_u\mathbf{u}(k) + \mathbf{B}_d\mathbf{v}(k) \\ \mathbf{y}(k) &= \mathbf{C}\mathbf{x}(k) \end{aligned}$$

where:

- \mathbf{k} is the time index (current control interval)
- \mathbf{x} is the state vector
- \mathbf{u} is the manipulated variables input vector
- \mathbf{v} is the measured disturbance input vector

- \mathbf{y} is the output vector
- \mathbf{A} is the state matrix
- \mathbf{B}_u is the input matrix
- \mathbf{B}_v is the disturbance input matrix
- \mathbf{C} is the output matrix

To solve the optimization problem, the MPC controller minimizes the following cost function for each time instant:

$$\begin{aligned}
 \min_u J &= \sum_{j=1}^{H_p} \|y(k+j|k) - y_{ref}(k+j|k)\| Q_y + \sum_{j=0}^{H_c-1} \|u(k+j|k)\| R_u \\
 \text{s.t. } &u(k+j+1|k) = Ax(k+j|k) + B_u u(k+j|k) + B_d v(k+j|k) \\
 &x(k|k) = x(k) \\
 &y(k+j|k) = Cx(k+j|k) \\
 &|u(k+j|k)| \leq u_{limit}
 \end{aligned} \tag{3.1}$$

Q_y and R_u are the weights for the output and the manipulated variables, H_p is the prediction horizon and H_c is the control horizon. The optimization problem's goal is to minimize the cost function by respecting the conditions, including those relating to the manipulated variables' limits.

As previously mentioned, there are two controller versions developed in this thesis work, the one with separate dynamics and the one with combined dynamics. The cost function remains the same in both configurations, but the definitions of the output and reference vectors are different. Consequently, the definition of weighted norm also changes.

The main difference between the two configurations is in the resolution of two cost functions in the separate configuration and the resolution of a cost function in the combined one.

3.2.1 Combined Dynamics Configuration

The output vector is equal to:

$$[v_x \ e_1 \ e_2]^T$$

The reference output vector is equal to:

$$[v_{ref} \ 0 \ 0]^T$$

The longitudinal velocity v_x tries to follow the reference velocity v_{ref} based on the road curvature, while the lateral deviation and the relative yaw angle have a reference equal to 0.

The weighted norm of the output vector is defined as follows:

$$\|y(k+j|k)\| = [v_x \ e_1 \ e_2] \begin{bmatrix} Q_{11} & 0 & 0 \\ 0 & Q_{22} & 0 \\ 0 & 0 & Q_{33} \end{bmatrix} \begin{bmatrix} v_x \\ e_1 \\ e_2 \end{bmatrix}$$

Q_{11} , Q_{22} and Q_{33} are the weights for the outputs that must be tuned to control the dynamics of the vehicle properly.

The optimal input vector corresponds to the **manipulated variables** and it is equal to:

$$[\dot{v}_x \ \delta]^T$$

3.2.2 Separated Dynamics Configuration

The output vector for longitudinal controller and for the lateral one are respectively equal to:

$$\begin{bmatrix} v_x \\ e_1 \ e_2 \end{bmatrix}^T$$

The reference output vectors are equal to:

$$\begin{bmatrix} v_{ref} \\ 0 \ 0 \end{bmatrix}^T$$

As in the configuration with combined dynamics, the longitudinal velocity v_x tries to follow the reference velocity v_{ref} based on the road curvature.

The weighted norm of the output vector for the longitudinal controller is defined as follows:

$$\|y(k+j|k)\| = v_x Q_{11} v_x^T$$

The weighted norm of the output vector for the lateral controller is defined as follows:

$$\|y(k+j|k)\| = [e_1 \ e_2] \begin{bmatrix} Q_{22} & 0 \\ 0 & Q_{33} \end{bmatrix} \begin{bmatrix} e_1 \\ e_2 \end{bmatrix}$$

Q_{11} is the weight for the longitudinal velocity, while Q_{22} and Q_{33} are the weights for the lateral deviation and relative yaw angle.[36]

Each controller has an optimal input vector. For the longitudinal controller this is equal to the **longitudinal acceleration** \dot{v}_x while for the lateral controller it is equal to the **steering angle** δ .

3.3 Reference Path Generator

The path planning problem is defined as the generation of the geometric path that must be followed by the vehicle. This problem can be formulated for any robotic system. Before introducing it, some definitions must be introduced.

- **Configuration space C-space** is the space of all the possible robot configuration

- **Obstacles' representation in the configuration space C -obs** is the image of the obstacles in the C -space
- **Space of free configurations C -free** is the space of all the allowed configuration. It is equal to the difference between C -space and C -obs

The path planning method used in this thesis work is based on a modified RRT algorithm for a non-holonomic car-like mobile robot. The RRT algorithm looks for a series of obstacle-free segments in the configuration space. This algorithm must work rapidly and uniformly. The final result of this method is the creation of various series of segments, called tree.

After creating the tree, a search through the branches of the tree is done to find a path without collisions in the robot environment. Due to the differential constraints of a non-holonomic car-like mobile robot, the set of potential configurations that the robot can reach is reduced. For this reason, the basic form of the RRT algorithm must be modified.[37]

Dubins curves are selected for the path planning part of the vehicle. The difference between basic and modified RRT algorithm on Dubins curves is how branches are formed in the search tree.

In the basic RRT, the branches are made of straight lines, while the modified algorithm uses Dubins curves for satisfy differential constraints. If the velocity has only positive values, which means that the vehicle can move only forward, the model of Dubins car is obtained. The vehicle motion can be described as a set of equations in the following form:

$$\begin{aligned} v_x &= v_{CG} \cos \theta \\ v_y &= v_{CG} \sin \theta \\ \dot{\theta} = r &= \frac{v_{CG}}{L} \tan \delta \end{aligned}$$

The two variables to control are vehicle velocity v_{CG} and steering angle δ . They are indicated with the following vector:

$$u = [u_v \quad u_\delta]$$

The vehicle motion can be described as:

$$\begin{aligned} v_x &= u_v \cos \theta \\ v_y &= u_v \sin \theta \\ \dot{\theta} = r &= \frac{u_v}{L} \tan u_\delta \end{aligned}$$

For the vector, u is useful to define the allowed range for each variable. The maximum steering angle is indicated with δ_{MAX} .

$$|u_\delta| \leq \delta_{MAX}$$

As mentioned above, the vehicle can move only forward, so the velocity can assume only positive values. To simplify this case for the algorithm, velocity is considered constant and can assume two possible values:

$$u_v \in \{0, 1\}$$

If u_v is equal to zero, the vehicle is not moving, while if it is equal to 1, the vehicle moves with a constant velocity. The equations above describe the mathematical model of the Dubins car.

The basic form of the RRT algorithm for path planning is unusable because it is impossible to reach all configurations from a specific state with Dubins car. The algorithm is modified, and Dubins curves are used in the construction of the search tree. Every branch represents the Dubins curve instead of a straight line.

Considering the model of Dubins car, the vehicle moves with a constant velocity ($u_v = 1$) and has maximum steering angle δ_{MAX} , which results in a minimum turning radius ρ_{min} . The vehicle travels from an initial configuration to a final one and the main task is to minimize the length of the curve between these two configurations. The cost function that must be minimized is equal to:

$$L_{curve}(\tilde{q}, \tilde{u}) = \int_0^{t_F} \sqrt{v_x(t)^2 + v_y(t)^2} dt$$

where \tilde{q} represents a general configuration, and t_F is the time in which the final configuration is reached.

Since the velocity is constant the system can be simplified to:

$$v_x = \cos \theta$$

$$v_y = \sin \theta$$

$$\dot{\theta} = u$$

u is in the range $[-\tan \delta_{MAX}, \tan \delta_{MAX}]$. For simplicity, $\tan \delta = 1$.

The shortest path for the Dubins Car can be expressed as a combination of three primitives. The variable u can assume three values that are associated with the primitives.

$$u \in \{-1, 0, 1\}$$

The primitives associated to the values of u are described below:

- S, $u = 0$, straight line
- L, $u = 1$, left turn
- R, $u = -1$, right turn

As mentioned earlier, a path can be described by a series of three primitives. Two primitives of the same type can be merged into one, so the possible sequences of primitives are equal to:

$$\{LRL, RLR, LSL, LSR, RSL, RSR\}$$

The shortest path between two configurations can be characterized by one of these sequences, called words. These are called the **Dubins curves**.

The primitives are transformed in image points in \mathbb{R}^3 through:

$$L_v(x, y, \theta) = (x + \sin(\delta + v) - \sin \delta, y - \cos(\delta + v) + \cos \delta, \delta + v)$$

$$R_v(x, y, \theta) = (x - \sin(\delta - v) + \sin \delta, y + \cos(\delta - v) - \cos \delta, \delta - v)$$

$$S_v(x, y, \theta) = (x + v \cos \delta, y + v \sin \delta, \delta)$$

where the index v indicates the motion along the line(circular or straight) of length v . [38]

Path planning returns a curve every 0.1 seconds. This curve is decomposed into a series of points of which the first corresponds to the current curvature of the road while the others correspond to the previewed curvature. The prediction horizon is equal to the number of points describing the predicted curvature.

Considering a curve $\alpha(s)$, where s is the arc length and Φ is the tangential angle, the road curvature is defined as:

$$\kappa = \frac{d\Phi}{ds}$$

A small value of the road curvature corresponds to a small curve, while a big value of κ corresponds to a very tight curve.

It is possible to define also the radius of road curvature as the inverse of road curvature:

$$R = \frac{1}{\kappa}$$

The radius of road curvature is equal to the radius of the circle positioned at the centre of curvature. This circle is called osculating circle.

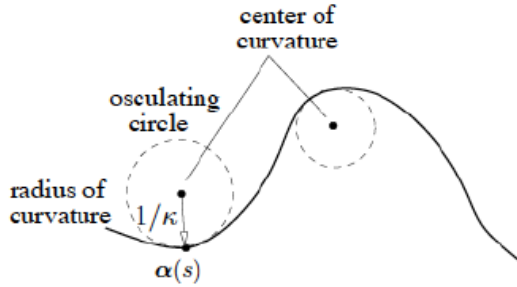


Figure 3.2: Curvature

3.4 Reference Velocity Generator

This section focuses on generating the longitudinal reference velocity based on information from the path planner. The reference velocity in the literature is calculated, considering the geometry of the road and lateral comfort. The developed controller is designed for an autonomous vehicle, so lateral comfort is not considered a parameter to decide the allowed speed.

The reference velocity must increase if the vehicle is travelling in a straight line, while it must decrease if the vehicle is about to approach a curve.

The maximum allowed velocity based on the curvature of the road is equal to:

$$v_{MAX} = \sqrt{\frac{g\mu}{\kappa}}$$

where g, μ and κ are respectively the acceleration of gravity, the friction coefficient and the road curvature.[39]

The road curvature value is chosen from the previewed curvature values. The highest value of the previewed curvatures is taken to give the vehicle time to brake when it is about to approach the curve. The described velocity is considered as the reference velocity of the vehicle.

The vehicle tries to match the reference velocity as it travels. It is necessary to apply a positive acceleration if the vehicle has a lower velocity than the reference velocity or a negative acceleration if the vehicle has a higher velocity than the reference one, therefore, when approaching a curve.

The acceleration the vehicle needs is equal to:

$$a_{MAX} = \sqrt{\frac{v_x^2 - v_{MAX}^2}{2(d - t_r v_x)}}$$

where v_x is the current longitudinal velocity of the vehicle, d is the distance from the curve and t_r is the time-delay.

The description of the reference velocity may, in some cases, be inappropriate or incomplete. For this reason, the National Highway Traffic Safety Administration(NHTSA) introduces a different calculation for the maximum allowed velocity in curves. The maximum allowed velocity is equal to:

$$v_{MAX} = \sqrt{\frac{g}{\kappa} \left(\frac{\Phi_r + \mu}{1 - \Phi_r \mu} \right)}$$

where Φ_r is the road camber angle.

3.5 Wheel Torque Calculation for Desired Acceleration

Considering the transmission in steady-state (not undergoing a gear shift) and the longitudinal tire slip negligible, the wheel rotational velocity ω_w is proportional to the engine velocity ω_e as follows:

$$\omega_w = R\omega_e$$

where R is the gear ratio.

The longitudinal velocity can be described by $v_x = r_{eff}\omega_w$ and consequently the longitudinal acceleration is equal to:

$$a_x = r_{eff}R\dot{\omega}_e$$

The longitudinal force equilibrium of the vehicle is equal to:

$$m a_x = F_x - R_x - F_{aero}$$

where F_x is the total longitudinal tire force, R_x is the rolling resistance force and F_{aero} is the aerodynamic drag force. Substituting the value of the longitudinal acceleration to the previous equation:

$$m r_{eff} R \dot{\omega}_e = F_x - R_x - F_{aero}$$

$$F_x = m r_{eff} R \dot{\omega}_e + R_x + F_{aero}$$

Considering the equation for the longitudinal force just obtained, the wheel rotational dynamics equilibrium is equal to:

$$I_w \dot{\omega}_w = T_w - r_{eff}(F_x) = T_w - m R r_{eff}^2 \dot{\omega}_e - r_{eff} R_x - r_{eff} F_{aero}$$

From the previous equation, it is possible to extrapolate the torque's value to the wheels necessary to obtain the desired acceleration T_w .

$$T_w = I_w R \dot{\omega}_e + m R r_{eff}^2 \dot{\omega}_e + r_{eff} R_x + r_{eff} F_{aero}$$

The engine acceleration $\dot{\omega}_e$ can be approximated as follows:

$$\dot{\omega}_e = \frac{a_{x des}}{R r_{eff}}$$

The torque to the wheels can be rewritten as:[40]

$$T_w = I_w R \frac{a_{x des}}{R r_{eff}} + m R r_{eff}^2 \frac{a_{x des}}{R r_{eff}} + r_{eff} R_x + r_{eff} F_{aero}$$

$$T_w = \frac{I_w}{r_{eff}} a_{x des} + m r_{eff} a_{x des} + r_{eff} R_x + r_{eff} F_{aero}$$

$$T_w = \left(\frac{I_w}{r_{eff}} + m r_{eff} \right) a_{x des} + (R_x + F_{aero}) r_{eff}$$

Rolling Resistance:

The tire and the road are subject to deformation in the contact area. The deformation of the road can be neglected, but the tire is made of an elastic material, so its deformation must be considered. Each area of the tire is subject to deformation due to the rotation of the wheel.

Normal load deflects the tire material vertically into the contact zone, and subsequently, the material returns to its original shape when it leaves the zone. Due to the tire material's internal damping, the energy expended deforming the tire material is not fully recovered when the material returns to its original form.

This energy loss can be represented by force on the tires called **rolling resistance**. This force opposes the motion of the vehicle.

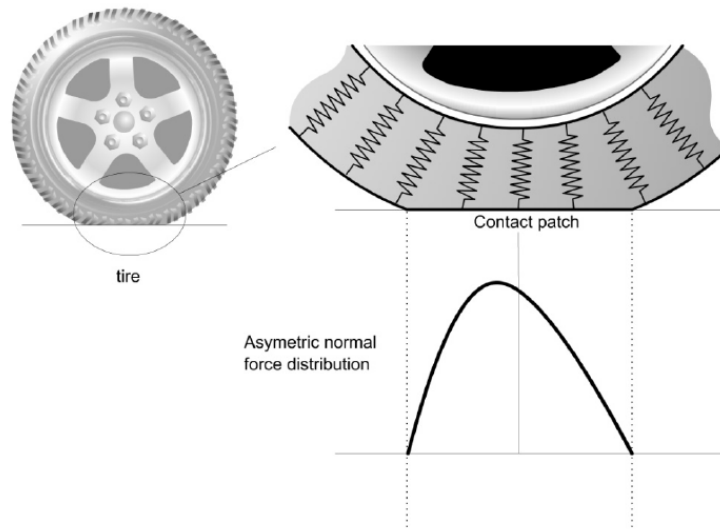


Figure 3.3: Rolling Resistance

The rolling resistance can be divided into the front axle component and the rear axle component. This force is proportionally dependent on normal loads through a rolling resistance coefficient. The equation is described below:

$$R_x = R_{xf} + R_{xr} = f(F_{zf} + F_{zr})$$

CHAPTER 4

Validation and Results

This chapter is related to the final results of this master thesis work. Every subsection presents the results obtained from the 3 DOF vehicle model and the model presented in the Simscape Vehicle Template.

It is divided into three subsections:

- The first subsection is related to the results obtained into Driving Scenario Simulator.
- The second subsection is related to the results obtained merging the path planning and lane following parts.
- The last subsection is related to the results of the Hardware implementation.

Two types of simulation are performed in the Driving Scenario Simulator: an acceleration test and a complete track test.

The first test is performed to test the MPC controller in the longitudinal behaviour fully. The vehicle increases its velocity until it reaches the maximum velocity, and there are no signals for steering. After maintaining the velocity equal to the maximum velocity for a certain period, the vehicle brakes until it reaches a velocity equal to zero.

The complete track test is used to analyze the vehicle's longitudinal and lateral behaviour if it has face curves. This test allows analyzing how the acceleration, brake and steering signals change according to the part of the track where the vehicle is located.

When the path planning part and the lane following part are merged, an acceleration test is performed using real-time data. To merge both parts, the path planner outputs are modified to obtain useful signals for the controller.

The results obtained are presented with the controller in separate form. The results obtained with the controller with combined dynamics lead to the same results, with the only difference that the controller's parameters with separate dynamics are easier to modify.

4.1 Driving Scenario Simulator

The Driving Scenario Simulator on MATLAB defines roads, vehicle, pedestrian and other aspects of the scenario. In this thesis work, it is used to define the road where the vehicle travels.

The road is defined in the Scenario Reader block, and the lane boundaries are defined in the Vision Detection Generator block. The Scenario Reader block is connected to the vehicle model to place the vehicle on the road.

The two scenarios defined are a straight road and a complete circuit. The straight road is used for the acceleration test and is 2km long. The road width of both scenarios is 8 m.

Below are the results obtained with the simulations with Driving Scenario Simulator. The parameters with which the MPC controller is described are indicated in each sub-chapter.

4.1.1 3 Degrees of Freedom validation and results

Straight Road:

- Initial global position: $x=0$ m, $y=0$ m, $z=0$ m
- Initial yaw angle : $\psi=0$ rad
- Output weights : $Q_{11}=10$, $Q_{22}=1$, $Q_{33}=0$
- Maximum and minimum acceleration command: $a_{MAX}=12$ m/s², $a_{min}=-12$ m/s²
- Maximum and minimum steer command: $\delta_{MAX}=\pi/12$ rad, $\delta_{min}=-\pi/12$ rad
- Maximum velocity: $v_{MAX}=40$ m/s
- Simulation time: 40 s

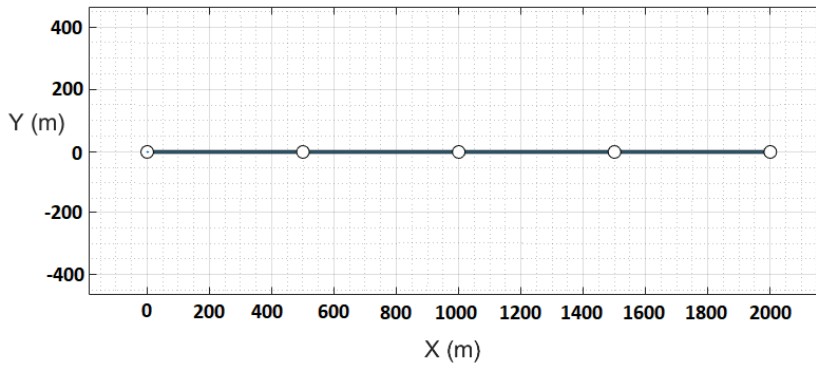


Figure 4.1: Straight Road Scenario

The acceleration test consists of three parts. In the first part, the reference velocity increases until it reaches the maximum allowed velocity. In the second part, the vehicle travels at a constant velocity over a period of time. The last part consists of braking the vehicle up to zero velocity.

The results show the comparison between the reference velocity and the longitudinal velocity, the acceleration and deceleration commands, the steering command and the behaviour of the lateral deviation and the relative yaw angle.

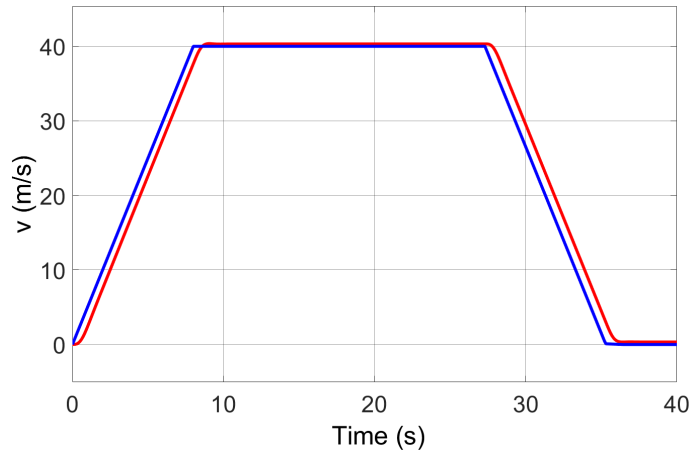


Figure 4.2: Reference velocity(blue line) and Longitudinal velocity(red line)- Straight Road 3 DOF Vehicle

In Figure 4.2, the longitudinal velocity is indicated with a red line, while the reference velocity is indicated with a blue line. After 8 seconds, the reference velocity is equal to the maximum velocity. The longitudinal velocity tries to follow the reference velocity and reaches the maximum velocity at 8.2 seconds. There is a slight overshoot, and small braking is applied to the vehicle to stabilize the longitudinal velocity equal to the maximum velocity. After 27 seconds, the reference velocity decreases and reaches the value zero at 35 seconds. The vehicle reaches zero speed at 36 seconds.

The behaviour of the acceleration and deceleration commands are shown below.

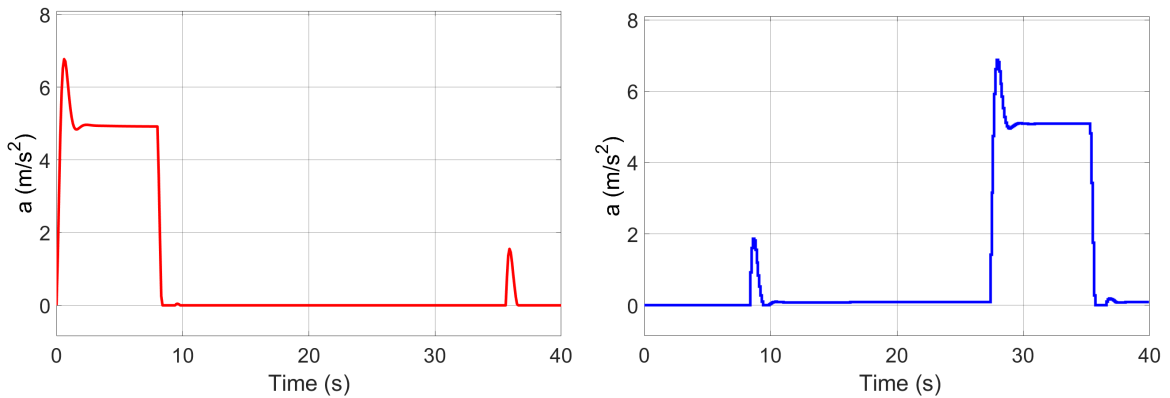


Figure 4.3: Acceleration(red line) and Deceleration(blue line) Commands - Straight Road 3 DOF Vehicle

The vehicle acceleration is equal to:

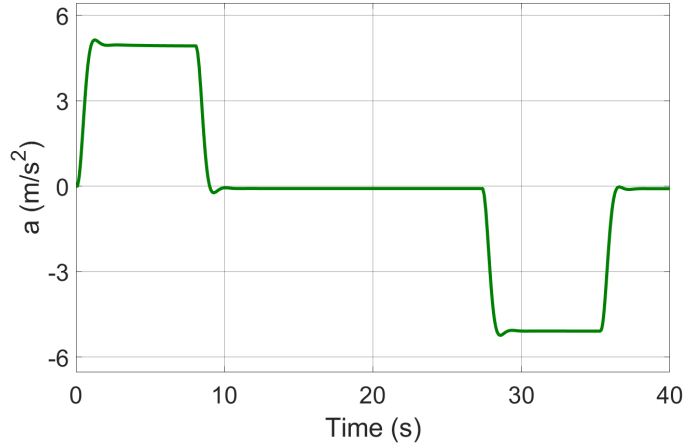


Figure 4.4: Vehicle Acceleration - Straight Road 3 DOF Vehicle

The steering control is activated if the lateral deviation or relative yaw angle is different from zero.

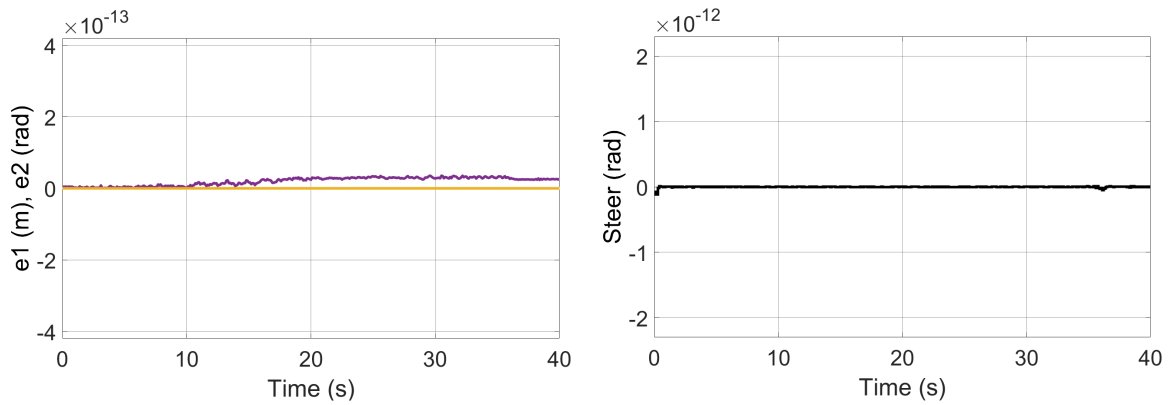


Figure 4.5: Lateral Deviation(purple line) and Relative Yaw Angle(yellow line). Steering Command(black line)- Straight Road 3 DOF Vehicle

The left figure shows the lateral deviation with a purple line, while the relative yaw angle is indicated with a yellow line. To see variations in the signals, the graph is zoomed in to the order of 10^{-13} . So these two signals are represented by minimal quantities. As a result, the steering control, in the figure on the right, changes with minimal variations. To see the first signal variations, the graph is zoomed to the order of 10^{-12} .

These results are consistent with the scenario in which the vehicle is traveling. In Figure 4.6, the route of the vehicle in the scenario is shown. The route is indicated with a red line.

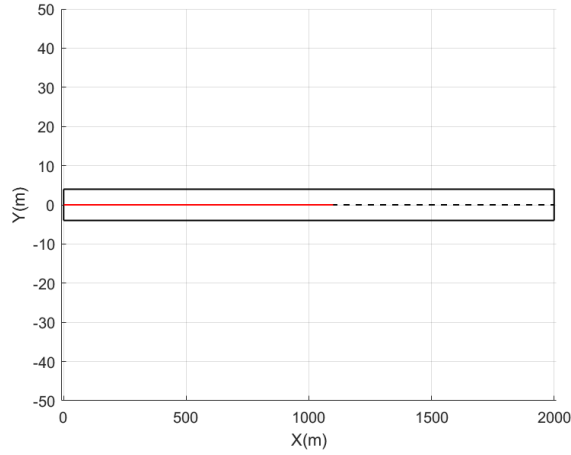


Figure 4.6: Vehicle Route - Straight Road 3 DOF Vehicle

Complete Circuit:

- Initial global position: $x=-0.0056$ m, $y=0.01$ m, $z=0$ m
- Initial yaw angle : $\psi=0.453$ rad
- Output weights : $Q_{11}=10$, $Q_{22}=5$, $Q_{33}=0$
- Maximum and minimum acceleration command: $a_{MAX}=8$ m/s², $a_{min}=-8$ m/s²
- Maximum and minimum steer command: $\delta_{MAX}=\pi/12$ rad, $\delta_{min}=-\pi/12$ rad
- Maximum velocity: $v_{MAX}=30$ m/s
- Simulation time: 160 s

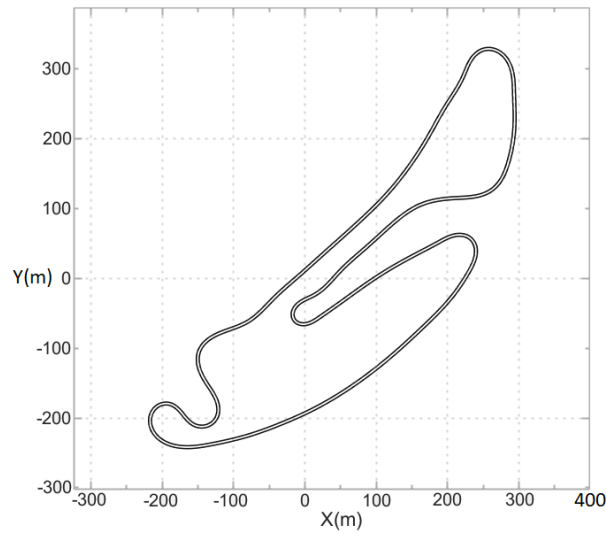


Figure 4.7: Berlin 2018 Race Track

The reference velocity adapts to the scene where the car is travelling. In the vicinity of a curve, this decreases, while in a straight line, it tends to assume the maximum value of 30 m/s.

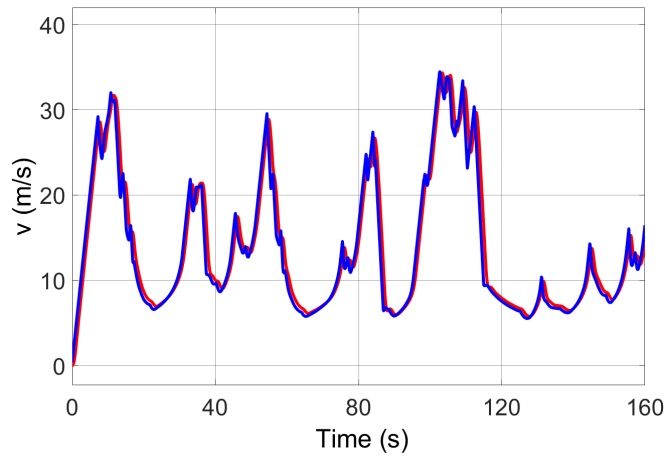


Figure 4.8: Reference velocity(blue line) and Longitudinal velocity(red line) - Berlin 2018 Race Track 3 DOF Vehicle

In the figure, it is possible to see how the longitudinal velocity follows the reference velocity signal.

The behaviour of the acceleration and deceleration commands are shown below.

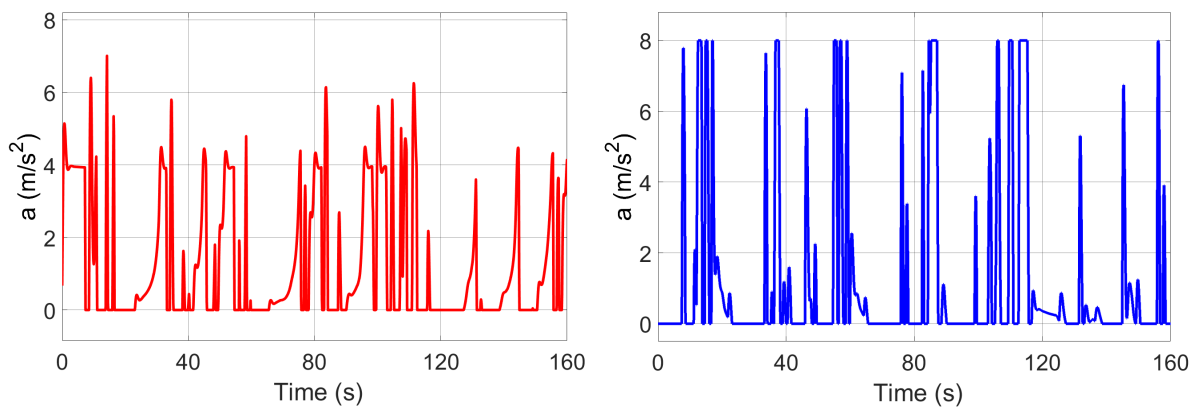


Figure 4.9: Acceleration(red line) and Deceleration(blue line) Commands - Berlin 2018 Race Track 3 DOF Vehicle

The vehicle acceleration is equal to:

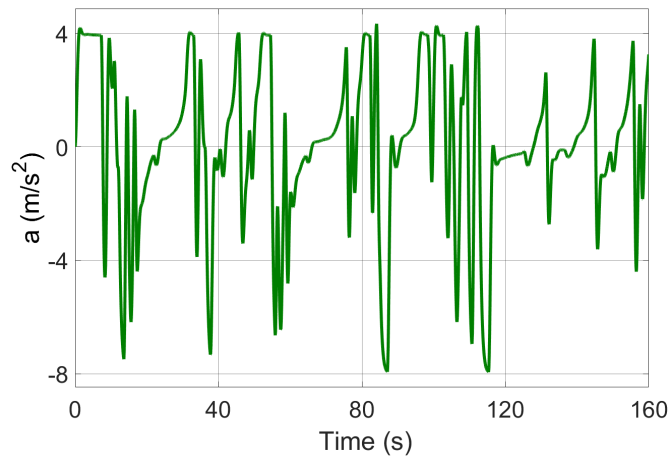


Figure 4.10: Vehicle Acceleration - Berlin 2018 Race Track 3 DOF Vehicle

The following figure shows how the steering command changes according to the lateral deviation and relative yaw angle values.

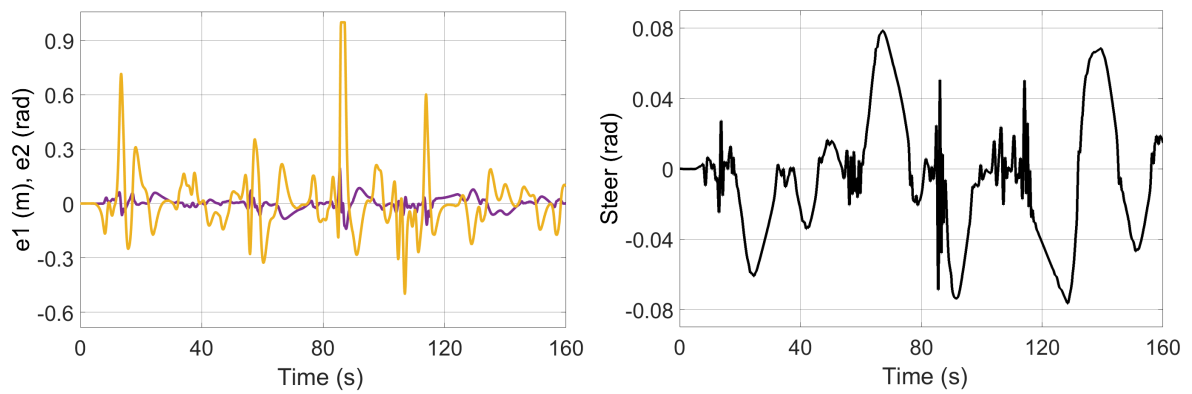


Figure 4.11: Lateral Deviation(purple line) and Relative Yaw Angle(yellow line). Steering Command(black line) - Berlin 2018 Race Track 3 DOF Vehicle

In Figure 4.12, the route of the vehicle in the scenario is shown. The route is indicated with a red line.

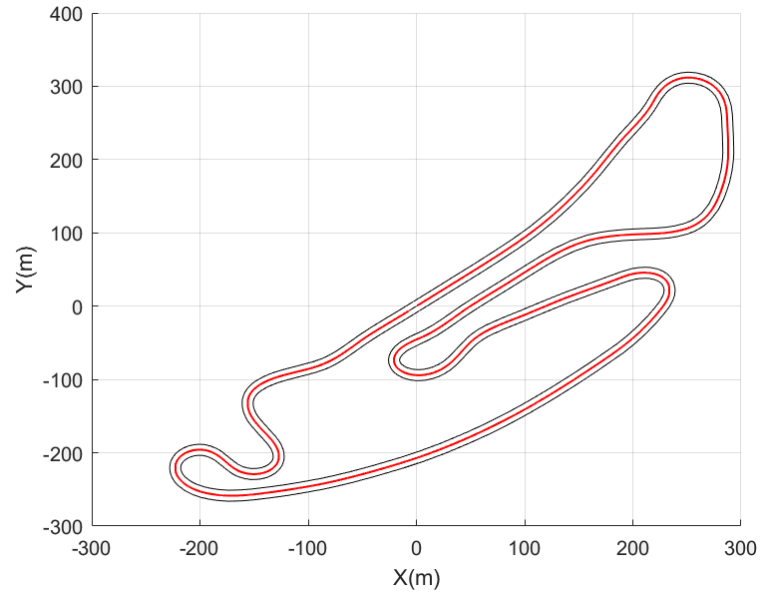


Figure 4.12: Vehicle Route - Berlin 2018 Race Track 3 DOF Vehicle

The results above are coherent with the value of curvature acquired by sensors and shown in Figure 4.13.

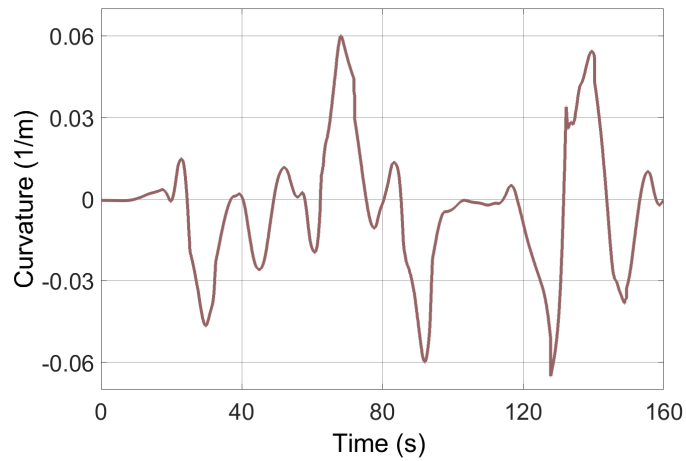


Figure 4.13: Curvature - Berlin 2018 Race Track 3 DOF Vehicle

4.1.2 15 Degrees of Freedom validation and results

Straight Road:

- Initial global position: $x=0$ m, $y=0$ m, $z=0$ m
- Initial yaw angle : $\psi=0$ rad
- Output weights : $Q_{11}=20$, $Q_{22}=1$, $Q_{33}=0$
- Maximum and minimum acceleration command: $a_{MAX}=9$ m/s², $a_{min}=-9$ m/s²
- Maximum and minimum steer command: $\delta_{MAX}=\pi/7$ rad, $\delta_{min}=-\pi/7$ rad
- Maximum velocity: $v_{MAX}=40$ m/s
- Simulation time: 50 s

The acceleration test consists of three parts. In the first part, the reference velocity increases until it reaches the maximum allowed velocity. In the second part, the vehicle travels at a constant velocity over a period of time. The last part consists of braking the vehicle up to zero velocity.

The results show the comparison between the reference velocity and the longitudinal velocity, the acceleration and deceleration commands, the steering command and the behaviour of the lateral deviation and the relative yaw angle.

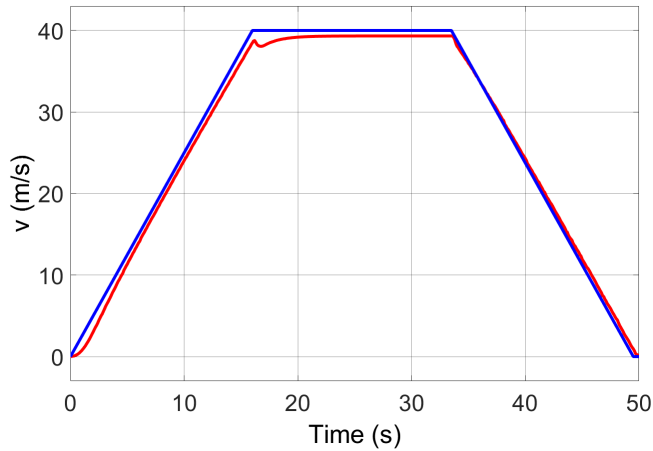


Figure 4.14: Reference velocity(blue line) and Longitudinal velocity(red line) - Straight Road 15 DOF Vehicle

In Figure 4.14, the longitudinal velocity is indicated with a red line, while the reference velocity is indicated with a blue line. After 16 seconds, the reference velocity is equal to the maximum velocity. The longitudinal velocity tries to reach the reference velocity, but it stops at 39.4 m/s. After 33.6 seconds, the reference velocity decreases and reaches the value zero at 49.5 seconds. The vehicle reaches zero speed at 50 seconds.

The behaviour of the acceleration and deceleration commands are shown below.

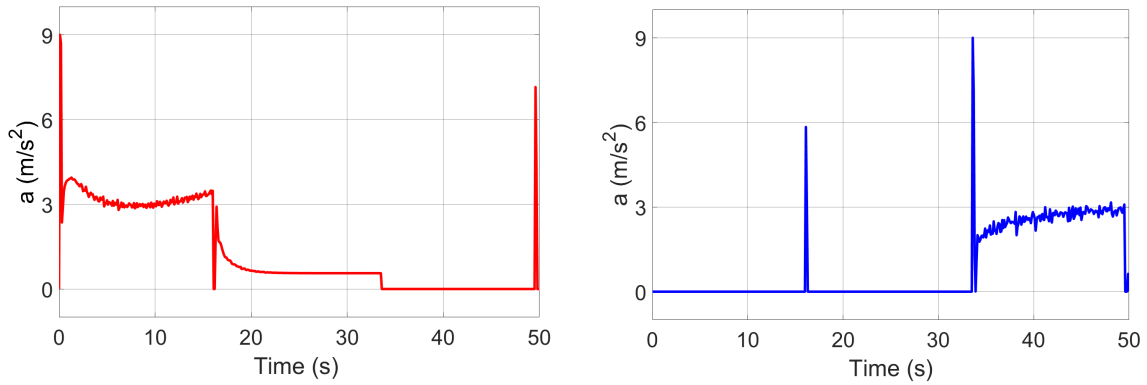


Figure 4.15: Acceleration(red line) and Deceleration(blue line) Commands - Straight Road 15 DOF Vehicle

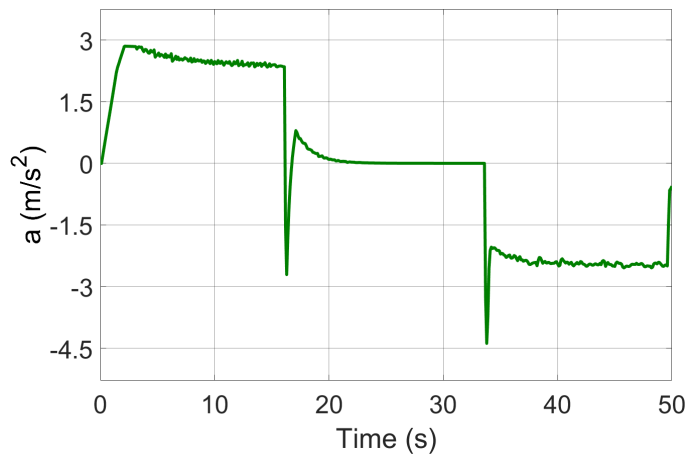


Figure 4.16: Vehicle Acceleration - Straight Road 15 DOF Vehicle

The steering control is activated if the lateral deviation or relative yaw angle is different from zero.

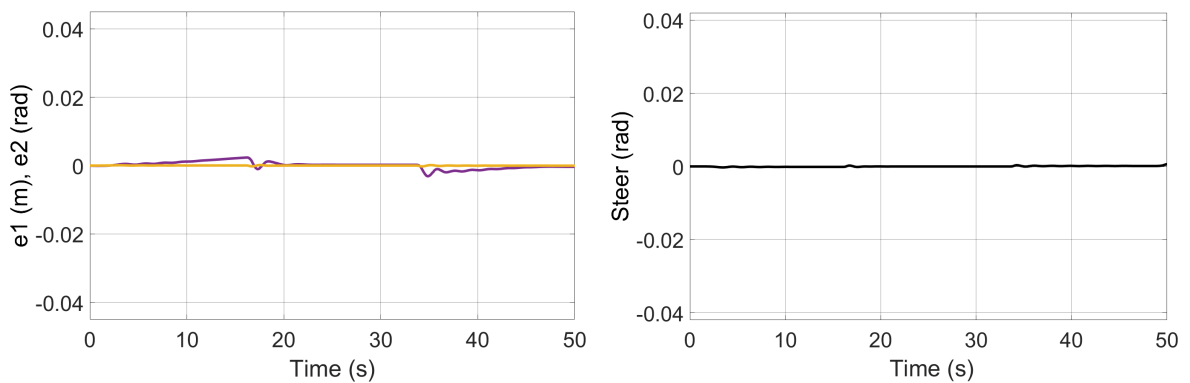


Figure 4.17: Lateral Deviation(purple line) and Relative Yaw Angle(yellow line). Steering Command(black line) - Straight Road 15 DOF Vehicle

The left figure shows the lateral deviation with a purple line, while the relative yaw angle is indicated with a yellow line. The steering control, in the figure on the right, changes with minimal variations.

These results are consistent with the scenario in which the vehicle is traveling. In Figure 4.18, the route of the vehicle in the scenario is shown. The route is indicated with a red line.

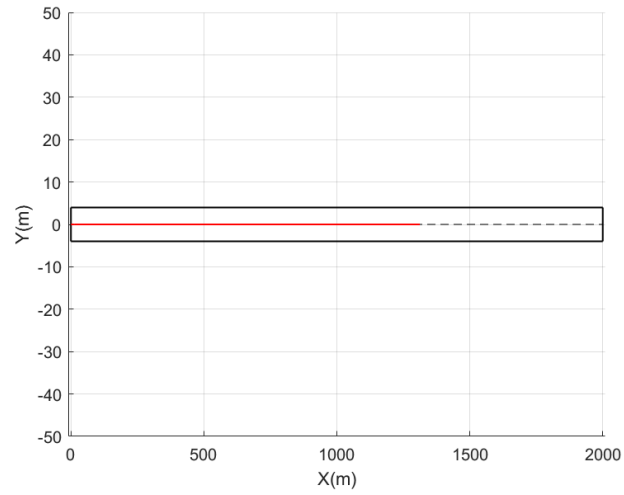


Figure 4.18: Vehicle Route - Straight Road 15 DOF Vehicle

Complete Circuit:

- Initial global position: $x=-0.0056$ m, $y=0.01$ m, $z=0$ m
- Initial yaw angle : $\psi=0.651$ rad
- Output weights : $Q11=10$, $Q22=20$, $Q33=0$
- Maximum and minimum acceleration command: $a_{MAX}=9$ m/s², $a_{min}=-9$ m/s²
- Maximum and minimum steer command: $\delta_{MAX}=\pi/7$ rad, $\delta_{min}=-\pi/7$ rad
- Maximum velocity: $v_{MAX}=40$ m/s
- Simulation time: 160 s

The reference velocity adapts to the scene where the car is travelling. In the vicinity of a curve, this decreases, while in a straight line, it tends to assume the maximum value of 40 m/s.

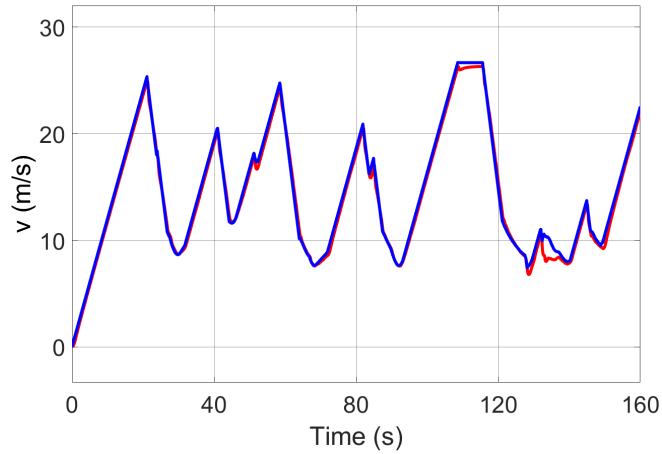


Figure 4.19: Reference velocity(blue line) and Longitudinal velocity(red line) - Berlin 2018 Race Track 15 DOF Vehicle

In the Figure 4.19, it is possible to see how the longitudinal velocity follows the reference velocity signal.

The behaviour of the acceleration and deceleration commands are shown below.

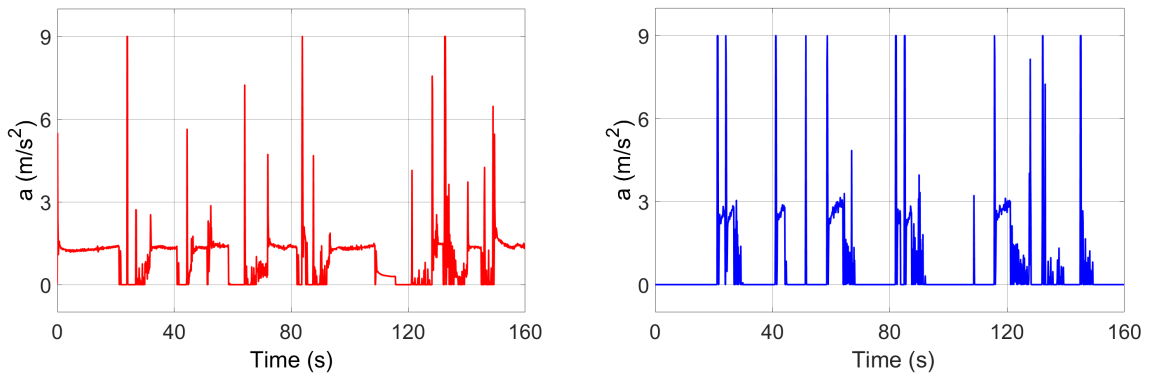


Figure 4.20: Acceleration(red line) and Deceleration(blue line) Commands - Berlin 2018 Race Track 15 DOF Vehicle

The vehicle acceleration is equal to:

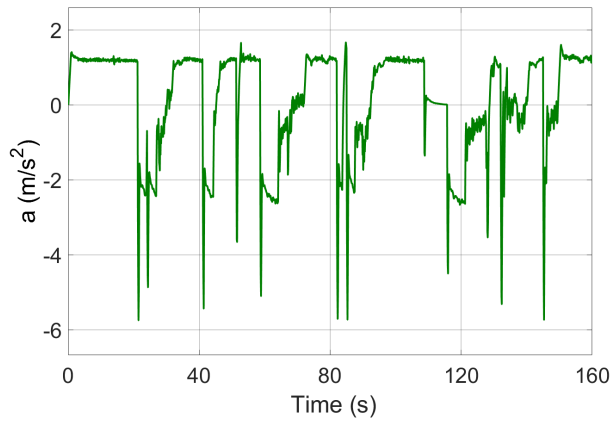


Figure 4.21: Vehicle Acceleration - Berlin 2018 Race Track 15 DOF Vehicle

In the following figure, it is possible to note how the steering command changes according to the lateral deviation and relative yaw angle values.

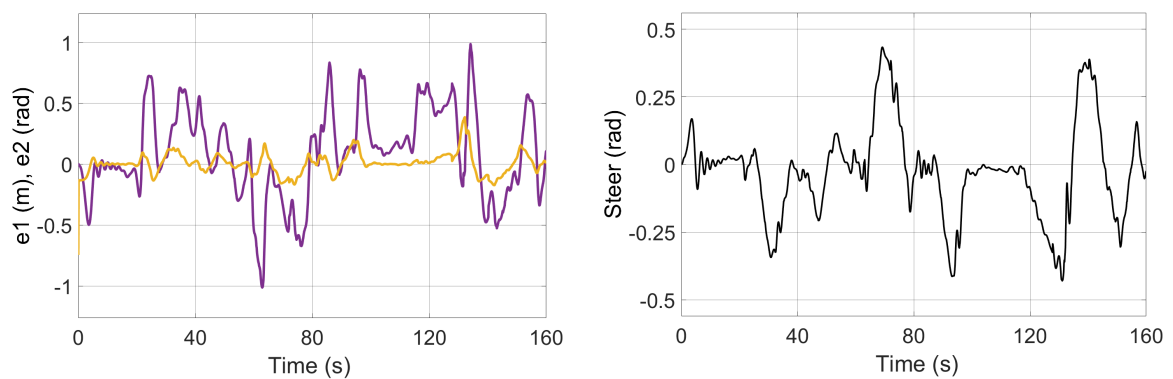


Figure 4.22: Lateral Deviation(purple line) and Relative Yaw Angle(yellow line). Steering Command(black line) - Berlin 2018 Race Track 15 DOF Vehicle

In Figure 4.23, the route of the vehicle in the scenario is shown. The route is indicated with a red line.

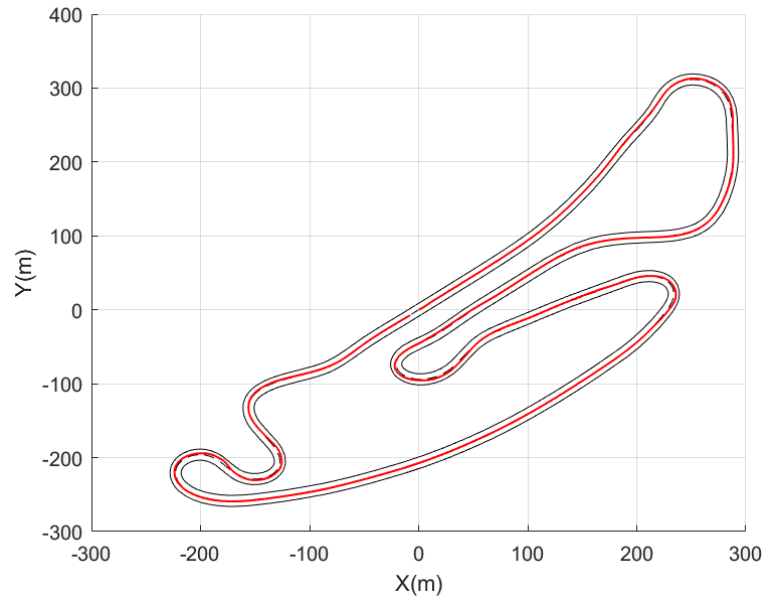


Figure 4.23: Vehicle Route - Berlin 2018 Race Track 15 DOF Vehicle

The results above are coherent with the value of curvature acquired by sensors and shown in Figure 4.24.

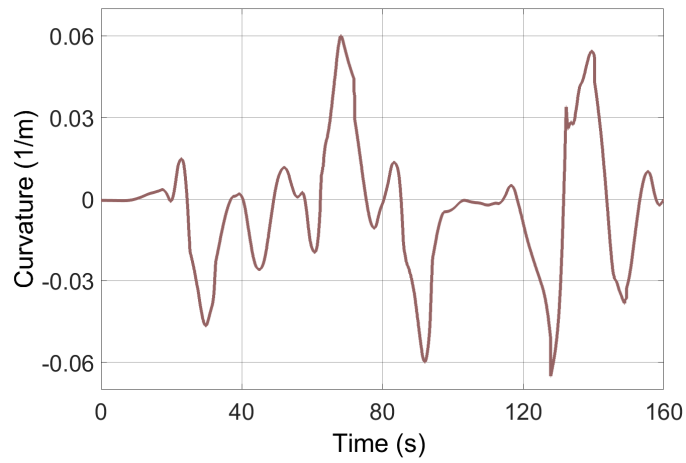


Figure 4.24: Curvature - Berlin 2018 Race Track 15 DOF Vehicle

4.2 Path Planning and Lane Following

The results obtained in this part of the thesis relate to the integration of the path planning part and the control part.

The path planning part is used to process the acquired data in real-time and supply the controller's processed signals. This part should simulate the behaviour of a Lidar.

The images acquired in real-time are used as input by path planning, which processes them and returns the road curvature value. The curvature's value is essential to define the reference speed of the vehicle and keep the vehicle in the centre of the road. The images used to refer to an acceleration test.

Initially, this part is applied to the 3 DOF model of the vehicle and later, it is all applied to the 15 DOF model of the vehicle.

The integration of the parts of path planning and control is fundamental to increase realism in simulations.

4.2.1 3 Degrees of Freedom validation and results

Straight Road:

- Initial global position: $x=0$ m, $y=0$ m, $z=0$ m
- Initial yaw angle : $\psi=0.033$ rad
- Output weights : $Q_{11}=10$, $Q_{22}=1$, $Q_{33}=0$
- Maximum and minimum acceleration command: $a_{MAX}=40$ m/s², $a_{min}=-40$ m/s²
- Maximum and minimum acceleration : $a_{MAX}=9$ m/s², $a_{min}=-9$ m/s²
- Maximum and minimum steer command: $\delta_{MAX}=\pi/12$ rad, $\delta_{min}=-\pi/12$ rad
- Maximum velocity: $v_{MAX}=30$ m/s
- Simulation time: 36 s

The acceleration test consists of three parts. In the first part, the reference velocity increases until it reaches the maximum allowed velocity. In the second part, the vehicle travels at a constant velocity over a period of time. The last part consists of braking the vehicle up to zero velocity.

The results show the comparison between the reference velocity and the longitudinal velocity, the acceleration and deceleration commands, the steering command and the behaviour of the lateral deviation and the relative yaw angle.

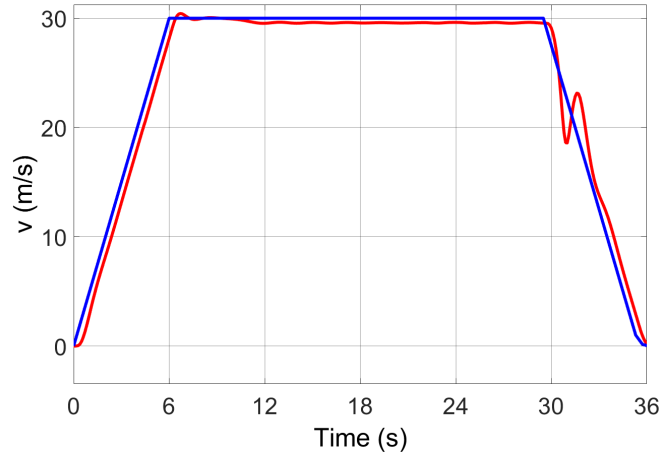


Figure 4.25: Reference velocity(blue line) and Longitudinal velocity(red line) - Straight Road 3 DOF Vehicle RRT + Control

In Figure 4.25, the longitudinal velocity is indicated with a red line, while the reference velocity is indicated with a blue line. After 6 seconds, the reference velocity is equal to the maximum velocity. The longitudinal velocity tries to follow the reference velocity and reaches the maximum velocity at 6.2 seconds. There is a slight overshoot, and small braking is applied to the vehicle to stabilize the longitudinal speed equal to the maximum velocity. After 29.7 seconds, the reference velocity decreases and reaches the value zero at 36 seconds. The vehicle reaches zero speed at 36 seconds.

The behaviour of the acceleration and deceleration commands are shown below.

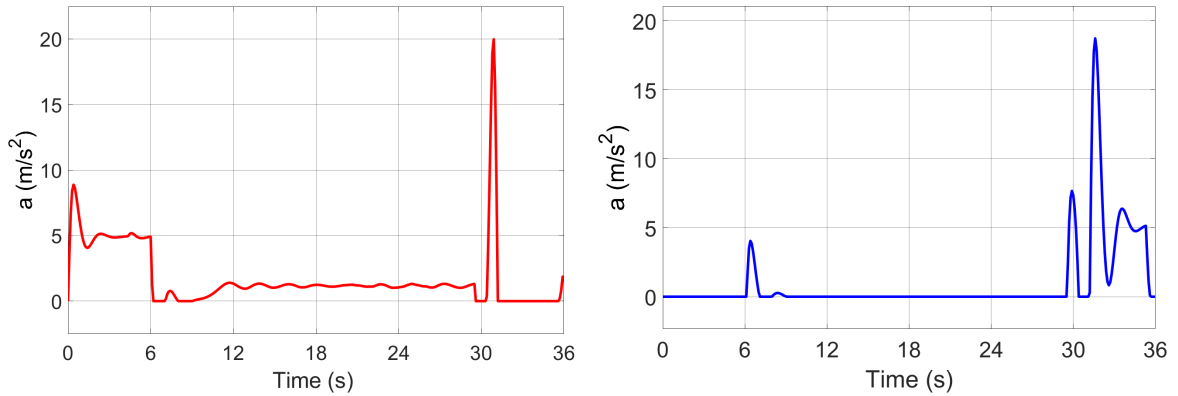


Figure 4.26: Acceleration(red line) and Deceleration(blue line) Commands - Straight Road 3 DOF Vehicle RRT + Control

The vehicle acceleration is equal to:

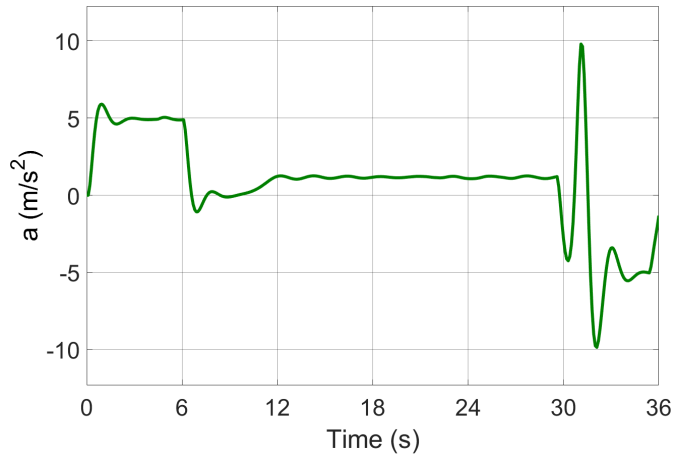


Figure 4.27: Vehicle Acceleration - Straight Road 3 DOF Vehicle RRT + Control

The steering control is activated if the lateral deviation or relative yaw angle is different from zero.

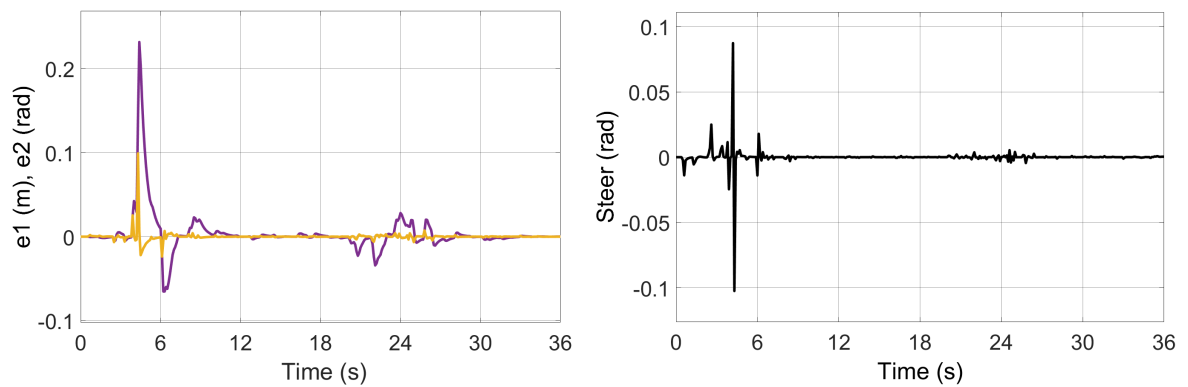


Figure 4.28: Lateral Deviation(purple line) and Relative Yaw Angle(yellow line). Steering Command(black line) - Straight Road 3 DOF Vehicle RRT + Control

The left figure shows the lateral deviation with a purple line, while the relative yaw angle is indicated with a yellow line. The steering control, in the figure on the right, changes with minimal variations. In the first 20 seconds, there are variations due to slight interference in the real data.

These results are consistent with the scenario in which the vehicle is traveling. In Figure 4.29, the route of the vehicle in the scenario is shown. The route is indicated with a red line.

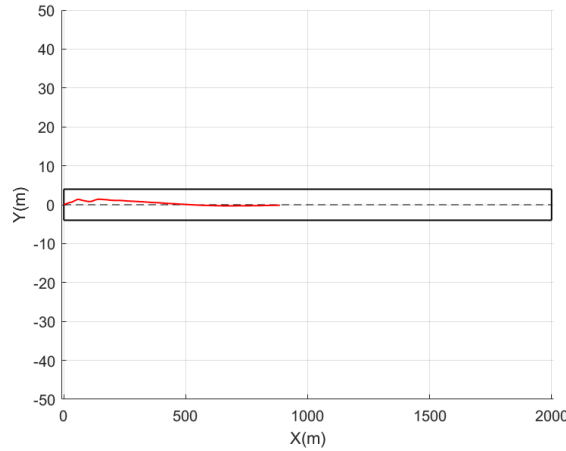


Figure 4.29: Vehicle Route - Straight Road 3 DOF Vehicle RRT + Control

4.2.2 15 Degrees of Freedom validation and results

Straight Road:

- Initial global position: $x=0$ m, $y=0$ m, $z=0$ m
- Initial yaw angle : $\psi=0$ rad
- Output weights : $Q_{11}=20$, $Q_{22}=1$, $Q_{33}=0$
- Maximum and minimum acceleration command: $a_{MAX}=9$ m/s², $a_{min}=-9$ m/s²
- Maximum and minimum steer command: $\delta_{MAX}=\pi/7$ rad, $\delta_{min}=-\pi/7$ rad
- Maximum velocity: $v_{MAX}=30$ m/s
- Simulation time: 36 s

The acceleration test consists of three parts. In the first part, the reference velocity increases until it reaches the maximum allowed velocity. In the second part, the vehicle travels at a constant velocity over a period of time. The last part consists of braking the vehicle up to zero velocity.

The results show the comparison between the reference velocity and the longitudinal velocity, the acceleration and deceleration commands, the steering command and the behaviour of the lateral deviation and the relative yaw angle.

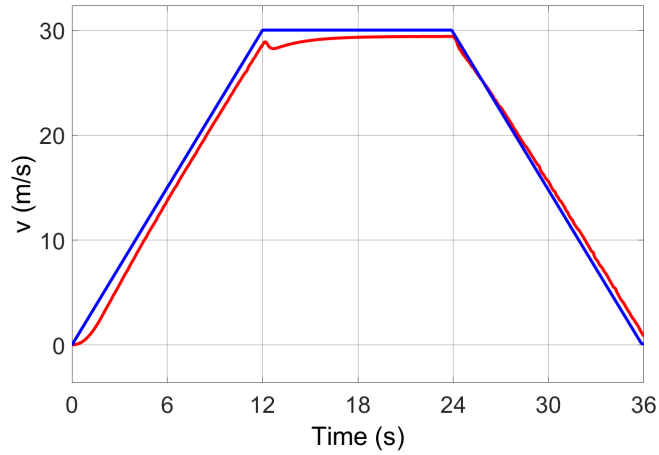


Figure 4.30: Reference velocity(blue line) and Longitudinal velocity(red line) - Straight Road 15 DOF Vehicle RRT + Control

In Figure 4.30, the longitudinal velocity is indicated with a red line, while the reference velocity is indicated with a blue line. After 12 seconds, the reference velocity reaches the maximum velocity. After 24 seconds, the reference velocity decreases and reaches the value zero at 36 seconds. The vehicle reaches zero speed at 36 seconds.

The behaviour of the acceleration and deceleration commands are shown below.

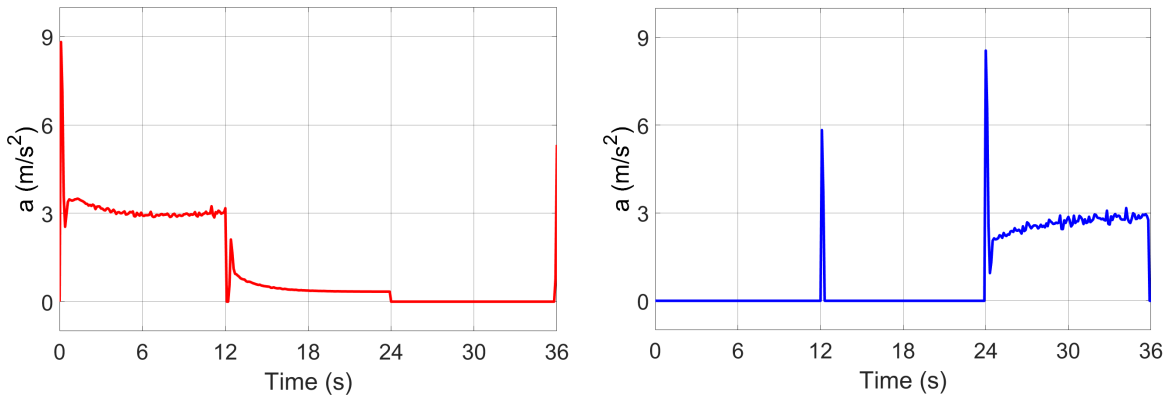


Figure 4.31: Acceleration(red line) and Deceleration(blue line) Commands - Straight Road 15 DOF Vehicle RRT + Control

The vehicle acceleration is equal to:

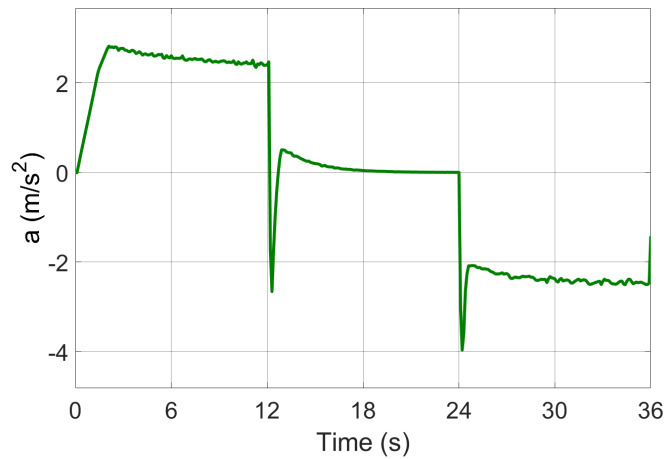


Figure 4.32: Vehicle Acceleration - Straight Road 15 DOF Vehicle RRT + Control

The steering control is activated if the lateral deviation or relative yaw angle is different from zero.

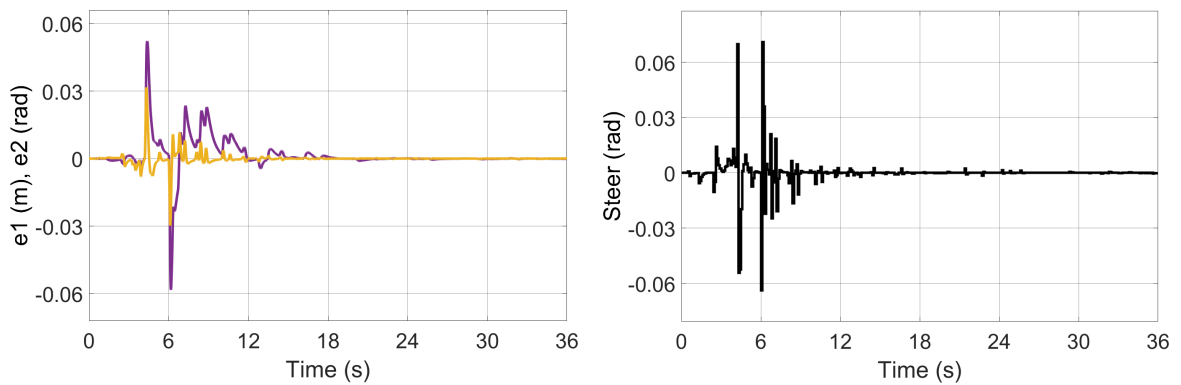


Figure 4.33: Lateral Deviation(purple line) and Relative Yaw Angle(yellow line). Steering Command(black line) - Straight Road 15 DOF Vehicle RRT + Control

The left figure shows the lateral deviation with a purple line, while the relative yaw angle is indicated with a yellow line. The steering control, in the figure on the right, changes with minimal variations.

These results are consistent with the scenario in which the vehicle is traveling. In Figure 4.34, the route of the vehicle in the scenario is shown. The route is indicated with a red line.

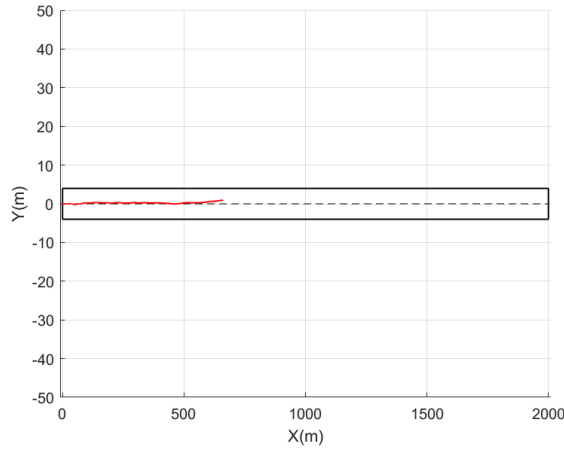


Figure 4.34: Vehicle Route - Straight Road 15 DOF Vehicle RRT + Control

4.3 Hardware Implementation

The last part of the thesis work concerns the implementation of the controller in a real-time target machine.

One of the major problems of the Hardware implementation concerns the C / C ++ Code Generation. If the Simulink elements that build the MPC controller are not compatible with the Code Generation, the model must be changed using compatible blocks. Before moving on to implementation, the controller must be validated with the 3 DOF vehicle model and the 15 DOF vehicle model.

This process can take a long time due to the blocks' incompatibility with the Code Generation and the replacement of these with new blocks that imitate their behaviour, always avoiding the incompatibility between the Simulink model and the Code Generation. Through the MinGW compiler, it is possible to see if the blocks on Simulink can support code generation. The Simulink model is modified, substituting the blocks that do not support code generation with blocks that support it.

The real-time target hardware platform used for implementing the controller developed in this thesis work is the SCALEXIO AutoBox, represented in Figure 4.35.



Figure 4.35: SCALEXIO AutoBox

SCALEXIO AutoBox is used in vehicles such as passenger cars, trucks, trains and agricultural and construction machinery. Optimized for in-vehicle use, it is ideal for test drives in the development of components such as electric powertrains and chassis control and functions for assisted, highly automated and autonomous driving(AD).

To produce a HIL procedure, after having collected all the inputs and outputs of a complete simulation, we transform the Simulink model by removing all the blocks that will not be included in the code generation phase. Through dSpace, the controller in Simulink is translated in C code through automatic code generation.

The generated code is inserted on SCALEXIO Auto-Box to perform real-time simulations. The simulations are done in a loop to check if the controller has problems over time. The generated code is built on SCALEXIO without error, and the controller works at six milliseconds.

CHAPTER 5

Conclusions and future works

In this thesis work, the design, validation and implementation phases for a controller with MPC strategy are developed. In the first part of the thesis work, vehicle dynamics is modeled using 3 degrees of freedom vehicle model, and simulations are performed in virtual scenarios created using Automated Driving Scenario Toolbox on MATLAB and Simulink. In the second part, there is an integration of the Path Planning and the Vehicle Control Strategy based on acquisitions performed in real-time. The third part of the thesis work is performed on Simscape Vehicle Template with the vehicle dynamics modeled using 15 degrees of freedom vehicle model. The last part of the work consists of implementing the developed controller into Real-Time Target Hardware Platforms.

The simulations performed in this work are an acceleration test and a complete circuit test. Through the Driving Scenario Designer other driving scenarios were built but the Berlin 2018 Race Track scenario was preferred as it represents a real circuit used as a Formula E electric car race on the Tempelhof airport street circuit at Tempelhof airport, on the outskirts of Berlin on 2018.

The results shown in the first part of chapter 4 highlighted the correct operation of the controller both in longitudinal and lateral dynamics. The longitudinal velocity follows the reference velocity in both the acceleration test and the complete circuit test. The controller provides an acceleration or deceleration command based on the longitudinal and reference velocity signals, while it provides a steering command based on the lateral deviation and relative yaw angle signals that the controller tries to bring equal to zero.

The simulations performed through the Driving Scenario Simulator allow to verify the controller and the other fundamental blocks for its operation as the reference speed generator. The path planning developed for this approach is limiting for the application that the vehicle has to perform. The vehicle will participate in the Formula SAE competitions in the near future, where the limits of the track are drawn with cones that delimit the left and right limits of the road ahead.

For this reason, after the validation of the controller with the 3 DOF and 15 DOF model, the controller is integrated with a path planning developed specifically for the application that the vehicle has to carry out.

The method used in path planning consists of generating a feasible trajectory with the vision sensors' information based on the positioning of the cones. This information is con-

stantly updated with a period equal to the sample time. The images acquired in real-time are used as input by path planning, which processes them and returns the road curvature value. The curvature's value is essential to define the reference speed of the vehicle and keep the vehicle in the centre of the road.

The results shown in the second part of chapter 4 are related to integration of the control part and the path planning part. The real data used for the simulations are used to perform an acceleration test using 3 DOF and 15 DOF vehicle models. The results are consistent with the scenario in which the vehicle is traveling.

The last part of the thesis work concerns the implementation of the controller in the real-time target machine. After the construction of a model compatible with the Automatic Code Generation, the controller model is inserted in the SCALEXIO AutoBox which performs real-time simulations. The controller is able to process the data and deliver it to the vehicle in six milliseconds, which corresponds to 6% of the sampling time.

Despite the good results obtained in this thesis, there are still many improvements that can be made. The first improvement is to build a 15 DOF vehicle model that respects the characteristics of the Squadra Corse vehicle using Simscape tools. Curve simulations can be performed with the model that integrates path planning and control. To perform these simulations, real-time data of the vehicle in curves must be collected.

Another improvement is to use a better algorithm for creating the reference velocity. The previous algorithm took into account the maximum velocity that the vehicle could maintain in the curve for the current curve, but this was limiting as the vehicle sometimes did not approach the curves correctly. In this thesis work, the reference velocity is calculated taking into account the predicted curves and therefore the vehicle can have time to brake promptly as it prepares for the curve. The algorithm used can be improved by considering other factors for vehicle stability for the reference speed.

Other improvements related to the vehicle model can be made by modifying the engine, brakes and other elements such as suspension and adapting them to the vehicle. The model can be implemented in the Speedgoat, a real-time target platform that allows code generation of the model in Simscape.

These and other improvements can be made by students who will become part of the Squadra Corse Team or who will collaborate with the LIM for the development of the thesis.

List of Figures

1.1	History of Autonomous Vehicle Technologies	2
1.2	Da Vinci's Self-Propelled Cart [3]	3
1.3	Whitehead Torpedo [4]	3
1.4	Mechanical Mike aircraft autopilot [5]	4
1.5	Teetor Cruise Control [6]	4
1.6	Stanford Cart [7]	5
1.7	Automatically Operated Car [8]	5
1.8	VaMoRs [9]	5
1.9	General Atomics MQ-1 Predator [10]	6
1.10	DARPA Challenges [11]	6
1.11	Tesla Model S [12]	6
1.12	SAE Autonomous Vehicle Standard levels [14]	7
1.13	Anti-lock Braking System	8
1.14	Electronic Stability Control	9
1.15	Cruise Control[17]	9
1.16	Adaptive Cruise Control	10
1.17	Autonomous Emergency Braking	11
1.18	Lane Departure Warning System [21]	11
1.19	Lane Keep Assist [22]	12
1.20	Automatic Lane Keeping Control [23]	12
1.21	Parking Assist System [24]	12
1.22	Partners Formula Student Germany 2021	13
1.23	Formula Student Competition	13
1.24	Formula Student Competition Classes	14
1.25	Formula Student Driveless vehicle during Formula Student Germany 2019	14
1.26	State of Art Flow Chart	16
1.27	Autonomous Vehicle Control Architecture	16
1.28	First Controller Architecture	17
1.29	First Controller Architecture	18
1.30	Second Controller Architecture	19
1.31	Second Controller Architecture	20
1.32	Lateral Controller	20
1.33	Longitudinal Controller	21

2.1	Local Coordinates System [28]	25
2.2	Global Coordinates System	26
2.3	3 DOF Vehicle Model	27
2.4	Vehicle Body 3 DOF Dual-Track [29]	28
2.5	Instantaneous Center of Motion	30
2.6	Deflected tread path and slip angle	31
2.7	Vehicle Body 3 DOF Single-Track	32
2.8	Ackermann Angle	32
2.9	Single-Track Kinematic	33
2.10	Single-Track Dynamic	36
2.11	Equilibrium of Vehicle Forces	37
2.12	Aerodynamic Drag Force	39
2.13	Static Load Distribution	40
2.14	Understeering / Oversteering	41
2.15	Lateral Deviation and Relative Yaw Angle[32]	42
2.16	15 DOF Vehicle Model	46
2.17	Double-Wishbone Suspension	54
2.18	Rack and Pinion Steering System	54
2.19	Anti Roll Drop Link	55
3.1	Autonomous Driving Building Blocks	59
3.2	Curvature	66
3.3	Rolling Resistance	69
4.1	Straight Road Scenario	72
4.2	Reference velocity(blue line) and Longitudinal velocity(red line)- Straight Road 3 DOF Vehicle	73
4.3	Acceleration(red line) and Deceleration(blue line) Commands - Straight Road 3 DOF Vehicle	73
4.4	Vehicle Acceleration - Straight Road 3 DOF Vehicle	74
4.5	Lateral Deviation(purple line) and Relative Yaw Angle(yellow line). Steering Command(black line)- Straight Road 3 DOF Vehicle	74
4.6	Vehicle Route - Straight Road 3 DOF Vehicle	75
4.7	Berlin 2018 Race Track	75
4.8	Reference velocity(blue line) and Longitudinal velocity(red line) - Berlin 2018 Race Track 3 DOF Vehicle	76
4.9	Acceleration(red line) and Deceleration(blue line) Commands - Berlin 2018 Race Track 3 DOF Vehicle	76
4.10	Vehicle Acceleration - Berlin 2018 Race Track 3 DOF Vehicle	77
4.11	Lateral Deviation(purple line) and Relative Yaw Angle(yellow line). Steering Command(black line) - Berlin 2018 Race Track 3 DOF Vehicle	77
4.12	Vehicle Route - Berlin 2018 Race Track 3 DOF Vehicle	78
4.13	Curvature - Berlin 2018 Race Track 3 DOF Vehicle	78

4.14 Reference velocity(blue line) and Longitudinal velocity(red line) - Straight Road 15 DOF Vehicle	79
4.15 Acceleration(red line) and Deceleration(blue line) Commands - Straight Road 15 DOF Vehicle	80
4.16 Vehicle Acceleration - Straight Road 15 DOF Vehicle	80
4.17 Lateral Deviation(purple line) and Relative Yaw Angle(yellow line). Steering Command(black line) - Straight Road 15 DOF Vehicle	80
4.18 Vehicle Route - Straight Road 15 DOF Vehicle	81
4.19 Reference velocity(blue line) and Longitudinal velocity(red line) - Berlin 2018 Race Track 15 DOF Vehicle	82
4.20 Acceleration(red line) and Deceleration(blue line) Commands - Berlin 2018 Race Track 15 DOF Vehicle	83
4.21 Vehicle Acceleration - Berlin 2018 Race Track 15 DOF Vehicle	83
4.22 Lateral Deviation(purple line) and Relative Yaw Angle(yellow line). Steering Command(black line) - Berlin 2018 Race Track 15 DOF Vehicle	83
4.23 Vehicle Route - Berlin 2018 Race Track 15 DOF Vehicle	84
4.24 Curvature - Berlin 2018 Race Track 15 DOF Vehicle	84
4.25 Reference velocity(blue line) and Longitudinal velocity(red line) - Straight Road 3 DOF Vehicle RRT + Control	86
4.26 Acceleration(red line) and Deceleration(blue line) Commands - Straight Road 3 DOF Vehicle RRT + Control	86
4.27 Vehicle Acceleration - Straight Road 3 DOF Vehicle RRT + Control	87
4.28 Lateral Deviation(purple line) and Relative Yaw Angle(yellow line). Steering Command(black line) - Straight Road 3 DOF Vehicle RRT + Control	87
4.29 Vehicle Route - Straight Road 3 DOF Vehicle RRT + Control	88
4.30 Reference velocity(blue line) and Longitudinal velocity(red line) - Straight Road 15 DOF Vehicle RRT + Control	89
4.31 Acceleration(red line) and Deceleration(blue line) Commands - Straight Road 15 DOF Vehicle RRT + Control	89
4.32 Vehicle Acceleration - Straight Road 15 DOF Vehicle RRT + Control	90
4.33 Lateral Deviation(purple line) and Relative Yaw Angle(yellow line). Steering Command(black line) - Straight Road 15 DOF Vehicle RRT + Control	90
4.34 Vehicle Route - Straight Road 15 DOF Vehicle RRT + Control	91
4.35 SCALEXIO AutoBox	91

Acronyms

ABS	Anti-lock Brake System
ACC	Adaptive Cruise Control
AD	Autonomous Driving
ADAS	Advanced Driver Assistance System
AEB	Autonomous Emergency Braking
ALKC	Automatic Lane Keeping Control
AMPC	Adaptive Model Predictive Control
AS	Autonomous System
CC	Cruise Control
CG	Center of Gravity
CPU	Control Program Unit
CV	Combustion Vehicle
DARPA	Defense Advanced Research Projects Agency
DAS	Driver Assistance System
DOF	Degrees of freedom
DV	Driverless Vehicle
EBS	Emergency Brake System
EPS	Electric Power Steering
ESC	Electronic Stability Control
ESP	Electronic Stability Program
EV	Electric Vehicle
FFW	Feedforward

FS	Formula Student
FSC	Formula Student Combustion
FSD	Formula Student Driverless
FSE	Formula Student Electric
FSDV	Formula Student Driverless Vehicle
FSG	Formula Student Germany
GPS	Global Positioning System
GUI	Graphical User Interface
HAV	Highly Automated Vehicles
HIL	Hardware-in-the-Loop
ICM	Instantaneous Center of Motion
ICT	Information and Communications Technology
IMU	Inertial Measurement Unit
ISO	International Organization for Standardization
LIM	Laboratorio Interdisciplinare di Meccatronica
LDWS	Lane Departure Warning System
LK	Lane Keeping
LKA	Lane Keep Assist
LMPC	Learning Model Predictive Control
MPC	Model Predictive Control
NHTSA	National Highway Traffic Safety Administration
PA	Park Assist
PAS	Park Assist System
PE	Point of Equilibrium
PID	Proportional Integral Derivative
RH	Receding Horizon
SAE	Society of Automotive Engineers
SIL	Software-in-the-Loop

- TCS** Traction Control System
- V2I** Vehicle-to-Infrastructure
- V2N** Vehicle-to-Network
- V2V** Vehicle-to-Vehicle
- V2X** Vehicle-to-Everything

Symbols

X	Longitudinal global direction
Y	Lateral global direction
Z	Vertical global direction
\vec{i}	Longitudinal local versor
\vec{j}	Lateral local versor
\vec{k}	Vertical local versor
\vec{e}_x	Longitudinal global versor
\vec{e}_y	Lateral global versor
\vec{e}_z	Vertical global versor
x	Longitudinal local direction
x_{in}	Initial longitudinal local direction
y	Lateral local direction
z	Vertical local direction
v_{CG}	Velocity of center of gravity
v_x, \dot{x}	Longitudinal velocity
v_y, \dot{y}	Lateral velocity
v_z, \dot{z}	Vertical velocity
$a_{CG}, v_{\dot{CG}}$	Acceleration of center of gravity
a_x, \dot{v}_x, \ddot{x}	Longitudinal acceleration
a_y, \dot{v}_y, \ddot{y}	Lateral acceleration
a_z, \dot{v}_z, \ddot{z}	Vertical acceleration
ϕ	Roll
θ	Pitch
ψ	Yaw
$\omega_x, \dot{\phi}$	Roll rate
$\omega_y, \dot{\theta}$	Pitch rate
$\omega_z, \omega, \dot{\Psi}, \dot{\phi}, r$	Yaw rate
$\alpha_x, \dot{\omega}_x, \ddot{\phi}$	Angular Roll acceleration
$\alpha_y, \dot{\omega}_y, \ddot{\theta}$	Angular Pitch acceleration
$\alpha_z, \alpha, \dot{\omega}_z, \dot{\omega}, \dot{\Psi}, \ddot{\phi}, \dot{r}$	Angular Yaw acceleration
l_f	Front wheelbase
l_r	Rear wheelbase
L	Wheelbase
T	Track

β	Vehicle body sideslip angle
r_{fl}	Distance from center of gravity to front left wheel ground contact point
r_{fr}	Distance from center of gravity to front right wheel ground contact point
r_{rl}	Distance from center of gravity to rear left wheel ground contact point
r_{rr}	Distance from center of gravity to rear right wheel ground contact point
θ_{lf}	Angle between chassis coordinate system and front left wheel ground contact point
θ_{lr}	Angle between chassis coordinate system and front right wheel ground contact point
θ_{rf}	Angle between chassis coordinate system and rear left wheel ground contact point
θ_{rr}	Angle between chassis coordinate system and rear right wheel ground contact point
v_{wfl}	Front left wheel velocity
v_{wfr}	Front right wheel velocity
v_{wrl}	Rear left wheel velocity
v_{wrr}	Rear right wheel velocity
R_{fl}	Curvature radius of front left wheel
R_{fr}	Curvature radius of front right wheel
R_{rl}	Curvature radius of rear left wheel
R_{rr}	Curvature radius of rear right wheel
R	Curvature radius of the vehicle
ρ	Road curvature of the vehicle
α_{fl}	Tire side slip angle of front left wheel
α_{fr}	Tire side slip angle of front right wheel
α_{rl}	Tire side slip angle of rear left wheel
α_{rr}	Tire side slip angle of rear right wheel
δ_{Ack}	Ackermann angle
v_f	Front wheel velocity
v_r	Rear wheel velocity
δ_f	Front wheel steering angle
δ_r	Rear wheel steering angle
δ	Vehicle steering angle
τ	Steer gear ratio
α_f	Front tire sideslip angle
α_r	Rear tire sideslip angle
F_{xf}	Longitudinal force acting on the front axle
F_{xr}	Longitudinal force acting on the rear axle
F_{yf}	Lateral force acting on the front axle
F_{yr}	Lateral force acting on the rear axle

F_{zf}	Normal force acting on the front axle
F_{zr}	Normal force acting on the rear axle
X_f	Longitudinal force on the front axle along local axis x
X_r	Longitudinal force on the rear axle along local axis x
Y_f	Lateral force on the front axle along local axis y
Y_r	Lateral force on the rear axle along local axis y
F_{aero}	Aerodynamic drag force
I_{zz}	Moment of inertia around the local vertical axis z
F_x	Driving force
C_f	Front cornering stiffness
C_r	Rear cornering stiffness
\tilde{a}_y	Steady-state lateral acceleration
ρ_{air}	Air density
S	Cross-sectional area of the vehicle
c_x	Drag coefficient
m	Vehicle mass
g	Gravity acceleration
F_{zf}^0	Static vertical load on front axle
F_{zr}^0	Static vertical load on rear axle
K	Understeer/oversteer gradient
v_{cr}	Critical velocity
e_1	Lateral deviation
e_2	Relative yaw angle
y_{cl}	Position of the center line of the road
ψ_{des}	Desired yaw angle
$\dot{\psi}_{des}$	Desired yaw rate
κ	Road curvature
τ	Time constant
\dot{a}_x, \ddot{v}_x	Longitudinal jerk
\dot{a}_y, \ddot{v}_y	Lateral jerk
\dot{a}_z, \ddot{v}_z	Vertical jerk
T_s	Sampling time
A	State matrix
B_u	Input matrix
B_d	Disturbance input matrix
C	Output matrix
k	Time index
x	State vector
u	Manipulated variables input vector
v	Measured disturbance input vector
y	Output vector
v_0	Initial longitudinal velocity
f	Rolling resistance coefficient
μ	Friction coefficient

r_{wheel}	Wheel radius
x_{CG}	Longitudinal vehicle position
y_{CG}	Lateral vehicle position
z_{CG}	Vertical vehicle position
z_{wfl}	Vertical movement of the front left wheel
z_{wfr}	Vertical movement of the front right wheel
z_{wrl}	Vertical movement of the rear left wheel
z_{wrr}	Vertical movement of the rear right wheel
θ_{wfl}	Rotation of the front left wheel
θ_{wfr}	Rotation of the front right wheel
θ_{wrl}	Rotation of the rear left wheel
θ_{wrr}	Rotation of the rear right wheel
y_{carv}	Movement of the front wheel angle
m_{ufl}	Mass of the front left wheel
m_{ufr}	Mass of the front right wheel
m_{url}	Mass of the rear left wheel
m_{urr}	Mass of the rear right wheel
m_u	Total unsprung mass
F_{xfl}	Driving force of front left wheel
F_{xfr}	Driving force of front right wheel
F_{xrl}	Driving force of left wheel
F_{xrr}	Driving force of right wheel
F_{yfl}	Yaw force of front left wheel
F_{yfr}	Yaw force of front right wheel
F_{yrl}	Yaw force of left wheel
F_{yrr}	Yaw force of right wheel
F_{sfl}	Suspension force of front left wheel
F_{sfr}	Suspension force of front right wheel
F_{srl}	Suspension force of left wheel
F_{srr}	Suspension force of right wheel
I_{xx}	Moment of inertia around longitudinal axis
I_{yy}	Moment of inertia around lateral axis
I_{zz}	Moment of inertia around vertical axis
h_r	Distance from center of gravity to roll axle
h_p	Distance from center of gravity to pitch axle
z_{fl}	Position of front left suspension and sprung mass connection point
z_{fr}	Position of front right suspension and sprung mass connection point
z_{rl}	Position of rear left suspension and sprung mass connection point
z_{rr}	Position of rear right suspension and sprung mass connection point
z_{ufl}	Vertical position of the front left unsprung mass

z_{ufr}	Vertical position of the front right unsprung mass
z_{url}	Vertical position of the rear left unsprung mass
z_{urr}	Vertical position of the rear right unsprung mass
k_{ufl}	Vertical stiffness of the front left wheel
k_{ufr}	Vertical stiffness of the front right wheel
k_{url}	Vertical stiffness of the rear left wheel
k_{urr}	Vertical stiffness of the rear right wheel
T_{xfl}	Driving torque of the front left wheel
T_{xfr}	Driving torque of the front right wheel
T_{xrl}	Driving torque of the rear left wheel
T_{xrr}	Driving torque of the rear right wheel
T_{bfl}	Braking torque of the front left wheel
T_{bfr}	Braking torque of the front right wheel
T_{brl}	Braking torque of the rear left wheel
T_{brr}	Braking torque of the rear right wheel
M_f	Rolling resistance of the wheels
I_{wfl}	Moment of inertia of the front left wheel
I_{wfr}	Moment of inertia of the front right wheel
I_{wrl}	Moment of inertia of the rear left wheel
I_{wrr}	Moment of inertia of the rear right wheel
α_{wfl}	Angular acceleration of the front left wheel
α_{wfr}	Angular acceleration of the front right wheel
α_{wrl}	Angular acceleration of the rear left wheel
α_{wrr}	Angular acceleration of the rear right wheel
k_{sfl}	Suspension stiffness of the front left wheel
k_{sfr}	Suspension stiffness of the front right wheel
k_{srl}	Suspension stiffness of the rear left wheel
k_{srr}	Suspension stiffness of the rear right wheel
\dot{z}_{ufl}	Vertical velocity of the front left unsprung mass
\dot{z}_{ufr}	Vertical velocity of the front right unsprung mass
\dot{z}_{url}	Vertical velocity of the rear left unsprung mass
\dot{z}_{urr}	Vertical velocity of the rear right unsprung mass
\dot{z}_{fl}	Variation of front left suspension and sprung mass connection point position
\dot{z}_{fr}	Variation of front right suspension and sprung mass connection point position
\dot{z}_{rl}	Variation of rear left suspension and sprung mass connection point position
\dot{z}_{rr}	Variation of rear right suspension and sprung mass connection point position
b_{sfl}	Suspension damping of the front left wheel
b_{sfr}	Suspension damping of the front right wheel
b_{srl}	Suspension damping of the rear left wheel
b_{srr}	Suspension damping of the rear right wheel

f_{ift}	Initial suspension force of front left wheel
f_{ifr}	Initial suspension force of front right wheel
f_{irl}	Initial suspension force of left wheel
f_{irr}	Initial suspension force of right wheel
u^*	Optimal manipulated variables vector
H_p	Prediction Horizon
H_c	Control Horizon
Q_y	Output weight
R_u	Manipulated variables weight
u_{limit}	Limits for manipulated variables
y_{ref}	Reference output vector
v_{ref}	Reference velocity
ω_e	Engine velocity
$\dot{\omega}_e$	Engine acceleration
R	Gear ratio
r_{eff}	Effective wheel radius
R_x	Rolling resistance
T_w	Necessary wheel torque to produce desired acceleration
S	Primitive straight line
L	Primitive left turn
R	Primitive right turn

References

- [1] Kiencke, Nielsen, *Automotive Control Systems 2nd edition*, Springer, 2004.
- [2] Steve Miller, *Simscape Vehicle Templates*, 2021.
- [3] Fryer T., *Leonardo-Design. Da Vinci drawings brought to life*, Engineering and Technology, article, 14(5), 18-21, 2019.
- [4] Barber F. M., *Lecture on the Whitehead Torpedo. US Torpedo Station*, article, 1874.
- [5] Moir I. and Seabridge A., *Aircraft Systems: Mechanical, electrical, and avionics subsystems integration*, John Wiley and Sons, vol.52, 2011.
- [6] Shaout, A. and Jarrah M. A., *Cruise control technology review*, Computers and electrical engineering, article, 23(4), 259-271, 1997.
- [7] Moravec H. P., *The Stanford cart and the CMU rover*, article, Proceedings of the IEEE, 71(7), 872-884, 1983.
- [8] Uno A., Sakaguchi T. and Tsugawa S., *A merging control algorithm based on inter-vehicle communication*, IEEE/IEEJ/JSAI International Conference on Intelligent Transportation Systems, 783-787, October 1999.
- [9] Maurer M., Behringer R., Dickmanns D., Hildebrandt T., Thomanek F., Schiehlen J., and Dickmanns E. D., *VaMoRs-P: An advanced platform for visual autonomous road vehicle guidance*, Mobile Robots IX, International Society for Optics and Photonics, 2352, 239-248, January 1995.
- [10] Green M. and Green G., *Remotely Piloted Aircraft: The Predators*, Capstone, 2004.
- [11] Buehler M., Iagnemma K. and Singh S., *The DARPA urban challenge: autonomous vehicles in city traffic*, Springer, vol.56, 2009
- [12] Dikmen M. and Burns C. M., *Autonomous driving in the real world: Experiences with tesla autopilot and summon*, Proceedings of the 8th international conference on automotive user interfaces and interactive vehicular applications, 225-228, October 2016
- [13] [Online], *A Brief History of Autonomous Vehicle Technology*, Available: <https://www.wired.com/brandlab/2016/03/a-brief-history-of-autonomous-vehicle-technology/>, 2016.

- [14] Kyriakidis M., Happee R. and de Winter J. C., *Public opinion on automated driving: Results of an international questionnaire among 5000 respondents*, Transportation research part F: traffic psychology and behaviour, 32, 127-140 ,2015.
- [15] Wei Z. and Xuexun G., *An ABS control strategy for commercial vehicle*, IEEE/ASME Transactions on Mechatronics, 20(1), 384-392, 2014.
- [16] Liebemann E. K., Meder K., Schuh J. and Nenninger G., *Safety and performance enhancement: The Bosch electronic stability control (ESP)*, SAE Technical Paper, 2004-21-0060, 2004.
- [17] [Online], *Open loop vs. closed loop control systems*, Available: <https://x-engineer.org/graduate-engineering/signals-systems/control-systems/open-loop-vs-closed-loop-control-systems-xcos/>.
- [18] Sado H., Sakai S. I. and Hori Y., *Road condition estimation for traction control in electric vehicle*, ISIE'99. Proceedings of the IEEE International Symposium on Industrial Electronics, Cat. No. 99TH8465, vol.2, 973-978, July 1999.
- [19] Marsden G., McDonald M. and Brackstone M., *Towards an understanding of adaptive cruise control*, Transportation Research Part C: Emerging Technologies, 9(1), 33-51, 2001.
- [20] Hulshof W., Knight I., Edwards A., Avery M. and Grover C., *Autonomous emergency braking test results*, Proceedings of the 23rd International Technical Conference on the Enhanced Safety of Vehicles (ESV), National Highway Traffic Safety Administration Washington, DC., pages 1-13, May 2013.
- [21] Jung C. R. and Kelber C. R., *A lane departure warning system based on a linear-parabolic lane model*, IEEE Intelligent Vehicles Symposium, IEEE, pages 891-895, June 2004.
- [22] Beglerovic H., Schloemicher T., Metzner S. and Horn M., *Deep learning applied to scenario classification for lane-keep-assist systems*, Applied Sciences, 8(12), 2590, 2018.
- [23] Wu S. J., Chiang H. H., Perng J. W., Lee T. T. and Chen C. J., *The automated lane-keeping design for an intelligent vehicle*, IEEE Proceedings. Intelligent Vehicles Symposium, IEEE, pages 508-513, June 2005.
- [24] Wada M., Yoon K. S. and Hashimoto H., *Development of advanced parking assistance system*, IEEE Transactions on Industrial Electronics, 50(1), 4-17, 2003.
- [25] [Online], *About Formula Student*, Available: <https://www.imeche.org/events/formula-student/about-formula-student>.
- [26] FSG Formula Student, *Official formula student rulebook*, 2020.
- [27] Morari M. and Lee J. H., *Model predictive control: past, present and future*, Computers and Chemical Engineering, 23(4-5), 667-682, (1999).

- [28] Kissai M., Monsuez B., Mouton X., Martinez D. and Tapus A., *Adaptive robust vehicle motion control for future over-actuated vehicles*, Machines, 7(2), 26, 2019.
- [29] Kiencke, Nielsen, *Automotive Control Systems 2nd edition*, Springer, 2004.
- [30] Hac A. and Simpson M. D., *Estimation of vehicle side slip angle and yaw rate*, SAE transactions, 1032-1038, 2000.
- [31] Polack P., Altché F., d'Andréa-Novel B. and de La Fortelle A., *The kinematic bicycle model: A consistent model for planning feasible trajectories for autonomous vehicles?*, 2017 IEEE intelligent vehicles symposium, vol 4, 812.-818, June 2017.
- [32] [Online], *Lane Keeping Assist System Using Model Predictive Control*, Available: <https://it.mathworks.com/help/mpc/ug/lane-keeping-assist-system-using-model-predictive-control.html>
- [33] , Li Gang, Yuan Hang, Shi Jing, Li Ning, Zhou Zhi-cheng, *Developing Simulation Model for Four In-wheel Motor Electric Vehicle Based on Simulink* Advanced Materials Research, Trans Tech Publications Ltd, vol. 846, 22-25, 2014.
- [34] Sancibrian R., Garcia P., Viadero F., Fernandez A. and De-Juan A., *Kinematic design of double-wishbone suspension systems using a multiobjective optimisation approach*, Vehicle System Dynamics, 48(7), 793-813, 2010.
- [35] Hanzaki A. R., Rao P. V. M. and Saha S. K., *The Rack and Pinion Steering*, Kinematic and sensitivity analysis and optimization of planar rack-and-pinion steering linkages, Mechanism and Machine theory, 44(1), 42-56, 2009.
- [36] Karthikeyan Manohar, *Performance analysis of model predictive based lane following controller and global path planning with trajectory tracking control system for autonomous race vehicle*
- [37] Steven M LaValle, *Rapidly-exploring random trees: A new tool for path planning*, 1998.
- [38] Steven M LaValle, *Planning algorithms*, Cambridge university press, 2006.
- [39] Irfan Khan, *Combined lateral and longitudinal control for autonomous driving based on Model Predictive Control*
- [40] B. Rajesh Rajamani, *Vehicle Dynamics and Control*, Springer US, 2012

Ringraziamenti

A mio Padre e mia Madre,
questa tesi è dedicata a voi,
ai vostri sacrifici e per aver creduto in me.

Ai professori Amati e Tonoli,
per avermi dato l'opportunità di partecipare a questo progetto.

Ai professori presenti e passati,
guide fondamentali in questo lungo percorso.

A Stefano, Sara e tutti i ragazzi del LIM,
per il vostro continuo supporto e per aver fatto parte, anche se per poco, di questo
meraviglioso gruppo.

A Jolanda,
punto di riferimento nella mia vita.

Alla mia famiglia e a chi mi protegge dall'alto.

Ad Andrea, Moceri e Luca,
per gli infiniti momenti di leggerezza.

A Giorgio e Alessandro,
per tutte le avventure e per i ricordi di questi anni.

A Claudio, Dario e Tanya,
sono orgoglioso di aver intrapreso questo percorso insieme a voi.

Ai ragazzi della Gang,
per tutti i giorni passati in aula studio.

A tutti voi dico GRAZIE.
Ognuno di voi mi ha aiutato a diventare la persona che sono oggi.

Infine vorrei ringraziare la persona più importante della mia vita.

A Martina,
Sai sempre come rendere la mia vita più luminosa.